Charles University

Faculty of Medicine in Pilsen

Study program: Anatomy, histology and embryology

Branch of study: D4AH5112

Mgr. Tereza Bělinová

Interactions of human cells with nanoparticles for bio-medical applications

Studium interakce buněk s nanočásticemi s využitím v bio-medicíně

PhD. Thesis

Supervisor: doc. RNDr. Marie Hubálek Kalbáčová, PhD.

Consultant: MUDr. Zuzana Humlová, PhD.

Pilsen, 2020

Prohlášení:

Prohlašuji, že jsem závěrečnou práci zpracovala samostatně a že jsem uvedla všechny použité informační zdroje a literaturu. Tato práce ani její podstatná část nebyla předložena k získání jiného nebo stejného akademického titulu.

Statement of authorship:

I declare that I prepared this Ph.D. thesis independently and that I stated all the information sources and literature. This work or a substantial portion thereof has not been submitted to obtain another academic degree or equivalent.

V Plzni / In Pilsen

Tereza Bělinová

Acknowledgements:

Here I would like to express my sincere gratitude to my supervisor Marie Hubálek Kalbáčová who supported me and provided me with valuable guidance. I am thankful for her patience, motivation and immense knowledge invested in me through the past years. My thanks also belong to MUDr. Zuzana Humlová, PhD.; Prof. Minoru Fujii, Ph.D.; Assoc. Prof. Ádám Gali, Ph.D.; prof. RNDr. Bohuslav Rezek, Ph.D.; Ing. Alena Řezníčková, Ph.D. and their teams for providing me with insight from different perspective and the chance to work with their unique and extraordinary nanomaterials. My sincere thanks belongs to Blanka Bílková, Pavla Sauerová, David Beke, Anna Fučíková, Štěpán Stehlík, Lucie Vrabcová, Iva Machová, Lucie Vištejnová and many other colleagues from Biomedical center in Pilsen and Institute of Pathological Physiology in Prague for creating helpful and friendly atmosphere. Without their support this thesis could have never be completed.

Last, but not least my thanks go to my family, without their support I would have never gone so far.

Abstract:

In the past decades, nanoparticles have been viewed as a potentially powerful platform for various applications in biomedical sciences. The possible application of nanoparticles varies from drug delivery agents to novel imaging platforms and surely, some application potential still remains hidden. Thus, it is necessary to broadly study their *in vitro* behavior in order to assess the precise theranostic potential as well as to distinguish possible threats to human health. Even though nanoparticles are getting more and more attention in current research, still only a limited amount of information is available, especially regarding interactions of ultra-small (< 5 nm) nanoparticles with biological environment and cells.

The aim of the work presented herein is to provide the reader with information concerning interactions of various ultra-small nanoparticles (silicon-based, gold, nanodiamonds) with biological environment and human cells. Dose- and time-dependent influence of the various nanoparticles on behavior of different human cells (osteoblasts, monocytes, keratinocytes, mesenchymal stem cells) was established under different conditions, stressing out the importance of protein corona (a layer of proteins originating from cultivation medium attached to nanoparticles). Biocompatibility of two different types of silicon-based nanoparticles was tested on different human cells, showing selectivity of one type of the nanoparticles (silicon carbide with different surface terminations) towards immune cells. Furthermore, deeper study of the silicon carbide nanoparticles in respect to their immunomodulatory potential and influence on behavior (e.g. doubling time, differentiation potential) and metabolism of monocytic cells was established. Biocompatibility of gold ultra-small nanoparticles and nanodiamonds was also tested on various human cells. Protein corona forming on these two types of nanoparticles was subsequently analyzed by mass spectrometry, showing that ultra-small nanoparticles are capable of interaction with quite large numbers of proteins. Furthermore, the nanoparticle-cell interactions were observed by various imaging methods, such as holographic microscopy, electron microscopy (TEM, SEM, cryoFIB-SEM SIMS-TOF), flow cytometry or Raman spectroscopic imaging.

This thesis not only presents the importance of basic research on proper characterization of nanoparticle-cell interactions but also suggests possible future directions for further research and possible applications of used nanomaterials in biomedical research.

Table of Contents

List of Abbreviations

A431 – Human keratinocyte cell line derived from skin carcinoma

ATP – Adenosine tri phosphate

AuNPs – Gold nanoparticles

cryoSEM – Scanning electron microscopy of cryogenically fixed sample

DAPI – 4′, 6-Diamidino-2-phenylindole dihydrochloride

DC – Dendritic cell-like phenotype

DMEM – Dubleco's Modified Eagle Medium

DNDs – Detonation nanodiamonds

ECAR – Extracellular acidification rate

FBS – Fetal bovine serum without heat inactivation

FC – Flow cytometry

FDA – Food and Drug Administration

FIB SEM – Focused ion beam scanning electron microscopy

H-DNDs – Detonation nanodiamonds with hydrogenated surface

HaCaT – Human keratinocyte cell line derived from healthy skin tissue

hMSC – Human mesenchymal stem cells

iFBS – Heat inactivated fetal bovine serum

LDH – Lactate dehydrogenase

LDL – Low density lipoprotein

MF – Macrophage-like phenotype

NDs – Nanodiamonds

NHDF – Normal human dermal fibroblasts cell line

NPs - Nanoparticles

NTA – Nano particle tracking analysis

OCR – Oxygen consumption rate

O-DNDs – Detonation nanodiamonds with oxidized surface

OXPHOS – Oxidative phosphorylation

PBS – Phosphate buffer saline

PC – Protein corona

PEG – Polyethylene glycol

QD – Quantum dot

ROS – Reactive oxygen species

SAOS-2 – Human osteoblastic cell line

SERS – Surface enhanced Raman scattering

SEM – Scanning electron microscopy

SDS-PAGE – Sodium dodecyl sulfate polyacrylamide gel electrophoresis

SiC-NH_2 – Silicon carbide nanoparticles with predominant –NH_2 surface termination

SiC-OH – Silicon carbide nanoparticles with predominant –OH surface termination

SiC-X – Silicon carbide nanoparticles with unspecified surface termination

SiQDs – Silicon quantum dots

TEM – Transmission electron microscopy

THP-1 – Human monocyte cell line

TOF-SIMS – Time of flight secondary ion mass spectrometry

USNPs – Ultra-small nanoparticles

αMEM – Alpha modified Eagle medium

1. Introduction

Even thought it might seem like that, nanoparticles (NPs) are not entirely a phenomenon of the past decades. NPs occur naturally, originating from cosmic fallout or geological processes such as volcanic eruptions or are even produced by living organisms (Plane 2012; Simakov 2018; Hosea et al. 1986). Some viruses can be also considered to be living NPs due to their size. Taking this long-term occurrence into account, human usage of NPs in colloidal state can be dated all the way into ancient Egypt in the form of various dyes (Walter et al. 2006; Johnson-McDaniel et al. 2013; Sciau et al. 2009; Artioli, Angelini, and Polla 2008). This ancient usage of NPs, however was probably without the artists knowing that they are working with nanomaterials. Even though the users of these colloids did not know it, they were the first to start the era of NPs production and wide usage. The first documented report of NPs preparations belongs to Michael Faraday on April 2nd 1856. He described in his notes the preparation of colloidal gold NPs and later published it (Faraday 1856, 1857). Since then, different NPs started to be more and more studied, characterized and utilized. Nowadays, beside still naturally occurring NPs, industrially engineered NPs take up a large portion of what humans come into contact. These NPs are produced by automobiles, cigarettes or construction dust (Kagawa 2002; Ning et al. 2006; Stefani, Wardman, and Lambert 2005). Furthermore, NPs are today being used widely in cosmetics and industrial production of cars and electronic parts (Raj et al. 2012; Santos et al. 2015). Humankind have been living in close contact with NPs since the beginning of their existence and will continue to live with them. Thus it is obvious why people seek deeper understanding of NPs and their existence.

2. Nanoparticles in Biomedicine

As NPs are omnipresent they pose an interesting platform for possible applications in industry, cosmetics or medicine. For biomedical application, it is crucial to define and describe characteristics and basic interactions of NPs with living structures, but also to consider their possible negative effects on human health.

2.1. Definition and Characterization of Nanoparticles

Nowadays there are multiple ways of NPs classification for example by size, shape or chemical properties.

Usually, structures ranging in their diameter from 1 nm to 100 nm are classified as NPs (Vert et al. 2012; "Nanotechnologies — Vocabulary — Part 2: Nano-objects" 2015). Most commonly used NPs in biomedical sciences have diameter at around 20-70 nm. This size is particularly advantageous for active endocytic (cellular process of transporting substances into cell) internalization of such NPs (Zhao and Stenzel 2018). In the past several years, a subsection of NPs called ultra-small NPs (USNPs) started to be distinguished. Such particles typically have diameter smaller than 5 nm. These small structures of different materials possess different electrical, optical or catalytic properties when compared to the bulk material itself. This is especially due to the increased surface/volume ratio (Fig. 1), the quantum effect that occurs in such small structures and their solubility in colloids. Thus, their size provides general properties common for all NPs regardless of other characteristics. Even though NPs can occur in form of dust or aerosol, they are predominantly bound to liquid milieu in the form of suspension or colloids (Buzea, Pacheco, and Robbie 2007).

Shape-wise, NPs can be spherical, cubic, star-shaped or even in the form of nano-tubes, as long as all of their dimensions fit in the 1-100 nm scale. The shape of NPs is one of the characteristics that defines possible interactions of them with cells. As reviewed by Wang et al. in some cases, rod shaped NPs are being internalized more easily than the same spherical NPs (Wang, Gaus, et al. 2019). It has also been showed that shape of NPs may influence the endocytic mechanism employed for their internalization (Xie et al. 2017). Some NPs can also possess porous structure that is particularly interesting in respect of their delivery properties. Such pores in NPs can be loaded with cargo which can then be delivered to desired cells (Arayne and Sultana 2006).

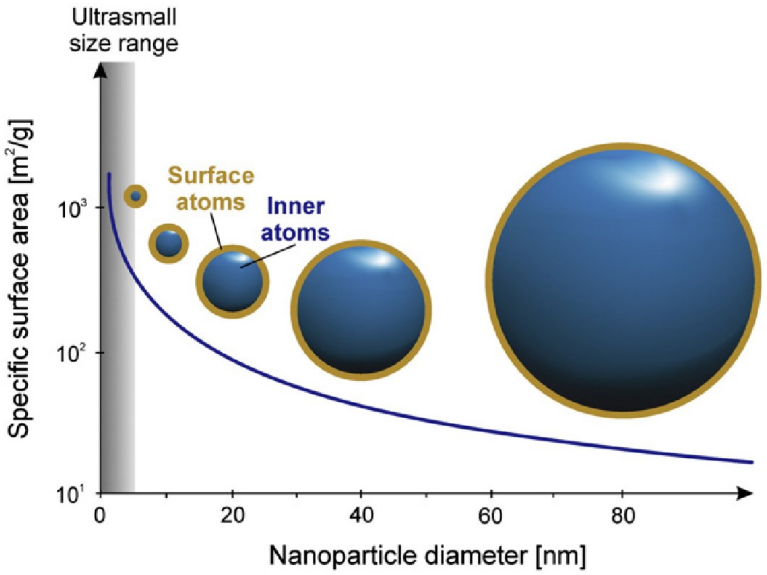

Figure 1: Schematic representation of size and surface/volume ratio of nanoparticles. Adapted from Zarschler et al. (Zarschler et al. 2016)

Further, more specific characteristics of NPs depend highly on the material of origin. They can be metallic (e.g. gold, silver, platinum or iron), carbon- or semiconductor-based, organic etc.

Metal-based (Au, Fe, Pt etc.) NPs possess similar mechanical characteristics as the bulk material itself, however their nano-size provides them with interesting opto-electrical properties. Surface plasmon resonance and surface-enhanced Raman scattering (SERS) marks conductive NPs for development of different bioassays (Petryayeva and Krull 2011). Some metal-based NPs also possess magnetic properties that can be utilized in phenomenon called magnetic fluid hyperthermia or in magnetic-based biosensing assays (Sharifi, Shokrollahi, and Amiri 2012; Kabe et al. 2019). Moreover, silver NPs have demonstrated antimicrobial activity, indicating potential to avoid over-using of antibiotics (Qing et al. 2018). In addition to being highly electron-dense and thus very useful in transmission electron microscopy (TEM), gold NPs (AuNPs) are also interesting due to the fluorescence resonance energy transfer (Horisberger and Rosset 1977; Dulkeith et al. 2005). This effect causes enhancement of fluorescent signal nearby the AuNPs which can be used to acquire higher quantum yield from weak fluorophores.

Semiconductor-based NPs can be manufactured from variety of materials such as silicon, germanium, zinc, cadmium and their oxides and other compounds (hydroxides, salts etc.). These NPs are particularly useful in electronics or as sensors thanks to their electro-conductivity. In biomedicine, these NPs are especially interesting for their

naturally occurring fluorescence stable to photo-bleaching (Flessau et al. 2014; Kailasa, Cheng, and Wu 2013). When semiconductor- or even metal-based USNP has this feature, it can be commonly called as a quantum dot (QD). Furthermore, semiconductor-based, and mainly silicon-based, NPs have often porous structure which allows for application as delivery platform for varying cargo (Stojanovic et al. 2016).

Carbon nanotubes, fullerens or nanodiamonds (NDs) are most common carbon-based NPs. Their major common characteristics is high conductivity and biocompatibility, as carbon is one of the main building blocks of organic structures. Carbon nanotubes are single- or multi-walled structures of rolled tightly bound hollow hexagonal lattice of carbon atoms. Beside their biocompatibility and good conductivity, carbon nanotubes are also exceptionally resistant to mechanical stress (Yu et al. 2000). Fullerens, atoms of carbon forming a meshed hollow sphere, have been viewed as potential imaging and cargo-delivery systems. Thanks to their relative biocompatibility and easy functionalization they can pose as an envelope for other substances (Lalwani and Sitharaman 2013). On the other hand, NDs are capable of forming so-called nitrogen vacancies leading to naturally occurring fluorescence and thus QDs formation (Kaur and Badea 2013). However, currently used carbon-based NPs have tendency to aggregate in liquid environment due to high Van der Waals and electrostatic interactions, which makes their application in biomedicine so far difficult (Koh and Cheng 2014).

NPs based on various organic polymers (polycaprolactone, polyethylene glycol (PEG), chitosan etc.) or lipids are promising platform especially for drug delivery. They can be designed as a specific carrier envelope which is biocompatible and biodegradable into monomeric state and then metabolized. Using surface functionalization and polymer design, such NPs can be used for targeted and controlled cargo delivery of therapeutics (El-Say and El-Sawy 2017). Their therapeutic potential is clearly visible as 50 % of NPs approved for clinical use by the American Food and Drug Administration (FDA) are polymers or lipids (Ventola 2017).

2.2. Nanoparticles in Biomedical Context

2.2.1. Nanoparticles' Interaction with Biological Environment

It is commonly accepted that interaction of NPs and biological environment is crucial for their further fate. Usually, NPs are administered to liquid biological environment, e.g.

cultivation medium *in vitro* or blood and lymph *in vivo*. Certain NPs can be administered directly to human cells through lungs, skin or gastrointestinal tract. However, even in this case the NPs still firstly interact with the cellular environment and form so called biomolecular corona, sometimes also referred to as protein corona (PC), as its main components are proteins (Gagner et al. 2012). This layer of proteins, lipids and other components forms the actual identity of NPs that cells can interact with. The proteins interact with NPs surface mostly non-covalently by Van der Waals forces, hydrogen bonds or electrostatic and hydrophobic interactions, or even by steric interactions (Yu, Liu, et al. 2019; Kumar et al. 2018).

PC in the true sense of the word is composed of two layers of biomolecules. The first, tightly bound layer is usually described as hard corona and the second, more loosely bound, is called soft corona (Fig. 2A). It is still a subject of investigation what are the key characteristics for protein binding. Usually, proteins with the highest electrochemical affinity to the NPs surface charge form the PC, however not strictly (Monopoli et al. 2012). This additional covering of NPs by biomolecules from the environment can be an issue, especially for NPs functionalized for specific cell targeting. Functionalized surface of NPs can be covered by the formed PC and thus the desired target does not have to be found (Mirshafiee et al. 2013; Salvati et al. 2013). To avoid this problem, protein repelling functionalization (e.g. by PEG) can be used (Pelaz et al. 2015). PEG coating, so called PEGylation, has several effects on NPs. Firstly, due to PEG charge, it can turn hydrophobic NP into hydrophilic one and thus allows for its easier solubility in aqueous solutions. Secondly, PEGylation makes NPs less recognizable for immune system and thus prolongs their circulation *in vivo* (Milla, Dosio, and Cattel 2012). Furthermore, it has been shown that functionalization of surfaces by PEG decreases the ability of proteins to bind to them (Bernhard et al. 2017). Other possible approach for avoiding PC to compromise targeting potential of functionalized NPs is protein pre-coating. NPs can be intentionally covered by selected proteins along with targeting agents, forming an "artificial" PC (Oh et al. 2018). However, both PCs must still be taken into account, as neither of the solutions is fully successful.

Until recently, it was hard to study both, hard and soft PC simultaneously. In the past years, however several new methods have been developed for this purpose (Winzen et al. 2015; Weber et al. 2018). Thus, new possibilities of PC characterization and its further manipulation have risen. This is especially important in respect to soft PC studies, as soft

PC is the main mediator of NPs-cell interaction and so far, very limited information of its composition is available.

However, the above-described commonly accepted PC design is applicable only to larger NPs (several tens of nm). USNPs cannot form this PC *sensu stricto*, as they are smaller or of the same size as most of the proteins. The way of interactions of these extremely small NPs with biological environment is still discussed among scientists. Two main ways of USNPs-protein interaction are proposed. Firstly, formation of protein network, connected by USNPs (Fig. 2B) and secondly, interaction of single protein with single USNP (Fig. 2C) (Piella, Bastus, and Puntes 2017; Chatterjee and Mukherjee 2014). Thus, USNPs may mediate formation of protein clusters by weak electrostatic interactions. Such interactions among different NPs or NPs and proteins then lead to formation of NPs-protein agglomerates. These agglomerates, in respect to their composition, influence cells and may cause varying effects (Bradac et al. 2018; Wang et al. 2018). Stearic interaction of single protein with USNP is so far predominantly just theorized and it is highly unlikely that such interaction occurs *in vivo* (Dravecz et al. 2018; Chatterjee and Mukherjee 2014). Under controlled conditions *in vitro*, however this might be possible and applied for example in enzyme function manipulation (Zhang et al. 2009).

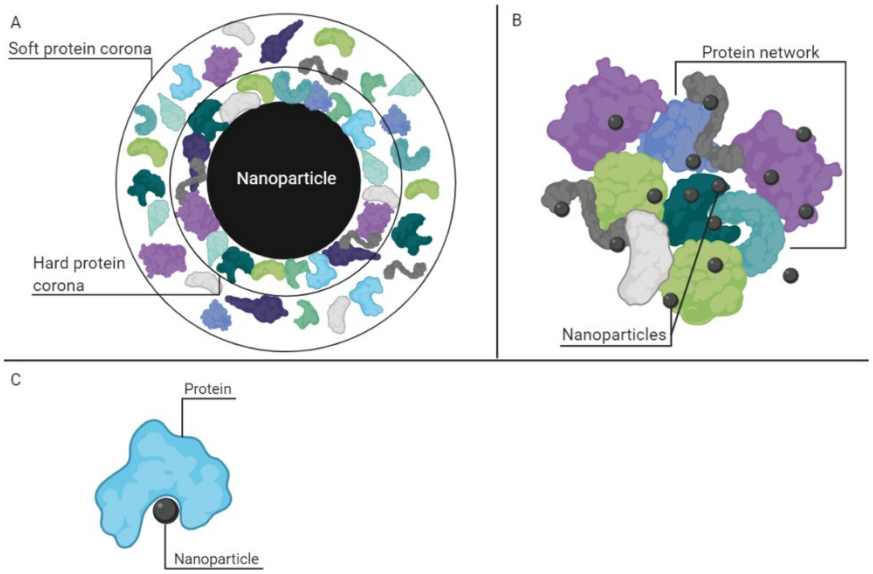

Figure 2: Schema of possible interactions of nanoparticles and proteins. Created *via* BioRender Software.

No matter the exact mechanism of NPs-protein interaction and the precise composition of PC, the interaction of NPs with biological environment has highly significant role in mediation of NPs-cell interactions and NPs further fate within the cells.

2.2.2. Nanoparticle-Cell Interaction

Once NPs are administered into biological environment (e.g. cultivation medium *in vitro* or blood *in vivo*) interaction with cells is unavoidable. Cellular internalization of NPs is highly debated topic in recent years and is strongly influenced especially by NPs characteristics (e.g. size, shape etc.). Prior to any cellular absorption, NPs need to interact with cellular membrane. It has been shown that NPs directly interacting with membranes (e.g. lipid bilayers) may affect membrane stability and stiffness (Contini et al. 2017; Lolicato et al. 2019).

Generally, NPs can enter cells by active (e.g. endocytosis) or passive ways. Active internalization pathways differ from passive by requirement of certain degree of energy. As written previously, NPs hardly interact with cells directly. The interaction is being mediated by proteins and other molecules covering the NPs. This might be one of the key determinants deciding the way of cellular uptake of NPs, as proteins forming PC might trigger receptor-mediated endocytosis (i.e. clathrin- or caveolin-dependent and clathrin- or caveolin-independent endocytosis and phagocytosis). Furthermore, NPs can also be internalized into cells by non-specific pathways such as pinocytosis (fluid-phase endocytosis) or *via* passive transport (i.e. direct transfer through cell membrane) (Fig. 3).

Precise endocytic mechanism is directed especially by NP´s (or USNP-protein aggregate) size. Particles of sizes above 500 nm can usually be internalized by phagocytosis, which is a specific endocytic mechanism reserved for immune cells (Aderem and Underhill 1999). Other cells, not capable of phagocytosis internalize such big NPs by the means of macropinocytosis (subsection of pinocytosis) (Kuhn et al. 2014). Smaller particles can enter cells by other, more specific mechanisms such as clathrin- and caveolin-dependent endocytosis or -independent mechanisms (Kettiger et al. 2013). USNPs under experimental conditions, are able to enter the cell directly through cell membrane in dependence on their size and surface charge (Wang et al. 2012; Jiang et al. 2015).

Clathrin-dependent endocytosis is highly connected with specific receptors (e.g. transferrin receptor, IL-13 receptor or LDL receptor) and usually concerns NPs approx. 100 nm in diameter (Kettiger et al. 2013). After binding of specific ligand to such receptors, clathrin-coated pit is formed and further process of invagination and uptake can progress. Endosome formed by this process are either recycled back to plasmatic

membrane or progress through the endosomal/lysosomal pathway (Kaksonen and Roux 2018). In order to allow for NPs to enter cells by this pathway they can be engineered to specifically bind to receptors that recruit clathrin to cellular membrane. Such specificity can be achieved for example by functionalization of NPs surface with ligand of specific receptor (Gao et al. 2013). This, however brings us back to the issue of formation and manipulation of PC (especially soft PC). Secondly, certain, mainly polymeric, NPs can be engineered to disintegrate in response to the decreasing pH or enzymatic activity within the endosomal pathway and thus releasing their cargo (Benyettou et al. 2015; Lv et al. 2016; Acar et al. 2017; Zhu et al. 2019).

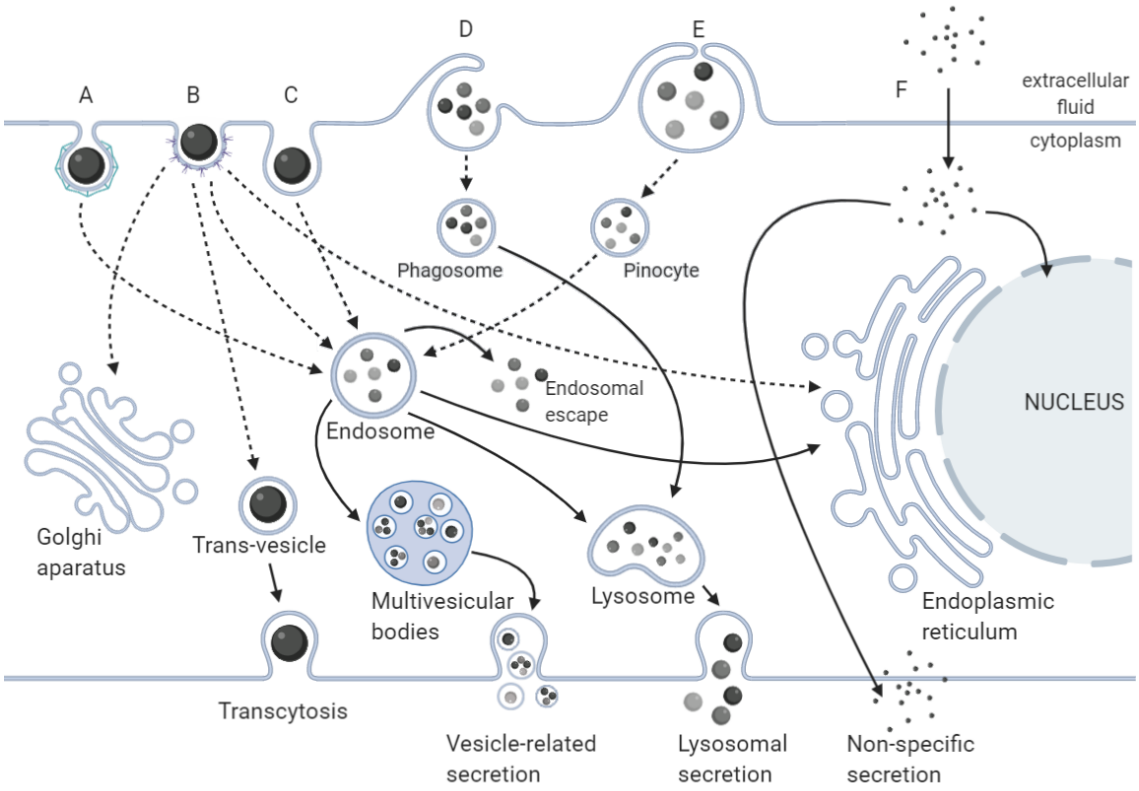

Figure 3: Simplyfied schematic representation of possible trafficking of nanoparticles in cell (A = clathrin-dependent endocytosis, B = caveolin-dependent endocytosis, C = clathrin/caveolin independent endocytosis, D = phagocytosis, E = pinocytosis, F = direct transfer). Created *via* BioRender Software.

Similarly to clathrin-dependent endocytosis, caveolin-dependent endocytosis is also receptor-specific. This type of endocytosis is mediated *via* caveolae, plasmatic membrane invaginations rich in cholesterol and sphingolipids, associated with caveolin-1. Receptors connected with this type of endocytosis are for example GPI-anchored proteins, growth hormone or IL-2 receptors (Parton and Simons 2007). NPs that have approx. 50 – 80 nm in diameter are usually engulfed by caveolin-dependent endocytosis (Kettiger et al. 2013).

Endosomes formed from caveolae can, besides undergoing classical endosomal pathway, be directed straight to Golgi apparatus or endoplasmic reticulum (Le and Nabi 2003). Thus, via directly targeting caveolin-dependent endocytosis NPs cargo can be delivered to these organelles (Xin et al. 2017). Furthermore, caveolin-dependent endocytosis has been shown as a potential way for overcoming barrier formed by endothelial cells (Wang et al. 2011; Oh et al. 2014). It has been shown, that these polarized cells are capable of internalization of NPs *via* caveolae and *via* transcytosis transport the NPs to the opposite side of the endothelia barrier. This could be used as possible shuttle for specific drugs to be delivered to specific tissues with high efficacy.

Clathrin- and caveolin-independent endocytosis (i.e. flotillin-mediated or ARF6-associated) is overall less-explored than clathrin- and caveolin–dependent mechanisms. Such endocytosis can be observed in engulfment of some virus-like particles (Damm et al. 2005). These special types of NPs utilize preferably regions on cytoplasm, called lipid rafts, associated with mediator proteins such as ADP-ribosylation factor 6 or Cdc42 protein (Kumari, Mg, and Mayor 2010). However, cases of such endocytic mechanisms for engineered NPs internalization are rare (Kasper et al. 2013).

Last widely used specific endocytic pathway, phagocytosis, is utilized only by specific cells – professional phagocytes (e.g. macrophages, dendritic cells or neutrophils). This mechanism is usually reserved for larger NPs (e.g. > 500 nm). Once again it is a receptor-mediated endocytosis, usually started by binding of debris or pathogen, which need to be cleared from body. Specific phagocytic receptors are for example Fc receptor, mannose receptor or complement receptor. This type of endocytosis is especially interesting, when intravenous application of NPs is considered. NPs are scavenged by phagocytes due to their opsonization (binding of molecules which increase affinity of phagocytic cells to opsonized structure) and cleared quickly from bloodstream (Tavano et al. 2018; Lazarovits et al. 2015). To avoid such fast clearance and prolong circulation lifetime of NPs, some researchers have been deploying NPs pre-coating with different solutions, such as PEG (Qie et al. 2016). These substances, however might cause adverse immunogenic effects and thus must be considered very carefully (Luo et al. 2017).

Beside the above-described specific cellular uptake mechanisms, NPs can also be internalized by the cells *via* non-specific constantly ongoing process called pinocytosis. Pinocytosis is sometimes referred to as “cellular drinking” as it is engulfment of

extracellular fluid, mediated by actin induced membrane protrusions. As stated previously, pinocytosis can be divided into subsections – macropinocytosis capable of engulfing large particles (> 500 nm) and micropinocytosis forming smaller vesicles. Thus, micropinocytosis can absorb very small NPs (< 10 nm) coincidentally when the NPs are dispersed in extracellular fluid. Vesicles formed by pinocytosis with sizes ranging from 100 to 500 nm are called pinosomes and are known to be prone to escape of internalized material from absorbed vesicle (Kerr and Teasdale 2009). Pinocytic uptake of NPs therefore can be exploited in order to upgrade delivery potential of differing drugs into cells (Iversen, Frerker, and Sandvig 2012; Liu and Ghosh 2019).

Direct transfer of NPs into cells is highly problematic to observe under standard conditions *in vitro* and nearly impossible *in vivo*. Direct penetration is highly dependent not only on NPs size and shape, but also on membrane stiffness (Torrano et al. 2016; Wang, Guo, et al. 2019). Although there have been some reports of naturally occurring cell membrane penetrating NPs, it is still more common to achieve translocation of NPs to cytoplasm by experimental approaches such as microinjection or electroporation (Tiefenboeck et al. 2017; Yu et al. 2016). Both of these approaches are applicable mainly *in vitro*, thus possible useful for *ex vivo* stimulation or manipulation of cells (Phonesouk et al. 2019). However, *in vivo* application of microinjection of NPs in order to cross biological barriers have been also reported for some experimental models (Paatero et al. 2017; Johansen et al. 2016). Main advantage of direct transport of NPs into cytoplasm is further sub-cellular targeting and even direct entry of NPs into cell nucleus without the need to engage endosomal escape mechanisms (Huo et al. 2014).

Endosomal escape is a potentially harmful mechanism that needs to be deployed by NPs in the case when their desired target is outside the classical endosomal pathway. All content of endosomes undergoes slow degradation. The acidic pH inside endosomes gradually decreases from 6.5 to approximately 4. The cargo is then either transported to cytoplasm for the cell to utilize it furtherly or to lysosome for complete degradation and subsequent elimination from the cell. Unless the NPs (i.e. polymeric NPs) are designed to unload their cargo or directly act (e.g. by change in fluorescence) in response to the decreasing pH or activity of endosomal enzymes, the endosomal entrapment must be overcome. Such escape can be achieved by NPs´ surface modification with cell penetrating peptides or other membrane disrupting modifications (Evans et al. 2019; Dalal and Jana 2017). Penetration of endosomal vesicles, however may lead to potentially

harmful outcomes and must be carefully considered (Melamed et al. 2018). When the NPs cannot undergo endosomal escape, they can either be directly excreted by the cell, or they can be cumulated in lysosomes. Such accumulation in lysosomes can be potentially highly toxic, even for initially non-toxic content of lysosomes. This effect is well demonstrated by rare metabolic lysosomal storage diseases (Winchester, Vellodi, and Young 2000).

Once inside cell, NPs may have various effects on them. As mentioned before, NPs can be designed as sensors and thus only reflect the environment in intracellular compartment where they are localized after endocytosis. Other NPs are simply used as an imaging agents and should not have any influence over cells whatsoever. NPs that serve as drug delivery platforms unload their cargo which then furtherly acts and alters the cell in its specific way. Beside this, NPs can also cause other effects such as genotoxicity, alter gene expression, cause mitochondrial function alteration (e.g. changes in mitochondrial potential) or even trigger apoptosis (programmed cell death) (Xie, Mason, and Wise 2011; Thakur et al. 2020; Gallud et al. 2019; Ma and Yang 2016). Mitochondrial function alteration is especially interesting as it may lead to various outcomes for cellular behavior. It has been reported that NPs can strongly impact mitochondrial respiration and in consequence affect overall cellular metabolism (Tucci et al. 2013).

Although endocytic mechanisms of NPs-cell interactions are broadly studied and well defined, exocytosis and subsequent clearance of NPs from organism are much less understood. It has been showed that in case of endosomal escape, NPs tend to accumulate inside the cell cytoplasm and do not undergo exocytosis (Stayton et al. 2009). In such case, biocompatibility of used NPs material is crucial. Several researchers have pointed out that NPs in fact undergo exocytosis and even tried to prolong their stay inside cells in order to give them enough time to influence such cells (Oh and Park 2014; Kim et al. 2015; Jiang et al. 2010). It has also been reported that NPs can be encapsulated by cells into extracellular vesicles called exosomes (Sancho-Albero et al. 2019). Such vesicles are very important in inter-cellular communication and pose highly interesting platform not only for NPs delivery, but also for alteration of exosomal secretion by NPs. To deeply study mechanisms of NPs excretion and exploit them, however still requires more sophisticated methods. Even less information than on cellular exocytosis of NPs is available in respect to clearance of NPs from organisms. Commonly, it is accepted that biocompatible and biodegradable nanoparticles, especially NPs with diameter under 8

nm, leave body by renal clearance (Ehlerding, Chen, and Cai 2016; Choi et al. 2007). However, certain NPs (e.g. metal-based or polymeric) also tend to accumulate in cells and are not furtherly cleared from organism (Satterlee et al. 2017; Miller et al. 2019). This can be used for example in targeted tumor therapy, however long-term studies of toxicity of such accumulated NPs are still lacking.

2.2.3. Nanoparticles and Immune System

Within any living organism, immune system is the first line of defense against all foreign substances entering the body. As stated previously, all living organisms have been exposed to NPs on daily basis and it has even be suggested, that these interactions might already be causing some damage (Hirai et al. 2016). Being so, our immune system (monocytes, macrophages, lymphocytes etc.) have surely developed a recognition and response system for NPs. Both components of complex immune system – innate and adaptive immunity – can respond to NPs and start immune reaction (Vivier and Malissen 2005). In respect to NPs it is necessary to determine the interactions with the immune system for two main reasons. First, possible toxic and inflammation potential of NPs must be evaluated before their application *in vivo*, as overreaction of the immune system may cause extensive damage. Second, new ways of evasion from immune system recognition and subsequent clearance is highly important in respect of prolonged circulation of NPs *in vivo* (Caracciolo et al. 2015).

Innate immune system generates non-specific inflammatory response to conserved immunogenic patterns. This response is mediated *via* pattern-recognition receptors of the cells. Thus, NPs surface modification or PC formation play key roles in this process. Specifically, PC corona was shown to mediate complement activation, which induces inflammatory response by cellular components of immune system (Ding and Sun 2019). Moreover, direct interaction of NPs with innate immune cells such as monocytes can also induce inflammatory response (Senapati et al. 2015). Furthermore, it has been shown that some NPs are capable of inflammasome activation and thus induce immune response (e.g. pro-inflammatory cytokine production) (Gomez, Urcuqui-Inchima, and Hernandez 2017). However, NPs have been shown not only to induce inflammation, but also to modulate already ongoing response (Gliga et al. 2020). Targeting certain components of innate immunity by NPs in order to manipulate subsequent adaptive immunity response in desired direction is also an interesting option. Using such mechanism may eventually

lead to enhancement of, for example, natural cancer immunity or mitigation of allergic reactions (Lee et al. 2019; Jatana et al. 2017).

In contrast to innate immune system, adaptive immunity is more sophisticated system involving highly specific mechanisms of antigen detection, including generation of immunological memory. This part of immune system is of particular interest in respect to cancer therapy and specific antibody production. For example induction of T-cell (cells responsible for assisting to development of immune response, immunological memory and killing of other cells infected by pathogens) mediated suppression of tumor growth by NPs administration was recently reported (Korangath et al. 2020). Other possible use of NPs-immune system interaction might lie in *ex vivo* stimulation of T-cells and their re-administration to body (Perica et al. 2015; Scholz et al. 2017). Furthermore, NPs showed a potential to lower allergic reaction in peanut allergy in mice by stabilizing T-cell response to the allergen (De S. Reboucas et al. 2014). B-cells, secretory cells responsible for production of specific antibodies, can also be targeted by NPs and lead to specific secretion of desired antibodies (Temchura et al. 2014).

In vivo, both of the two previously described systems always work closely together in order to correctly respond to internal and external dangers. NPs could potentially exploit this complex mechanism in terms of immunomodulation. Immunomodulation – an umbrella term describing both reinforcement and impairment of immune system function – could help us to fight against cancer and other diseases currently swiping the population.

2.2.4. Possible Applications of Nanoparticles in Biomedicine

There is a wide variety of NPs in research, clinical trials or even experimental application in current biomedicine. Herein, just the application potential of silicon-based, gold NPs and NDs (NPs studied in this thesis) will be described briefly.

Silicon-based NPs are a wide group of particles consisting of silicon (Si), its oxides or compounds with other elements. Usually, the main advantage of silicon-based materials is derived from their semiconductor nature. However, degradation and clearance of Si-based NPs have much larger potential than of any other semiconductor for biological applications. Silicon NPs can be degraded into orthosilicic acid, being then excreted from body by urine (Park et al. 2009). As such, Si-based NPs are predominantly used in the form of QDs for bio-imaging or in their porous form (i.e. mesoporus) as drug delivery systems. In bio-imaging, Si-based NPs are viewed as counterpart to commonly used QDs

that are predominantly highly toxic (Pramanik et al. 2018). Si-based QDs proved to be non-toxic and easily detected both, *in vitro* and *in vivo* (Tamba et al. 2015; Erogbogbo et al. 2011). Furthermore, the use of mesoporous silicon NPs for either direct photodynamic therapy, or as a coupling agent for its delivery, have also been reported (Secret et al. 2013; Kim et al. 2017).

Thanks to their physico-chemical and photo-optical properties, AuNPs have been broadly studied for the use in biomedicine. The combination of AuNPs and a sensitizer proved to be particularly effective in photodynamic cancer therapy, where light-induced reactive oxygen species (ROS) kill cancerous cells (Yang et al. 2015; Meyers et al. 2015). Significantly higher potential for AuNPs application, however lies in photo-thermal therapy. The ability of AuNPs to absorb light in visible or near infra-red spectrum and subsequently generate heat in order to damage cancerous cells proved to be efficient (Park et al. 2019; Ali, Wu, and El-Sayed 2019). Some types of AuNPs beside their photo-thermal effect have also been reported to directly cause ROS production. The combination of these two mechanisms strengthens the damage caused to cancerous cells, killing them in more efficient way (Guerrero-Florez et al. 2020). Beside the above-mentioned cancer therapy applications, AuNPs can also be utilized as drug-delivery agens, bio-sensing platforms or in bio-imaging (Kong et al. 2017; Jiang et al. 2018; Wu et al. 2019).

As carbon is a main building block of life, biocompatibility of carbon-based NPs is without any doubt. NDs possess the sp^3 formation and inert core of classical diamond. Furthermore, they also have prominent hardness, superb thermal conductivity, tunable surface modification options and in some cases natural fluorescence derived from nitrogen vacancies (Kaur and Badea 2013). These properties mark NDs as potential material for biomedical usage. Natural fluorescence of NDs derived from the presence of nitrogen vacancies does not suffer from photobleaching as much as conventionally used fluorophores. As such, surface-modified NDs can be targeted and used as non-toxic staining agents for bio-imaging (Chang et al. 2013; Su et al. 2017). Thanks to the fact, that NDs are easily surface-modified, drug-delivery application or even enhancement of photo-thermal therapy are envisioned (Yu, Yang, et al. 2019; Harvey et al. 2019). Interesting NDs' application is achieved in biocompatible bone scaffold design. It has been shown that NDs can act as potent adjuvant for bone cell adhesion and proliferation and thus improve the scaffold mechanical properties (Wu et al. 2017; Yassin et al. 2017).

3. Aims of the Thesis

3.1. Interactions of Silicon Quantum Dots with Human Cells

To determine the influence of silicon quantum dots on different types of human cells in culture with the focus on the importance of protein corona formation.

3.2. Interactions of Silicon Carbide Nanoparticles with Human Cells

To test the interactions of silicon carbide nanoparticles with different human cells and subsequently their potential as immunomodulatory agents with the focus on surface termination importance.

3.3. Interactions of Gold Nanoparticles with Human Cells

To describe the influence of ultra-small PEGylated gold nanoparticles on human osteoblasts.

3.4. Nanodiamond Nanoparticles Interaction with Proteins and Human Cells

To assess basic interactions of nanodiamonds with proteins from fetal bovine serum in culture media and subsequently with human cells.

4. Materials and Methods

In this section, methods used to acquire data for publications are stated in short, as detailed descriptions can be found in the publication full texts enclosed at the end of this thesis. Methods used in unpublished data sections are described in detail and clearly marked. If not stated otherwise, the described methods were performed solely by the Author.

4.1. Nanoparticles

Silicon Quantum Dots – Section 6.1.

Silicon QDs (SiQDs) were provided by the group of Dr. Minoru Fujii (Department of Electrical and Electronic Engineering, University of Kobe, Japan). Silicon crystals, co-doped with boron (B) and phosphorus (P) with diameter of approximately 4 nm were fully water-soluble with stable fluorescence (405 nm/700-850 nm) (Fujii, Sugimoto, and Imakita 2016). Particles were provided in methanol solution, from which they were transferred to water directly prior to use. Methanol to water transition was achieved by mixing NPs-methanol solution with sterile deionized H_2O (50:50) and subsequently subjected to evaporation of half of the volume at 70°C.

Silicon Carbide Nanoparticles – Section 6.2.

Silicon carbide (SiC) based NPs with different terminations (-x/-NH_2/-OH) were prepared by the group of prof. Gali (Wigner Research Centre for Physics and Department of Atomic Physics, Budapest University of Technology and Economics, Hungary). They were provided as a suspension in water with size range of 1-2.5 nm (Beke et al. 2012; Szekrényes et al. 2014) and diluted directly into cell culture media after brief (30 min) sonication in a sonication bath.

Gold Nanoparticles – Section 6.3.

Gold NPs (AuNPs) originated from Dr. Řezníčková (Department of Solid State Engineering, University of Chemistry and Technology, Czech Republic) and were prepared as a colloid in PEG/PEG-NH_2/PEG-SH solution by direct sputtering. Their size distribution varied from 1-4 nm in diameter (Reznickova et al. 2019; Reznickova et al. 2017). They were directly diluted into cell-culture media.

Detonation Nanodiamonds – Section 6.4.

DNDs used in this work were provided by the group of Dr. Stehlík and Dr. Rezek (Institute of Physics of the Czech Academy of Sciences and Faculty of Electrical Engineering, Czech Technical University, Czech Republic, respectively). They were prepared as a suspension in water of surface-oxidized (O-DNDs) and surface-hydrogenated (H-DNDs) 4 and 2 nm NPs (Stehlik et al. 2016; Stehlik et al. 2017).

4.2. Cells and Culture Conditions

Cell lines of human osteoblasts (SAOS-2), human monocytes (THP-1) and human keratinocytes derived from healthy skin tissue (HaCaT) and skin carcinoma (A431) were used. Primary human mesenchymal stem cells (hMSC) acquired from bone marrow of healthy donors were also used.

Standard sub-cultivation conditions (75 cm^2 cell culture flasks, TPP) for each cell type were as follows:

- SAOS-2: McCoy's 5A medium with addition of 15% heat-inactivated fetal bovine serum (iFBS), L-glutamine and penicillin/streptomycin antibiotic mixture
- THP-1: RPMI 1640 medium supplemented with 10 % iFBS, L-glutamine and penicillin/streptomycin antibiotic mixture
- hMSC: Alpha Modified Eagle Medium (αMEM) medium with phenol red supplemented with 10 % iFBS, L-glutamine and penicillin/streptomycin antibiotic mixture
- HaCaT: Dulbecco's Modified Eagle Medium (DMEM) supplemented with 10 % iFBS, L-glutamine and penicillin/streptomycin antibiotic mixture
- A431: DMEM medium supplemented with 10 % iFBS, L-glutamine and penicillin/streptomycin antibiotic mixture

Experimental conditions (96 or 6-well dishes, TPP) for all types of cells included variable of 5 % non-heat-inactivated fetal bovine serum (FBS) supplementation or 6 hours cultivation completely without FBS to allow direct NPs-cell interaction without formation of PC (referred to as serum-free conditions or medium without serum/FBS supplementation throughout the thesis). Identical batch of FBS was used for all NPs-related experiments:

- SAOS-2/HaCaT/A431: DMEM medium supplemented with 5 % FBS, L-glutamine and penicillin/streptomycin antibiotic mixture
- THP-1: RPMI 1640 medium supplemented with 5 % FBS, L-glutamine and penicillin/streptomycin antibiotic mixture
- hMSC: Alpha Modified Eagle Medium (αMEM) medium with phenol red supplemented with 10 % FBS, L-glutamine and penicillin/streptomycin antibiotic mixture

Differentiation of THP-1 cells into macrophage-like (MF) or dendritic cell-like (DC) phenotype was done as follows:

- MF: THP-1 cells were seeded at a concentration of 157 000 cells/cm^2 in 2 ml of standard cultivation medium with addition of 1 µM or 100 nM phorbol-myristate acetate (PMA) in 6-well plate and cultivated for 72 hours
- DC: THP-1 cells were seeded at a concentration of 157 000 cells/cm^2 in 2 ml of standard cultivation medium with addition of 0.1 µg/ml of each GM-CSF and IL-4 and then cultured for 5 days. After 3 days of cultivation, additional 1 ml of fresh medium with 3 µg/ml of each of the supplements was added to the cells.

4.3. Doubling Time of Cells

In order to assess influence of SiC-based NPs on cellular proliferation (i.e. time needed for the cell population to double) of monocytic THP-1 cells, doubling time was established (*Section 6.2.2.*).

The cells were seeded in 6-well dishes at a concentration of 10 000 cells/cm^2 on a shaker in the medium with 5% FBS supplementation with 100 µg/ml of SiC-based NPs for 6 hours. After that time shaker was turned off and cultivation continued until 24 and 48 hours. After 4, 24 and 48 hours, one whole 6-well dish was harvested and cell count in each well was determined by counting in Bürker chamber. From this count, doubling time was determined by using doubling time computational website (http://www.doubling-time.com/compute.php?lang=en).

4.4. Metabolic Activity

Metabolic activity of cells was assessed by colorimetric dehydrogenase-dependent MTS assay by Promega (Cell Titer961 AqueousOne). 10% MTS solution was added to experimental culture media with cells for 2 hours (37°C, CO_2) and then absorbance was measured at 455 nm (620 nm as reference) using Labsystem Multiskan MS reader or Tecan Spark reader. The results were then correlated to cell count (either counted by flow cytometer, in Bürker chamber (monocytic THP-1) or by Cy-Quant staining (adherent cells)), as increase in cell number may manipulate the results significantly. The lowering of metabolic activity under 75 % of control level was considered cytotoxic (Flahaut et al. 2006).

4.5. CyQuant Cell Count

In order to determine relative changes in cell count, measurement of DNA content by fluorescent staining with CyQuant NF (no freeze) cell proliferation assay (Invitrogen) was employed. After MTS assay, cells were washed and 50 µl of staining solution (1:500 CyQuant dye in HBSS buffer, both provided with the assay) was added to cells for 1 hour (37°C, CO_2) and then fluorescence intensity was measured (excitation 485 nm, emission 530 nm) with Tecan Spark reader.

4.6. Cytokine Detection

Production of wide panel of 42 cytokines was detected by Human Cytokine Antibody Array from Abcam. Supernatant harvested from cells with NPs was incubated with array membrane overnight at 4°C on rocking shaker, all other steps were done in accordance with manufacturers manual (*Section 6.2.1.*). Obtained data were processed by ImageLab software (BioRad).

4.7. Flow Cytometry

Flow cytometry (FC) measurements were applied for cell count of THP-1 cells and for mitochondrial mass and potential measurements. The method thereof is described in Publication C.

Furthermore SiQDs detection in SAOS-2 cells was conducted using FC (*Unpublished data - Section 6.1.2.*). The cells were pre-seeded at a concentration of 10 000 cells/cm^2 on 6-well dishes in the standard cultivation medium for 24 hours. After that, the cells

were washed in phosphate buffer saline (PBS) and incubated with 100 μg/ml SiQDs for 2 hours in DMEM with or without 5 % FBS. Subsequently cells were harvested by trypsin/EDTA and SiQDs were detected by BD FACS Aria at excitation wavelength 405 nm and emission was acquired at 750-810 nm. Only live cells were gated and furtherly processed in comparison to unstained control *via* FlowJo software.

4.8. Imaging

Multiple differing imaging techniques were applied in order to achieve detection of used USNPs in cells. Standard light and fluorescent microscopy (Olympus IX71 with a color camera DP74), was used in order to periodically check cellular morphology in subcultures and perform histological staining evaluation (*Section 6.2.1.*).

In order to observe SiQDs interaction with the cells, following method was applied (*Unpublished data - Section 6.1.2.*).

- Live-cell imaging of SiQDs interacting with SAOS-2 cells was conducted using Nanolive 3D Cell Explorer-fluo holographic microscope (Nanolive). Cells were pre-seeded under standard cultivation conditions at concentration of 10 000 cells/cm^2 on glass bottom 35 mm dishes (Ibidi) for 24 hours, then 100 μg/ml of SiQDs in DMEM + 5 % FBS were added and cells were incubated in controlled atmosphere, humidified and heated chamber (OKOlab) directly in the microscope. The acquired data were furtherly processed *via* STEVE software (Nanolive).

Detection of AuNPs in cells was conducted using transmission electron microscopy (TEM) and Raman spectroscopy (*Unpublished data – Section 6.3.2.*).

- For TEM imaging SAOS-2 cells were pre-seeded at a concentration of 10 000 cells/cm^2 in the standard cultivation medium into 35 mm Petri dishes with inserted sterilized 12 mm cover glasses on the bottom. After 24 hours, medium was discarded and cells were washed with PBS. Fresh DMEM medium with 5% FBS containing 14 μg/ml of AuNP-PEG-SH was added to cells and incubated for 24 hours. After this time, cells were washed twice in PBS and fixed by combination of 2% glutaraldehyde and 2% paraformaldehyde. Samples were then repeatedly washed in PBS and

subsequently dehydrated by ethanol row (10 min in 20%, 40%, 50%, 60%, 70%, 100% ethanol and 10 min in acetone). After dehydration, cells were mounted in resin and submerged in liquid nitrogen. Cover glass was then discarded and ultrathin slices were made. The samples were observed by TEM FEI Morgani microscope equipped with MegaView II CCD camera. TEM samples (resin mounting and microtome slicing) were prepared and images of AuNPs were taken at Institute of Biology and Medical Genetics (1LF, UK) with kind cooperation of Dr. Pavla Bažantová.

- For Raman spectroscopy SAOS-2 cells were pre-seeded at a concentration of 10 000 cells/cm^2 in the standard cultivation medium into 35 mm Petri dish with sterilized 12 mm quartz glass cover slips (SPI Supplies). After 24 hours, medium was discarded and cells were washed with PBS. Fresh DMEM medium with 5% FBS medium containing 14 μg/ml of AuNP-PEG-SH NPs was added to cells and incubated for 24 hours. After 24 hours, supernatant was discarded and cells were washed in PBS and fixed by 4% paraformaldehyde. Subsequently, samples were mounted to quartz glass slide and sealed by CoverGrip sealant (Biotium). Raman imaging was performed with kind cooperation of doc. Mojžeš at Division of Biomolecular Physics (MFF, UK) at WITec alpha300 RSA (WITec) and oil-immersion objective UPlanFLN 100x (NA 1.30, Olympus) at 647.1 nm line of Kr^+ ion laser using 20 mW power at the focal plane. Raman maps were analyzed by the means of the True Component Analysis from the software packet WITec Project Plus 5.1 (WITec) decomposing spectral datasets to individual spectral components differing in their relative contribution throughout the investigated object.

The presence of SiC NPs inside SAOS-2 cells was tested employing special technique described below (Unpublished data – *Section 6.2.2.*).

- A special method called cryo-TOF-SIMS FIB SEM microscopy developed by Tescan was tested in order to obtain information of intracellular localization of SiC-based NPs. SAOS-2 cells were pre-seeded in the standard cultivation medium at a concentration of 10 000 cells/cm^2 for 24 hours on gold grids provided by Tescan. Cells were then transferred to Brno and after media change left in CO_2 incubator for stabilization for 4 hours. Subsequently, media was discarded and changed for the medium with 5 % FBS and 100 μg/ml SiC-

x and incubated overnight. In the control cells, medium was changed but no particles were added. After overnight incubation, the cells were washed with the fresh medium and vitrified at Tescan facility (-183° C, Leica GP2). The vitrified samples were measured by Dr. Jakub Javůrek (Tescan s.r.o., Brno) at Tescan facility using Tescan Lyra3 Ga+ FIB SEM (focused ion beam scanning electron microscopy) equipped with a compact TOF-SIMS (time of flight secondary ion mass spectrometry) allowing for elemental analysis of milled material.

All microscopic images were processed for smoothness and brightness correction *via* ImageJ software (NIH).

4.9. Agilent Seahorse Cell Metabolism Detection

Glycolysis versus oxidative phosphorylation (OXPHOS) adenosine-tri-phosphate (ATP) production rate was determined in respect to SiC-based NPs and THP-1 cells (*Unpublished data – Section 6.2.2.*).

The cells were cultured in 6-well dish at a concentration of 10 000 cells/cm^2 on a shaker in the medium without FBS supplementation with 100 μg/ml of SiC-based NPs for 6 hours. Then the shaker was turned off and FBS was added in order to provide a final concentration of 5 % FBS. Cells were subsequently cultured for another 18 hours. After this time, cells were harvested by centrifugation (210 g, 5 min), split in two samples and processed in accordance with a standard Seahorse procedures for Seahorse ATP rate assay protocol. Briefly, cells were re-suspended in a Seahorse RPMI Medium and seeded on Seahorse cartridges pre-coated with poly-L-lysine (Sigma-Aldrich). Furthermore, cellular metabolism was measured in a Seahorse XFP mini analyzer (all Seahorse materials and instruments provided by Agilent). After the measurement, supernatant was discarded and the cell-containing cartridges were frozen (-20 °C) overnight. Subsequently, cell nuclei were stained with 4′,6-Diamidino-2-phenylindole dihydrochloride (DAPI, Sigma-Aldrich). Fluorescent images of DAPI stained cells were obtained using an Olympus IX71 microscope. Cell count for data normalization was determined using CellProfiler Analyst software (Cell Profiler). Data regarding oxygen consumption rate (OCR) and extracellular acidification rate (ECAR) of the cells were processed *via* Wave software (Agilent).

4.10. Exosome isolation and detection

Production of small extracellular vesicles – exosomes – by THP-1 cells stimulated with SiC-based NPs was assessed (*Unpublished data – Section 6.2.2.*).

The cells were cultured in a 6-well dish at a concentration of 10 000 cells/cm^2 in the medium without FBS supplementation with 100 µg/ml of SiC-x NPs on a shaker for 6 hours. Then, the shaker was turned off and FBS was added in order to provide the final concentration of 5 % FBS. The cells were subsequently cultured for another 18 hours. After this time, the cells were harvested by centrifugation (210 g, 5 min). The supernatant from the cells was transferred to a clean sterile tube and was furtherly processed by a differential ultracentrifugation. Shortly, supernatant was sequentially centrifuged (at 300 g for 10 min, 2000 g for 10 min and 10 000 g for 30 min) and always transferred to a fresh tube. After these steps, an ultracentrifugation was performed at 100 000 – 200 000 g for 70 min twice with supernatant elimination after each step. The resulting pellet was analyzed by Browns' motion analysis (Nano-particle tracking analysis (NTA), NanoSight NS300, Malvern Panalytical Ltd) and by Western blot against CD81 human exosomal marker. The Western blot and NTA were prepared with kind cooperation of Dr. Petr Přikryl (Institute of Pathological Physiology, 1LF UK) and Prof. František Štěpánek (Chemical Robotics Laboratory, VŠCHT), respectively.

4.11. Mass spectrometry

Presence of PC (i.e. proteins associated with NPs) was tested for PEGylated AuNPs (*Section 6.3.2.*). The same method was also employed for analysis of PC on DNDs (*Section 6.4.1.*, Publication D), where detailed procedure can be found.

Briefly, 14 mg/ml of AuNP-PEG and AuNP-PEG-SH was incubated in DMEM medium supplemented with 5 % FBS at room temperature under constant rotation on a rotator overnight. The samples were then centrifuged (10 510 g, 4°C, 30 min). Supernatant was discarded and resulting pellet was re-suspended in 500 µl of PBS and again centrifuged. This washing step was employed 5 times. After washing, the resulting pellet was dissolved in 30 ul of passive lysis buffer (PLB, Promega). 15 µl of resulting sample was used for mass spectrometry analysis as described in Publication D (i.e. liquid chromatography–mass spectrometry/mass spectrometry (LC–MS/MS)). Remaining 15 µl

was analyzed by a 12% Sodium dodecylsulfate polyacrylamide gel electrophoresis (SDS-PAGE). The sample preparation and SDS-PAGE were prepared with kind cooperation of Dr. Iva Machová (Biomedical Center, LFP UK). Mass spectrometry was performed and data analyzed by Dr. Martin Hubálek (Mass spectrometry group, ÚOCHB, VŠCHT).

4.12. Statistical Analysis

Statistical analysis was conducted in Statistica software (StatSof) employing non-parametric matched pair Wilcoxson test and two factor ANNOVA with post-hos Fischer-LSD analysis

5. List of Authors' Original Publications

Publication A: Ostrovska, Lucie, Antonin Broz, Anna Fucikova, **Tereza Belinova**, Hiroshi Sugimoto, Takashi Kanno, Minoru Fujii, Jan Valenta, and Marie Hubalek Kalbacova. "**The Impact of Doped Silicon Quantum Dots on Human Osteoblasts**." RSC Advances 6, no. 68 (2016): 63403-13, IF = 3,289

Tereza Bělinová was responsible for metabolic activity assessment, assisted in confocal imaging and writing of the original draft.

Publication B: Belinova, Tereza, Lucie Vrabcova, Iva Machova, Anna Fucikova, Jan Valenta, Hiroshi Sugimoto, Minoru Fujii, and Marie Hubalek Kalbacova. "**Silicon Quantum Dots and Their Impact on Different Human Cells**." physica status solidi (b) 255, no. 10 (2018). IF = 1.729

Tereza Bělinová was responsible for metabolic activity measurements, LDH detection and cell imaging and evaluation thereof as well as for writing the publication.

Publication C: Bělinová, Tereza, Iva Machová, David Beke, Anna Fučíková, Adam Gali, Zuzana Humlová, Jan Valenta, and Marie Hubálek Kalbáčová. "**Immunomodulatory Potential of Differently-Terminated Ultra-Small Silicon Carbide Nanoparticles.**" Nanomaterials 10, no. 3 (2020), IF = 4.324

Tereza Bělinová was responsible for all cell-related data collection and evaluation, preparation of samples for zeta potential measurements and writing of the publication.

Publication D: Reznickova, A., N. Slavikova, Z. Kolska, K. Kolarova, **T. Belinova**, M. Hubalek Kalbacova, M. Cieslar, and V. Svorcik. "**Pegylated Gold Nanoparticles: Stability, Cytotoxicity and Antibacterial Activity**." Colloids and Surfaces A: Physicochemical and Engineering Aspects 560 (2019): 26-34, IF = 2.829

Tereza Bělinová was responsible for metabolic activity measurements, statistical analysis and review of the publication draft.

Publication E: Machova, Iva, Martin Hubalek, **Tereza Belinova**, Anna Fucikova, Stepan Stehlik, Bohuslav Rezek, and Marie Hubalek Kalbacova. "**The Bio-Chemically Selective Interaction of Hydrogenated and Oxidized Ultra-Small Nanodiamonds with Proteins and Cells**." Carbon (2020), IF = 8.821

Tereza Bělinová was responsible for metabolic activity measurements, SEM sample preparation and review of the publication draft, assisted with mass spectrometry samples preparation and SEM imaging.

6. Results

In order to maintain consistency the results are presented in the same order as Aims of the thesis. Each aim is divided into a chapter regarding already published data and a chapter regarding unpublished data, if any, related to the same topic.

6.1. Interactions of Silicon Quantum Dots with Cells

6.1.1. Published Data (Publications A and B)

Publication A: Ostrovska, Lucie, Antonin Broz, Anna Fucikova, **Tereza Belinova**, Hiroshi Sugimoto, Takashi Kanno, Minoru Fujii, Jan Valenta, and Marie Hubalek Kalbacova. "**The Impact of Doped Silicon Quantum Dots on Human Osteoblasts**."

Publication B: Belinova, Tereza, Lucie Vrabcova, Iva Machova, Anna Fucikova, Jan Valenta, Hiroshi Sugimoto, Minoru Fujii, and Marie Hubalek Kalbacova. "**Silicon Quantum Dots and Their Impact on Different Human Cells**

The two above-mentioned publications summarize the long term work regarding SiQDs and their influence on different human cells. Commonly used QDs are usually made of heavy metals and thus tend to be toxic and not biocompatible. SiQDs are a promising platform to replace these commonly used QDs with relatively biocompatible and non-toxic material. Publication A was written while the author of the thesis was finishing Master studies at Faculty of Science. However, the work was not used to obtain any academic title of the author of this thesis and combined with publication B (where the thesis author is the first author) provides the reader with more complex overview of the matter of SiQDs and their potential in biomedicine, thus it is included herein.

In the Publication A novel SiQDs co-doped with phosphorus and boron were tested in respect to their behavior in biological environment and their influence on osteoblastic SAOS-2 cells. Two sizes of SiQDs were fabricated – SiQD 1100 and 1050 with diameter of 4 and 3 nm, respectively. Both NPs exhibited relatively high external quantum yield of 12 % and in long-time storage stable fluorescence with excitation of 405 nm and emission of 750 and 850 nm for SiQD 1050 and 1100, respectively. Both of the particles exhibited strong colloidal stability and slight (approx. 50 nm) fluorescence emission decrease in time.

After broad physico-chemical characterization, the NPs were cultivated with SAOS-2 cells under two different conditions – serum free (i.e. without PC formation) and 5% FBS containing medium (i.e. with PC formation) and their influence on metabolic activity of the cells was assessed in respect to increasing concentration (5, 25 and 125 μg/ml) and time (6, 24 and 48 hours). The results can be seen in Figure 5 in Publication A. SiQD 1100 have proved to be more toxic under both applied conditions, however much earlier effect was observed without the presence of FBS (thus without PC). In serum-free medium, the cells showed a decrease in metabolic activity earlier and with rising time also at lower concentrations than in medium with 5 % FBS. SiQD 1050 on the other hand showed cytotoxic effect only after longer incubation (24 hours) and only in serum-free medium. In medium with 5% FBS, the cells exhibited cytotoxic response (i.e. metabolic activity under 75% of control) only with the highest (125 μg/ml) concentration of NPs after 48 hours of incubation.

The cells with NPs were then subjected to microscopic examinations which revealed significant and quite interesting differences (Figures 6 and 7 in Publication A). SiQD 1050 showed formation of huge aggregates in the cultivation medium covering the cultivation surface and exhibited in low, foggy fluorescence emission, almost exclusively outside cells. Quite surprisingly, cluster formation remained under serum-free conditions, while detected fluorescence even decreased, making the NPs almost invisible. The most interesting results were obtained from SiQD 1100 and thus, further work was focused only on this type of SiQDs. With rising time (from 2 to 6 to 24 hours), the signal from SiQDs 1100 was getting stronger in medium with 5% FBS and started to change localization from medium around cells (2 hours) to not only the medium surrounding cells, but into the cells themselves (6 hours). After 24-hour incubation of cells with 50 μg/ml of SiQD 1100 in medium with 5% FBS, strong signal localized in intracellular vesicles was observed. In serum-free medium, still strong, however highly diffuse and non-localized signal was detected. After 2 hours under serum-free conditions, the fluorescent signal was already observed inside cells. After 6 hours of cultivation, FBS was added to the cultivation medium to avoid cell death due to the lack of nutrients and SiQD 1100 clusters with FBS-originating proteins were detected in culture medium. After 24 hours, strong, but not localized (i.e. diffused) fluorescent signal was detected in the cells cultivated with NPs without PC. Thus, presence of FBS (therefore presence of PC)

not only influenced cellular metabolic activity, but also had impact on intracellular localization of SiQDs.

From results described above, SiQD 1100 proved to be more interesting for further studies and thus, Publication B was focused on influence of only these NPs on different types of human cells. Beside osteoblastic SAOS-2 cells representing well-described stable cell line, suspension immune THP-1 cells in monocytic (*in vivo* freely circulating in blood) and macrophage-like (MF, tissue-specific adherent immune cells) state and primary healthy human mesenchymal stem (hMSC) cells were used in order to assess cell-type specific response of the cells to SiQDs. The cells were incubated with growing concentration of NPs (25, 50 and 100 μg/ml) for 6, 24 and 48 hours in FBS supplemented and serum-free medium. The results confirmed the importance of FBS presence and thus PC formation (Figure 2 in Publication B). All the cell types tested were sensitive to NPs presence significantly more in serum-free medium (thus without PC). Cell-type dependent response to SiQDs was clearly detected. Whereas clear concentration-dependent decrease in metabolic activity was observed in SAOS-2 cells, simple decrease without any concentration dependence in hMSC was detected. Immune cells (monocytic THP-1 and MF) proved to be particularly responsive in respect of the NPs. While supplemented with 5 % FBS, monocytic THP-1 cells showed significant increase of metabolic activity after 6 hours, which disappeared after 24 hours, where the metabolic activity was comparable to control level. In serum-free medium (i.e. without PC) the cells did not show such rapid increase of metabolic activity after 6 hours, however strong dose-dependent cytotoxicity was observed after 24 hours. In MF THP-1 cells, no effect was observed under either condition after 6 hours, however after 24 hours, significant decrease in metabolic activity was detected in serum-free medium, while only slight decrease was visible in FBS supplemented medium.

The results acquired from metabolic activity tests of SAOS-2 and hMSC cells were furtherly accompanied by testing of mechanism of the observed inhibition. Presence of lactate dehydrogenase (LDH) in cell supernatant reflects cell membrane rupture and thus resulting necrosis (Figure 3 in Publication B). Human mesenchymal stem cells (hMSC), showing decrease in metabolic activity only after 24 hours did not show any significant levels of LDH in the supernatant and thus cell membrane rupture could be ruled out. SAOS-2 cells, on the other hand, showed increasing levels of LDH detected in the medium with increasing incubation time. The levels were however significantly

higher than control levels of LDH only after 48 hours of incubation. This finding was in correspondence with metabolic activity results, where significant metabolic activity inhibition was observed at that time point.

When the results from the two above-mentioned publications are combined, SiQDs are shown as possible substitute for commonly used, highly toxic, QDs. Cell type dependent and specifically dose-dependent toxicity was observed in higher doses of NPs, however even lower dose proved to be clearly detectable in cells with sufficient fluorescence intensity. More importantly, both of the publications stressed out the importance of formation of PC caused by FBS supplementation of culture medium.

6.1.2. Unpublished Data

Even though the above-mentioned published results showed interesting results regarding SiQDs-cell interaction, more proof of direct contact and intracellular localization of the NPs was still needed. Two imaging techniques were applied in order to obtain further information.

Nanolive Holographic Microscopy

As a non-invasive live-cell imaging without photo-induced cellular stress is needed, holographic imaging techniques are a rising opportunity. This method is based on light diffraction and described in detail in corresponding patents (US patent No. 8,937,722 and EU patent No. 2011/121523). Even though SiQDs used herein have the potential to be detected by fluorescent microscopy, their excitation wavelength does not allow long term fluorescent live-cell imaging, as the 405 nm excitation wavelength is highly toxic for cells.

In the previous results the earliest time point of 6 hours was employed and resulted in significant decrease in metabolic activity of SAOS-2 cells treated with 100 μg/ml of SiQDs 1100. The evolution of SiQDs-cell interaction in time points leading to this toxic event was observed by non-invasive method of holographic microscopy. Surprisingly, the cells showed morphological textbook example of apoptosis within particularly short time of approx. 185 min (Fig. 4, Video 1 in electronic supplement) with continuous effect up until 6 hours of incubation. The results obtained in Publication B showed that toxicity of 100 μg/ml of SiQD 1100 after 6 hours of incubation in the medium with FBS was not connected with necrosis, as no LDH was detected in the cell supernatant (Figure 3a in

Publication B). The results from live-cell imaging suggested mechanism responsible for the cytotoxic lowering of metabolic activity after 6 hours in the medium with FBS might be apoptosis.

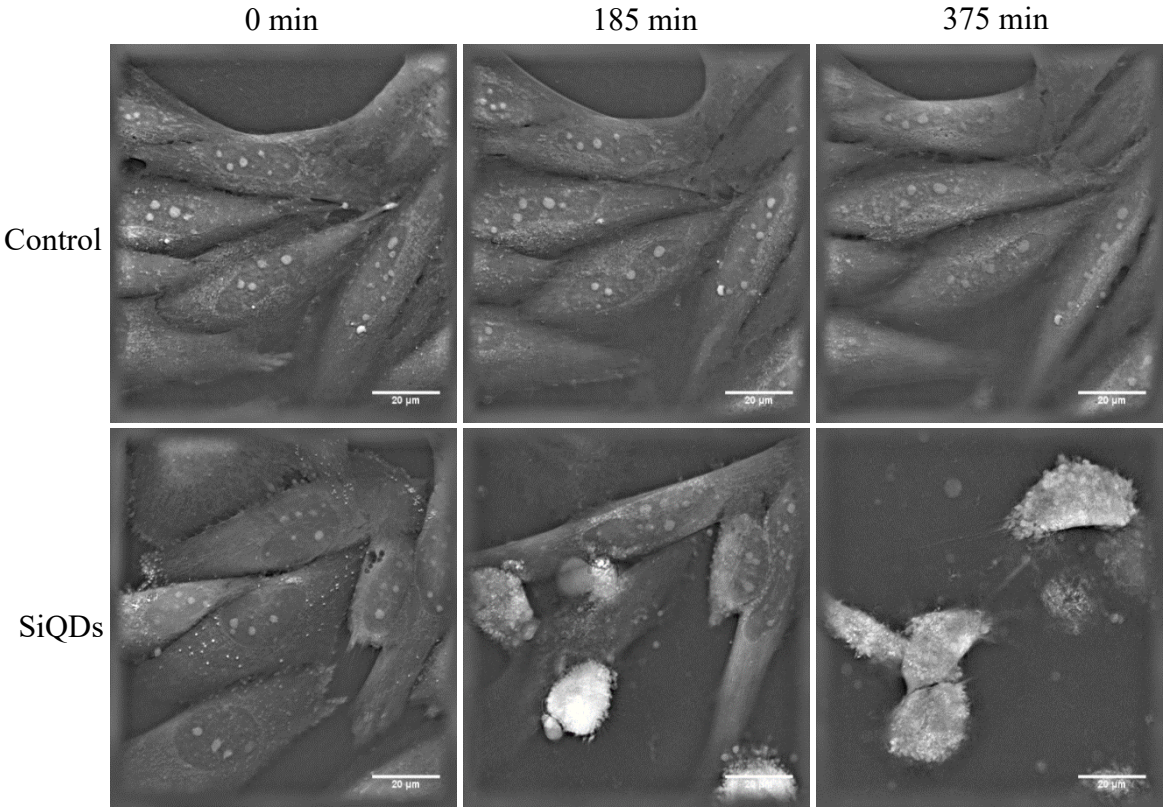

Figure 4: Holographic images of SiQDs influence on SAOS-2 cells. Representative images of changes in cellular morphology of SAOS-2 cells after treatment with 100 µg/ml of SiQDs in DMEM supplemented with 5 % FBS. The scale bar represents 20 µm

Detection of SiQDs in SAOS-2 Cells by Flow Cytometry

As the holographic microscopy data showed, SiQDs interact with cells almost immediately after their administration. To furtherly show the importance of PC formation, as was suggested in Publication A (Figures 6 and 7 in Publication A), on SiQDs, FC assessment of SiQDs uptake by SAOS-2 cells was conducted after 2 hours of incubation in the medium containing 100 µg/ml SiQDs with and without 5 % FBS supplementation.

Figure 5B shows SAOS-2 cells in 5% DMEM medium with 100 µg/ml of SiQDs. Approx. 17 % of live cells show fluorescence closely connected with SiQDs presence which is in correspondence with microscopic observations reported in section 6.1.1. In the medium without FBS supplementation, vast majority (98 %) of the healthy cells

exhibits SiQDs related fluorescence. Short-term incubation of SAOS-2 cells with SiQD 1100 showed, that the presence of FBS (and thus PC) has determining influence on NPs interaction with the cells.

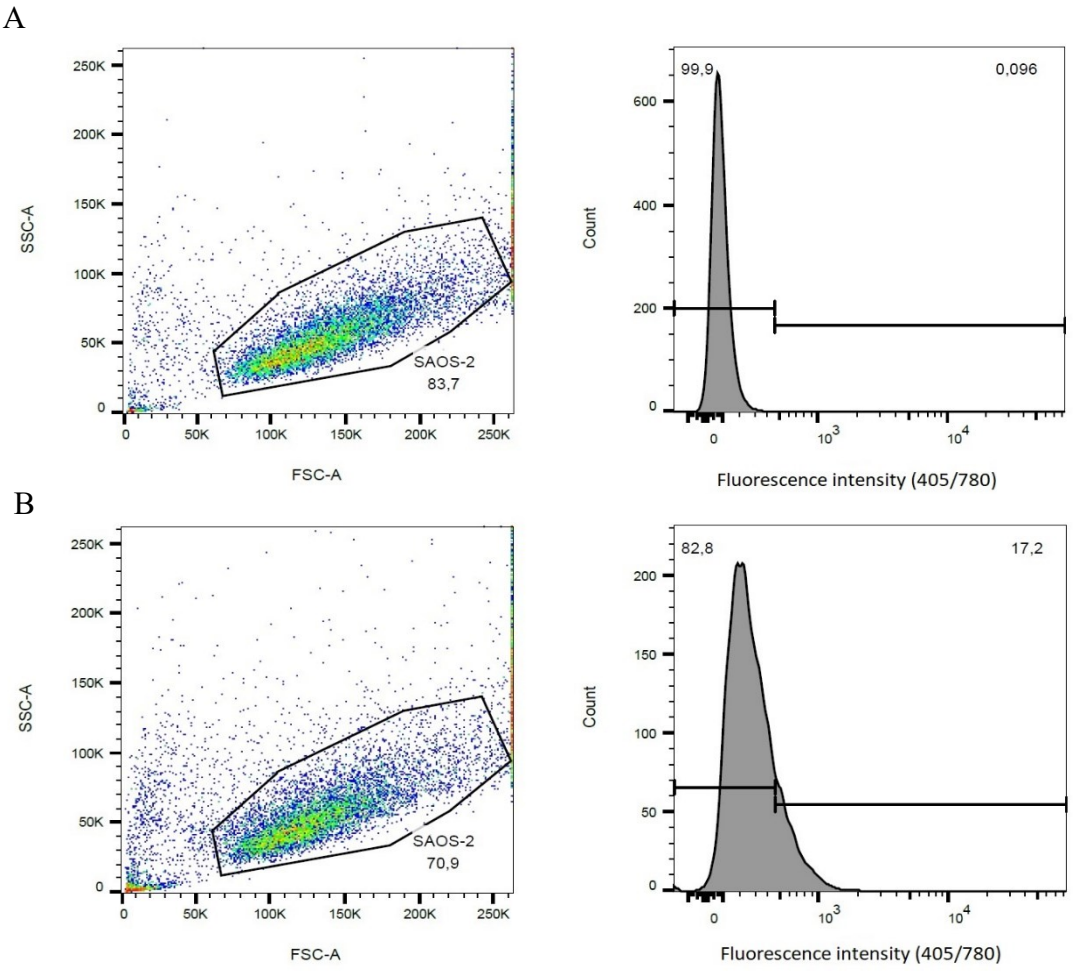

Figure 5: Flow cytometry analysis of SAOS-2 cells with 100 µg/ml of SiQDs in the medium with 5 % FBS. Histograms show fluorescence intensity and layout at excitation of 405 nm and emission of 780 – 810 nm for control, SiQDs untreated, cells (A) and cells with 100 µg/ml of SiQDs (B).

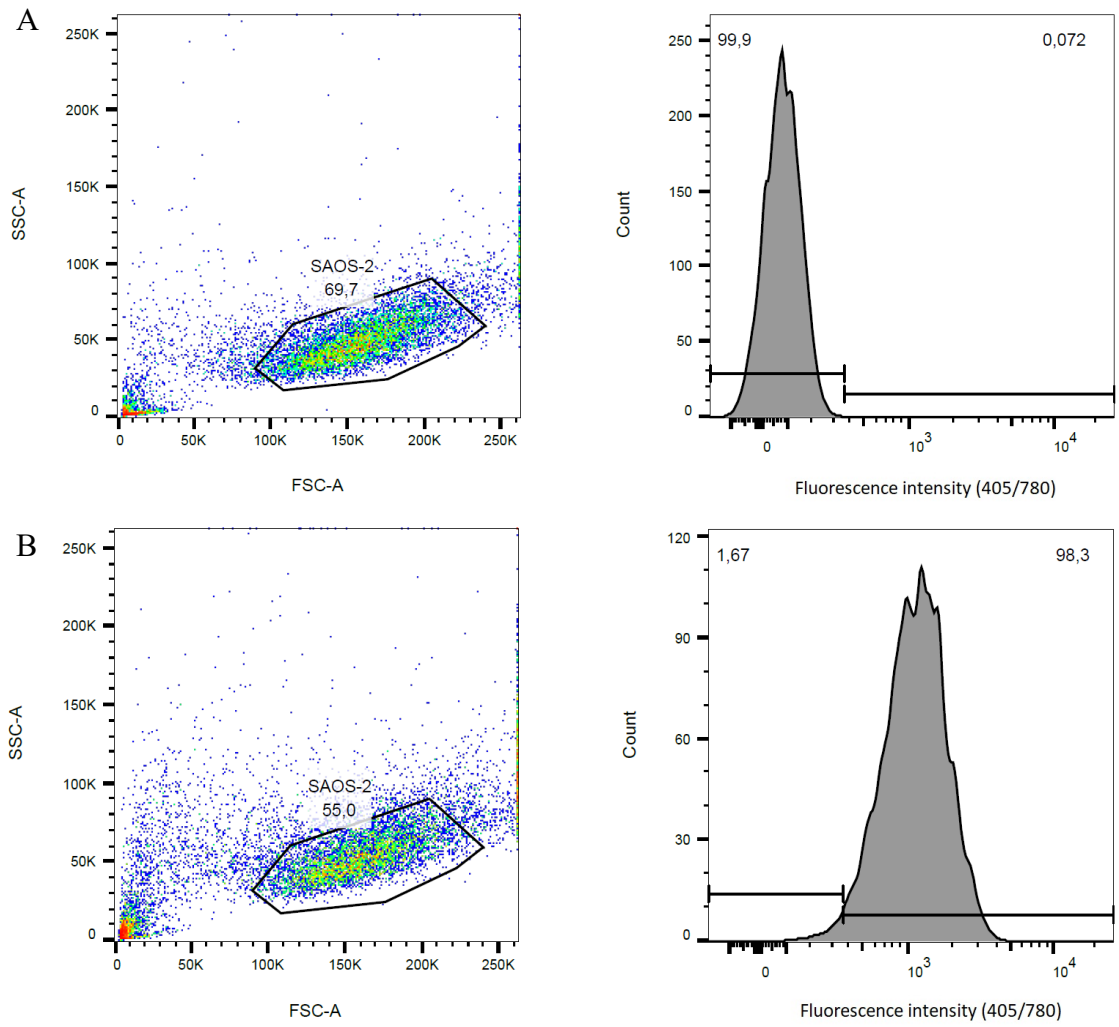

Figure 6: Flow cytometry analysis of SAOS-2 cells with 100 µg/ml of SiQDs in the medium without FBS. Histograms show fluorescence intensity and layout at excitation of 405 nm and emission of 780 – 810 nm for control, SiQDs untreated, cells (A) and cells with 100 µg/ml of SiQDs (B).

6.2. Interactions of Silicon Carbide Nanoparticles with Human Cells

6.2.1. Published Data (Publication C)

Publication C: Bělinová, Tereza, Iva Machová, David Beke, Anna Fučíková, Adam Gali, Zuzana Humlová, Jan Valenta, and Marie Hubálek Kalbáčová. "**Immunomodulatory Potential of Differently-Terminated Ultra-Small Silicon Carbide Nanoparticles.**"

The main biology-relevant advantage of USNPs lies in their size, which is often comparable to pores in differing cellular membranes (e.g. plasmatic membrane, nuclear membrane). Silicon carbide (SiC) has huge potential in biomedical applications for its combined biocompatibility and biodegradability of silicon and carbon. The combination of advantages of USNPs and SiC-based material is thus very promising for applications in biomedicine.

In Publication C, immunomodulatory effects of differently terminated SiC-based USNPs were assessed. NPs made out of SiC with average diameter of approx. 4 nm were prepared with three different surface terminations; SiC-x NPs called as prepared, which had variety of oxygen species and a high concentration of carboxyl groups on their surface, SiC-OH NPs, which had portion of the carboxyl groups substituted for –OH groups and SiC-NH_2 NPs where the –OH terminations were once again substituted for amine groups. These particles exhibited great colloidal stability not only in water, as their original deposition milieu, but also in the cell culture medium and even in medium supplemented with FBS (Figure 2 in Publication C). This is a remarkable property not often seen for NPs, as protein interactions usually lead to their agglomeration and increase in zeta potential (key parameter showing NPs colloidal stability).

The prepared NPs were cultured in rising concentrations (25, 50 and 100 μg/ml) with SAOS-2 cells, monocytic THP-1 and macrophage-like (MF) THP-1 for 6 and 24 hours (Figure 3 in Publication C). The influence of protein supplementation was also included as a variable. The results showed that no matter the surface termination and incubation conditions, SiC-based USNPs are inert in respect to SAOS-2 cell line. However, highly interesting results were obtained for both of the immune cell types. MF cells responded by a decrease of the metabolic activity only to SiC-x NPs after 24 hours

in the medium with FBS, whereas the in serum-free medium, all of the NPs caused significant cytotoxicity after 6 hours, which continued to exhibit in concentration-dependent manner even after 24 hours with SiC-x and SiC-OH, but not SiC-NH_2.

The most interesting results were obtained from monocytic THP-1 cells. Under both conditions, the cells showed only a slight response to all NPs after 6 hours. However, after 24 hours three completely different responses were obtained, especially with the highest concentration (i.e. 100 μg/ml) of NPs. SiC-x NPs exhibited strong metabolic activity inhibition, SiC-OH NPs retained inert behavior and metabolic activity was at the same level as the control, while SiC-NH_2 NPs resulted in significant metabolic activation of cells. Based on these results and the presumption that the metabolic activity test employed (i.e. MTS) is closely connected to mitochondrial dehydrogenase activity, determination of mitochondrial mass and membrane potential after 24 hours in the serum-free medium was employed (Figure 4 in Publication C). Mitochondrial mass remained unchanged in all SiC-based NPs treated cells. A mitochondrial potential determination showed that the decrease of metabolic activity in SiC-x treated cells was connected to the decrease in mitochondrial membrane potential. SiC-OH treated cells, which seemed similar to control cells in respect to the metabolic activity retained also the same mitochondrial membrane potential. Surprisingly, SiC-NH_2 treated cells which showed significant increase of metabolic activity (200 % of the control cells) had the mitochondrial potential at the same level as the SiC-x treated cells.

These interesting results showing the influence of SiC-based NPs on immune cells were followed by determination of cytokine production of these cells, in response to SiC-NPs stimulation. All of the particles resulted in increased production of IL-8, GRO-α and RANTES pro-inflammatory cytokines, copying the profile of LPS stimulated cells as inflammatory positive control (Figure 5 in Publication C) while at significantly lower levels.

No significant changes in morphology were observed after the short term (24 hours) incubation. In order to assess the possible influence of SiC-based NPs on differentiation potential of monocytic THP-1 cells, long term cultivation of 7 days (Figure 6 in Publication C) was performed. SiC-x NPs, as predicted from observed metabolic inhibition after 24 hours resulted in nearly no living cells after 7 days. SiC-OH on the other hand resulted in interesting mixture of morphologies of monocytic cells, MF and

even DC. SiC-NH_2 NPs after 7 days resulted in increase of cell number with significant number of MF morphology.

This work comprehensively described the potential immunomodulatory effect of SiC-based USNPs with different terminations. The surface termination herein proved to be of extreme significance from biological point of view. The immunomodulatory potential of these NPs deserves to be studied in more detail as a rising opportunity for their application.

6.2.2. Unpublished data

Influence of SiC-x NPs on Metabolic Activity of Human Keratinocytes and hMSC Cells

In order to test if SiC-based NPs alter metabolic activity selectively in immune cells (represented by THP-1 cell line) as suggested in Publication C, influence of SiC-x NPs was tested on two keratinocyte cell lines – HaCaT (representing non-cancerous cells) and A431 (representing cancerous cells) cells. In order to assess influence of these NPs in respect to primary cells, metabolic activity of human mesenchymal stem cells (hMSC) changes after the treatment with SiC-x NPs was tested. All the cell types were incubated with gradually increasing concentrations of SiC-x in the medium with 5% FBS for 24 hours. The results showed some slight statistically significant decrease in the metabolic

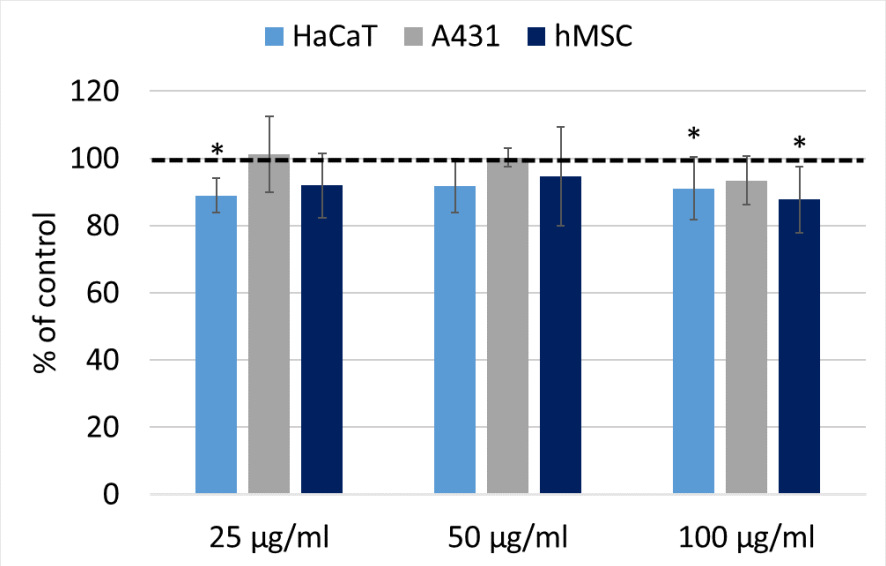

Figure 7: Metabolic activity of human keratinocytes (HaCaT and A431) and primary human mesenchymal stem cells (hMSC) after incubation with increasing concentrations of SiC-x for 24 hours in medium with 5% FBS. Dashed line shows 100 %, asterisk marks statistically significant results ($p < 0.05$)

activity of HaCaT (with 25 µg/ml and 100 µg/ml) and hMSC (100 µg/ml), but such reduction (to approx. 85 % of control levels) should not be considered as biologically significant (Fig. 7).

Doubling Time of THP-1 Cells after Treatment with SiC-based NPs

In order to establish the influence of different SiC-based NPs on ability of THP-1 cells to proliferate, doubling time was established. Doubling time represents a number of hours that the cells need to double their number. As seen in Figure 8 SiC-NH_2 NPs shorten doubling time of THP-1 cells to 28 hours, whereas SiC-x NPs prolong their proliferation to 51 hours. SiC-OH NPs retain approx. the same doubling time as control cells. Thus, it can be concluded that the surface termination of SiC-based NPs has determinant effect on THP-1 cell proliferation.

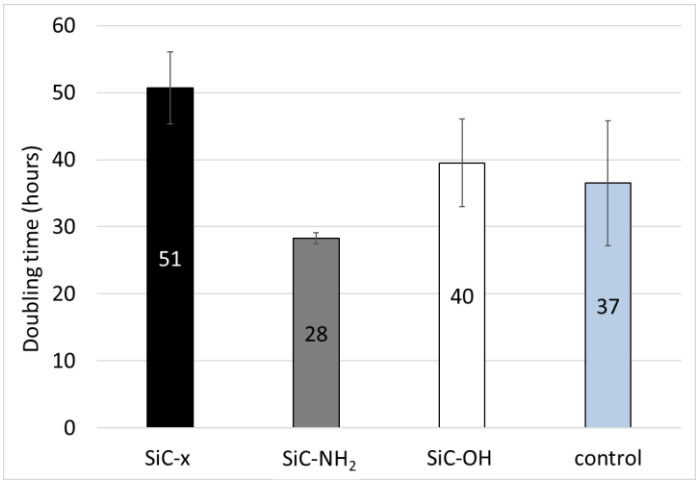

Figure 8: Doubling time of THP-1 cells after treatment SiC-based NPs. The cells were treated by 100 µg/ml of SiC-based NPs in DMEM medium with 5 % FBS for 4, 24 and 48 hours.

Metabolism Dependence of THP-1 Cells Based on SiC-based NPs Influence

As Publication C suggested, the observed metabolic activity stimulation in THP-1 monocytic cells was most probably not connected with strictly mitochondrial dehydrogenases. To assess changes in the metabolism of THP-1 monocytic cells, Seahorse ATP production rate analysis was employed. In this assay OCR (oxygen consumption rate) and ECAR (extracellular acidification rate) basal values are assessed and furtherly ATP production from OXPHOS and glycolysis is determined. After basal values are measured, injection of oligomycin is employed which leads to partial mitochondrial ATP synthesis inhibition (significant reduction of electron flow).

Subsequent complete inhibition of mitochondrial respiration is then achieved by injection of rotenone/antimycin A mixture. From the acquired ECAR and OCR data glycolytic and oxidative ATP production is calculated. The obtained results showed interesting shifts in ATP production (Fig. 9B). Control cells rely predominantly (59.1 %) on OXPHOS for ATP ptoduction. The treatment of cells with 100 µg/ml SiC-x NPs shifts the metabolism even more towards OXPHOS-dependent one (70.1 %). These cells previously showed significant decrease in metabolic activity (Fig. 9A). The SiC-OH and SiC-NH_2 treated cells showed shift from OXPHOS to slightly more glycolytic metabolism (46.9 and 51.4 % ATP produced by glycolysis respectively).

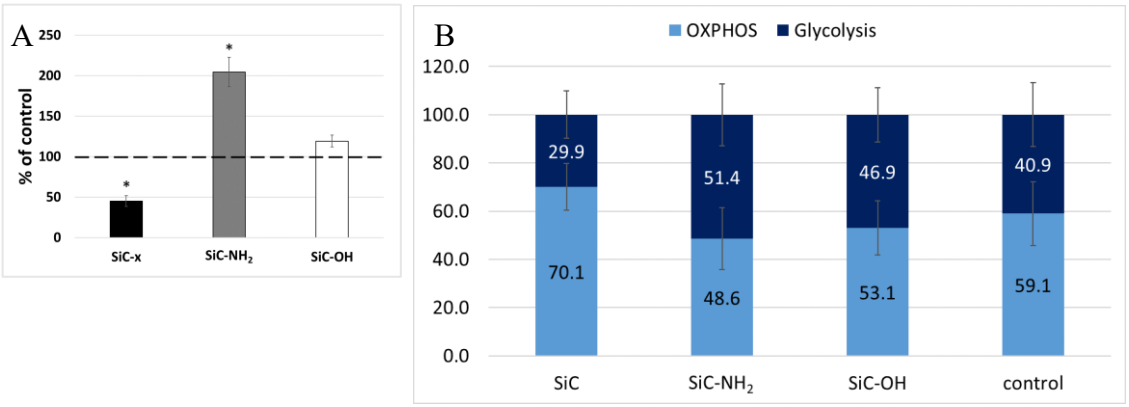

Figure 9: ATP production distribution between glycolysis and OXPHOS. The cells were treated by 100 µg/ml of SiC-based NPs for 24 hours in serum-free medium, their metabolic activity (A, Fig. 4 in Publication C) and glycolysis/OXPHOS ATP production (B) were measured.

Production of Exosomes from THP-1 Cells Stimulated by SiC-x NPs

Exosomes are one of the key mechanisms used by cells to communicate with each other. Usually, exosomes are small vesicles (30 – 100 nm) containing various signaling molecules or small RNA fragments. They proved to be particularly interesting in modulating the response of both, adaptive and innate immune system. Thus, a pilot test of SiC-based NPs influence on exosomal secretion was conducted on THP-1 cells to deeper study the potential immunomodulatory effects of these NPs.

The cells were incubated with 100 µg/ml of SiC-x NPs for 24 hours in the medium without FBS. As this was a pilot study, only SiC-x NPs were used, as the most consistent results were obtained from other methods with these NPs. The results showed that SiC-x treated cells produce significantly (by two orders) more exosomes than untreated control

cells (Fig. 10B and 10A, respectively). After 6 hours of incubation, FBS containing exosomes was added to the cultivation medium, thus the particles detected by NTA analysis could be considered of FBS origin. Subsequent western blot analysis, however confirmed that the acquired vesicles are truly exosomes by staining against human CD81, which is typically enriched in exosomal membrane (Fig. 10C). However, no significant difference in signal strength was detected and thus the difference in number of extracellular vesicles detected by NTA could not be correlated to exosome count.

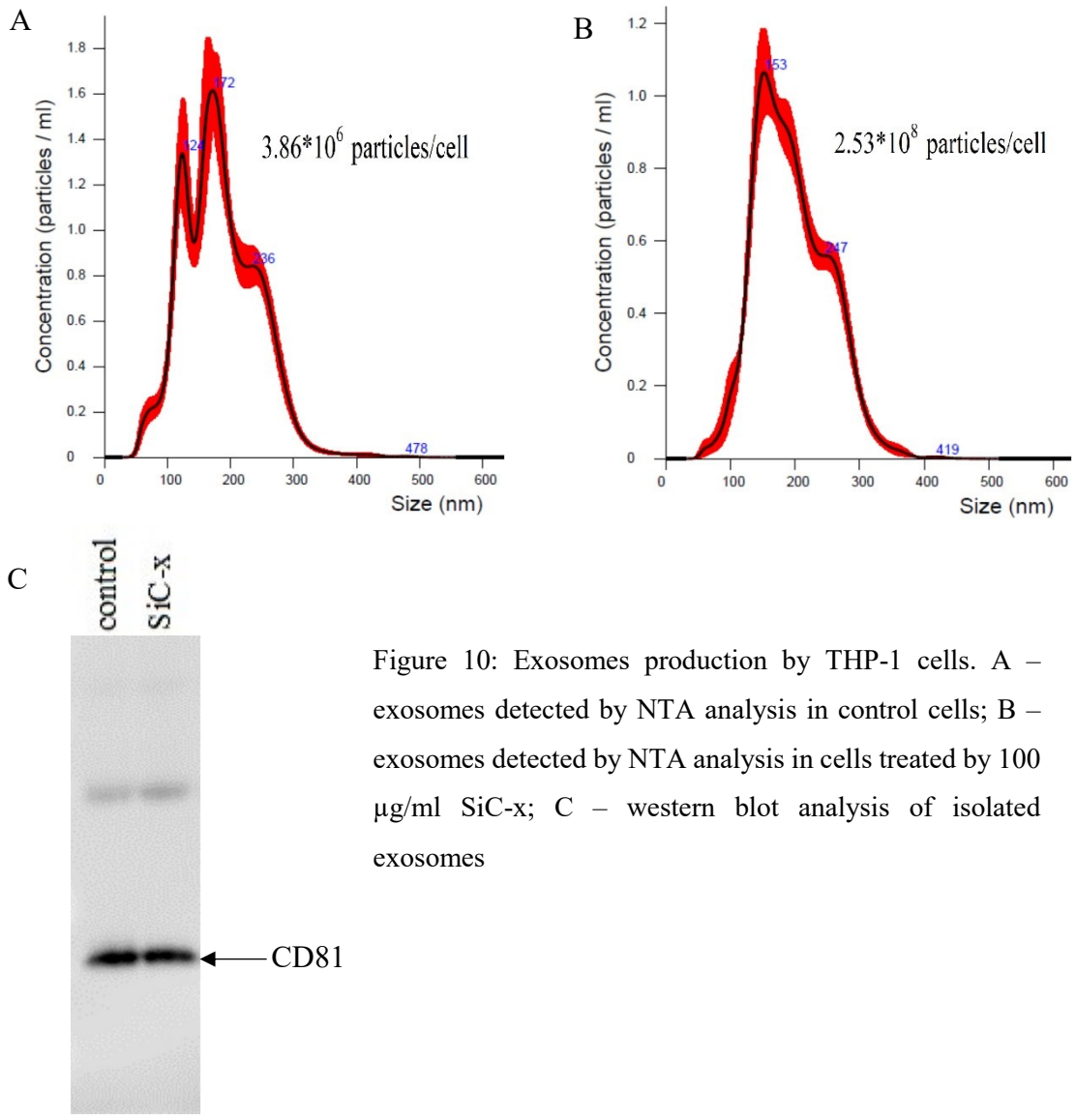

Figure 10: Exosomes production by THP-1 cells. A – exosomes detected by NTA analysis in control cells; B – exosomes detected by NTA analysis in cells treated by 100 µg/ml SiC-x; C – western blot analysis of isolated exosomes

Detection of SiC-x NPs in SAOS-2 Cells by Cryo-TOF-SIMS FIB SEM Microscopy

The SiC-based USNPs described above suffered from high fluorescence signal quenching after administration to cell-culture medium, thus making them hard to detect and establish if they are inside cells using fluorescence-based microscopic techniques.

Silicon and carbon are both not particularly electron dense materials that could be positively distinguished from cellular background by the means of standard or even high resolution TEM. Thus, in search for adequate imaging technique a cooperation with Czech technological company Tescan was established. Their unique cryoSEM microscope provided interesting results. The principle of the employed cryo-TOF-SIMS FIB SEM lies in a combination of FIB where focused beam of high-energy ions is systematically etching and milling the sample observed by SEM and TOF-SIMS directly detects the elemental composition of the milled area. Retrospective software reconstruction then theoretically provides precise map of element composition of the original sample.

The method seemed highly promising in respect to mapping of SiC-x presence inside the cells on nearly molecular level, however proved to be unpredictable. Samples were pre-cultured in Prague and then transferred to Brno. There the cells were kept in an incubator to adjust after the transfer for 4 hours and furtherly processed. Only after the whole measurement was finished, an issue was observed as nearly no cells were detectable on control grids and thus background for Si presence in the cells could not be established properly (Fig. 11). The reason for the lack of cells on control grids is unknown, however it might have been caused by the transport-related stress or unwary

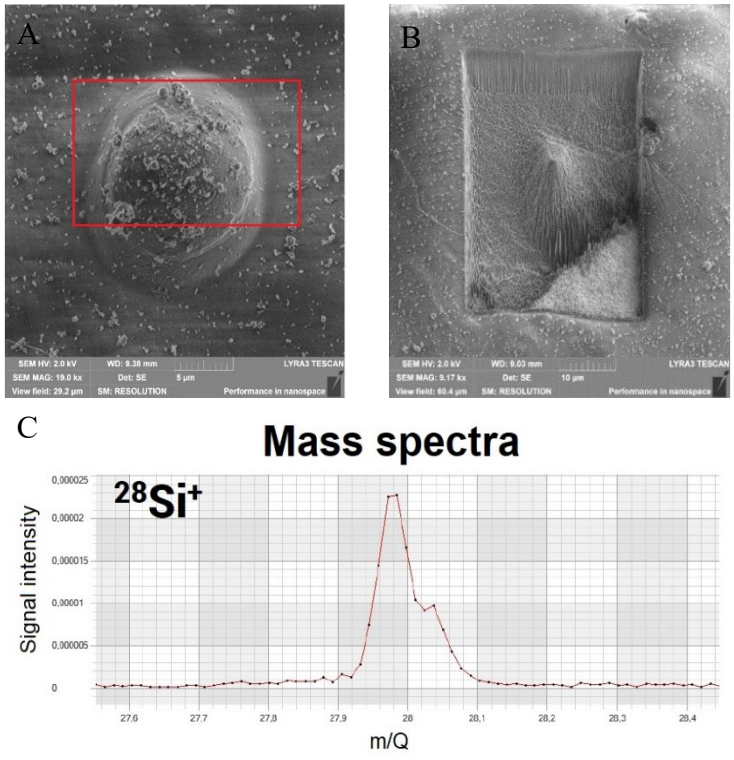

Figure 11: SEM images and spectral analysis of SiC-x treated cells by cryo-TOF-SIMS FIB SEM microscopy. SEM image of cell prior FIB-SEM (A) and after (B). Mass spectra of cell area marked by red rectangle (C).

handling of the grids. The results of measured control grid can be found in supplementary data (Fig.18 in *Section 9*). Contrary to control, the samples containing SiC-x NPs were still nicely covered with cells and Si was detected in milled area (Fig. 11). However, the Si concentration was almost at noise level.

6.3. Interactions of Gold Nanoparticles with Cells

6.3.1. Published Data (Publication D)

Publication D: Reznickova, A., N. Slavikova, Z. Kolska, K. Kolarova, **T. Belinova**, M. Hubalek Kalbacova, M. Cieslar, and V. Svorcik. "**PEGylated Gold Nanoparticles: Stability, Cytotoxicity and Antibacterial Activity**."

The research presented in above-mentioned publication was mainly focused on determination of the preparation and characterization of gold USNPs conducted by laboratory of dr. Řezníčková. AuNPs as mentioned before have a huge potential in biomedical applications, especially in imaging and possibly also in photo-thermal therapy. Metal NPs are commonly prepared by several methods, one of which is direct sputtering onto a surface or into a fluid, creating either modified surface or NPs solution, respectively. In order to lessen the interactions of NPs with each other or with other biomolecules (and thus the formation of clusters or PC respectively), NPs can be directly prepared into solutions of stabilizing molecules. Most commonly used, and also FDA approved, stabilizing agent for NPs is PEG. Herein, three types of PEG were employed for direct AuNPs deposition – pure PEG, amine-terminated (-NH_2) and thiol-terminated (-SH), differing in their properties (e.g. colloidal stability, size of polymer).

The results showed that direct sputtering of Au into the three types of PEG solution produced NPs with narrow size distribution of 1-6 nm in diameter, with the best homogeneity achieved by deposition into thiol-terminated PEG (1-3 nm). Such small structures, however resulted in loss of surface plasmon resonance and related absorption. All of the AuNPs proved to be thermo-stable and also retain their dispersibility and size distribution in time (up to 14 days after sputtering). After broad characterization of AuNPs deposited in different PEG solutions, their cytotoxicity was assessed on SAOS-2 cells. The cells were cultured with AuNPs for 24 hours and then their metabolic activity was determined (Fig. 7 in Publication D). From the results, it is obvious that AuNPs deposited in PEG-SH solution are the most bio-compatible option, as even the highest

used concentration of NPs (14 mg/l) did not result in cytotoxic effect on cells. The other two AuNPs (AuNP-PEG and AuNP-PEG-NH_2) resulted in significantly decreased cell metabolic activity and their overall bad shape was also confirmed by light microscopy (Fig. 8 in Publication D).

Overall, the result of research conducted for this publication showed, that USNPs of gold deposited into thiol-terminated PEG have superior properties to the ones deposited in pure PEG or amine-terminated PEG. Direct deposition for 900 sec provides sufficiently dense colloid, while retaining great thermal-stability, narrow size distribution and dispersibility in short- and long-term storage. These NPs also proved to be the least cytotoxic and thus most biocompatible in respect to osteoblastic cells and also showed mild antibacterial activity, which however can be neglected.

6.3.2. Unpublished data

Influence of FBS Supplementation of Medium on Metabolic Activity of SAOS-2 cells with AuNP-PEG-SH

In order to test influence of FBS supplementation (and thus PC formation) osteoblastic SAOS-2 cells were cultured with rising concentrations of AuNP-PEG-SH in the DMEM medium either with 5 % FBS or serum-free for 24 hours (Fig. 12). The results showed that the presence of FBS in the culture media within the first 6 hours of incubation is crucial. In the medium with 5 % FBS, the cells decreased metabolic activity slightly under the level of the control cells. The cells incubated with NPs in the serum-free medium increased their metabolic activity with increasing concentration of AuNP-PEG-

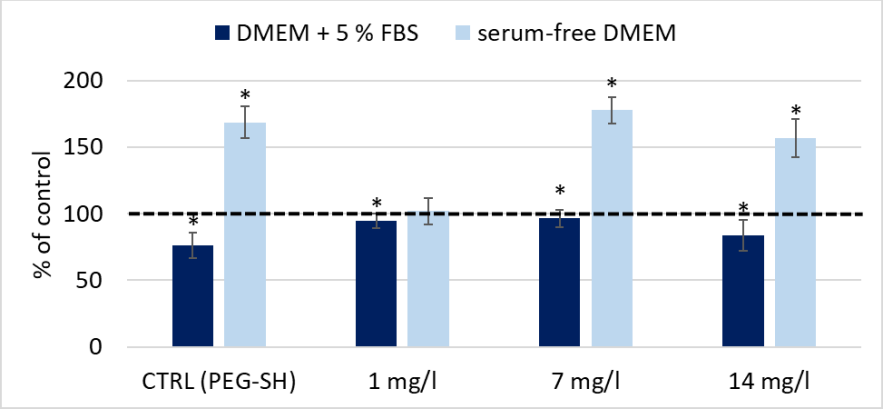

Figure 12: Metabolic activity of SAOS-2 cells treated with AuNP-PEG-SH. Cells were treated with rising (1, 7 and 14 mg/l) concentration of AuNP-PEG-SH in DMEM with 5% FBS or serum-free DMEM for 24 hours. Dashed line shows 100 %, asterisk represents statistical significant change ($p>0.05$)

SH. In order to test if the observed influence is caused by NPs or PEG-SH in which the NPs were deposited, PEG-SH treated control was employed (CTRL (PEG-SH) in Fig. 14). This control was achieved by addition (volume-vise) of the same amount of pure PEG-SH without NPs as in the highest concentration of NPs (i.e. 14 mg/l). It can be concluded that the effects observed under both conditions are more likely connected with PEG-SH acting as influencer than the AuNPs deposited in it.

Mass Spectrometry Analysis of PC formed on AuNP-PEG

Mass spectrometry analysis of PC formed in DMEM medium with 5% FBS on AuNP-PEG and AuNP-PEG-SH was performed. While samples were prepared for both, AuNP-PEG and AuNP-PEG-SH, detectable pellet containing AuNPs was acquired only for AuNP-PEG. No observable pellet and thus sample was acquired from AuNP-PEG-SH and thus no analysis was performed with it. After throughout analysis of protein adsorbed on AuNP-PEG, 39 proteins originating from FBS have been detected (Tab. 1). All the proteins identified to associate with the NPs have origin in plasma (i.e. FBS) and are somehow connected either to serum complement activation (main innate immune system enhancing immune response; complement component C3, complement C1Q subunit C, complement component C1q, alpha-2-antiplasmin) or play significant role in cytoskeletal formation and cellular adhesion (vitronectin, albumin, talin etc.). Detailed function of each protein can be found in Table 2A and 2B (*Section 9*).

Accession	Name	Accession	Name
Proteins with cholesterol transfer, heparin and lipase binding and low-density lipoprotein (LDL) particle receptor binding activity		**Proteins with hemostatic role in plasma**	
E1BNR0	Apolipoprotein B	F1MSZ6	Antithrombin-III
Q03247	Apolipoprotein E	P02081	Hemoglobin fetal subunit beta
P15497	Apolipoprotein A-I	P01966	Hemoglobin subunit alpha
Proteins associated with hyaluronan metabolic processes		Q9N2I2	Plasma serine protease inhibitor
F1MNW4	Inter-alpha-trypsin inhibitor heavy chain H2	P02769	Albumin
Q0VCM5	Inter-alpha-trypsin inhibitor heavy chain H1	**Proteins associated with immune system function**	
Q3T052	Inter-alpha-trypsin inhibitor heavy chain H4	Q2UVX4	Complement C3
Proteins with cytoskelet and adhesion associated function		P12763	Alpha-2-HS-glycoprotein
Q28178	Thrombospondin-1	Q1RMH5	C1QC protein
M0QVY0	Intermediate filament rod domain-containing protein	Q5E9E3	Complement C1q subcomponent subunit A
P06394	Keratin, type I cytoskeletal 10	P28800	Alpha-2-antiplasmin
Q3ZBS7	Vitronectin	E1BH06	Uncharacterized protein
A0A140T8C8	Kininogen-1	**Proteins with various proteinase and inhibitory activity**	
Q5XQN5	Keratin, type II cytoskeletal 5	Q7SIH1	Alpha-2-macroglobulin
F1MDH3	Talin 1	A6QPP2	SERPIND1 protein
P63261	Actin, cytoplasmic 2	P00760	Cationic trypsin
F1MC11	Keratin, type I cytoskeletal 14	P34955	Alpha-1-antiproteinase
G3MZ71	Keratin 2	**Proteins associated with cellular metabolism**	
Q3SX14	Gelsolin	Q3MHL4	Adenosylhomocysteinase
P08728	Keratin, type I cytoskeletal 19	P10096	Glyceraldehyde-3-phosphate dehydrogenase
A1L595	REVERSED Keratin, type I cytoskeletal 17	A5D984	Pyruvate kinase
G3N0V2	Keratin 1	P19858	L-lactate dehydrogenase A chain

Table 1: Mass spectrometry analysis of proteins on AuNP-PEG nanoparticles. All proteins originate from *Bos Taurus*.

Furthermore, SDS-PAGE electrophoresis was conducted from each washing step (Fig. 16, line number 1-5) and 15 µl of final pellet (Fig.13, line P). The gel electrophoresis demonstrated washing of extra FBS proteins not tightly associated with NPs. The gel electrophoresis of the acquired pellet also showed, that sufficient (detectable) amount of proteins is bound to AuNP-PEG to be detectable by this method.

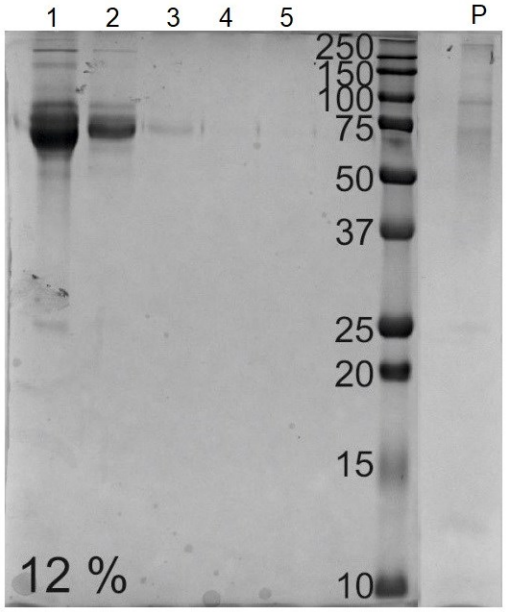

Figure 13: SDS-PAGE gel of AuNP-PEG. Numbers mark supernatant sample from corresponding washing step. P marks 15 µl of dissolved final pellet of AuNP-PEG.

Transmission Electron Microscopy of AuNP-PEG-SH in SAOS-2 Cells

The osteoblastic SAOS-2 cells were cultured with 14 mg/l of AuNP-PEG-SH for 24 hours in the medium supplemented with 5 % FBS and subsequently subjected to analysis by TEM in order to assess their intracellular localization. After throughout analysis of the sample, precisely distinguishable structures with high electron density were located both, inside of cells (Fig. 14) and in vesicle outside of cell (Fig. 15). One can only speculate the origin of both vesicles, however it can be concluded that these NPs in FBS supplemented medium undergo vesicle-related trafficking and are not diffusely distributed in cytoplasm.

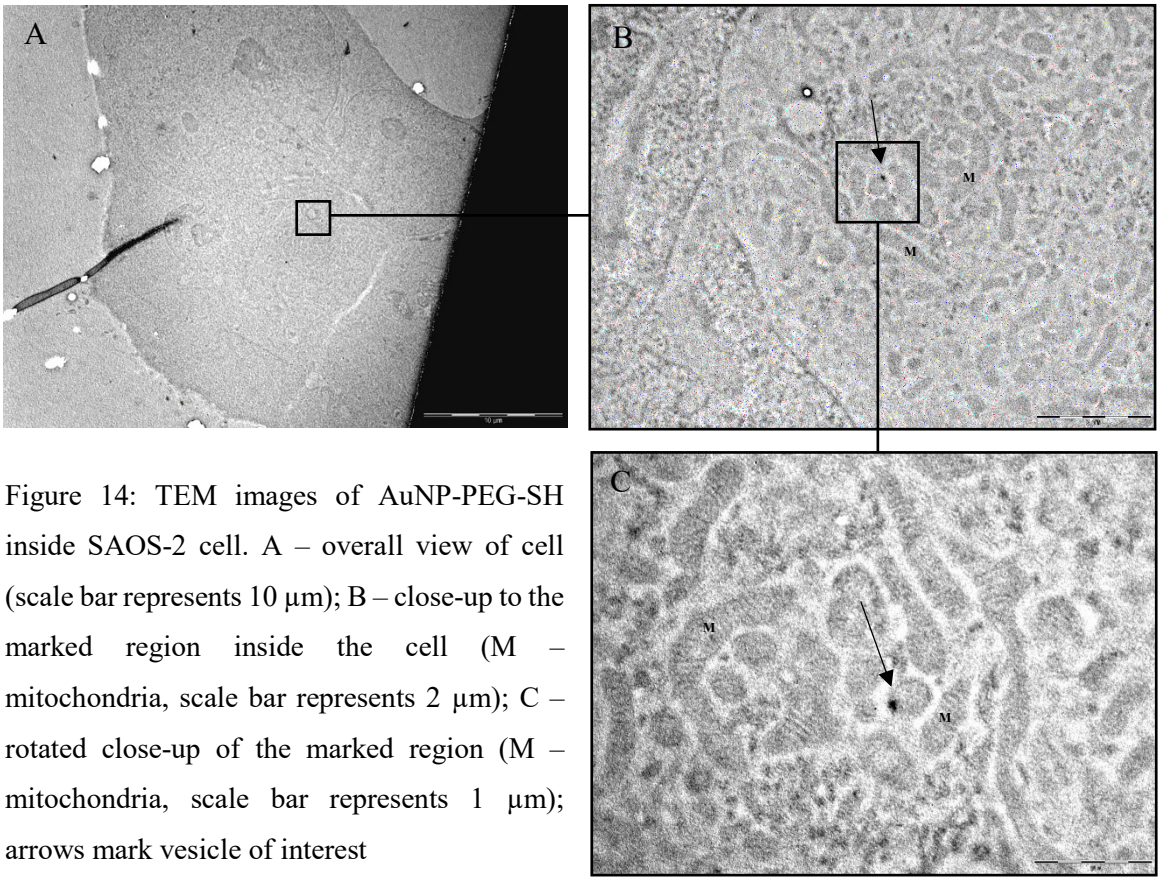

Figure 14: TEM images of AuNP-PEG-SH inside SAOS-2 cell. A – overall view of cell (scale bar represents 10 µm); B – close-up to the marked region inside the cell (M – mitochondria, scale bar represents 2 µm); C – rotated close-up of the marked region (M – mitochondria, scale bar represents 1 µm); arrows mark vesicle of interest

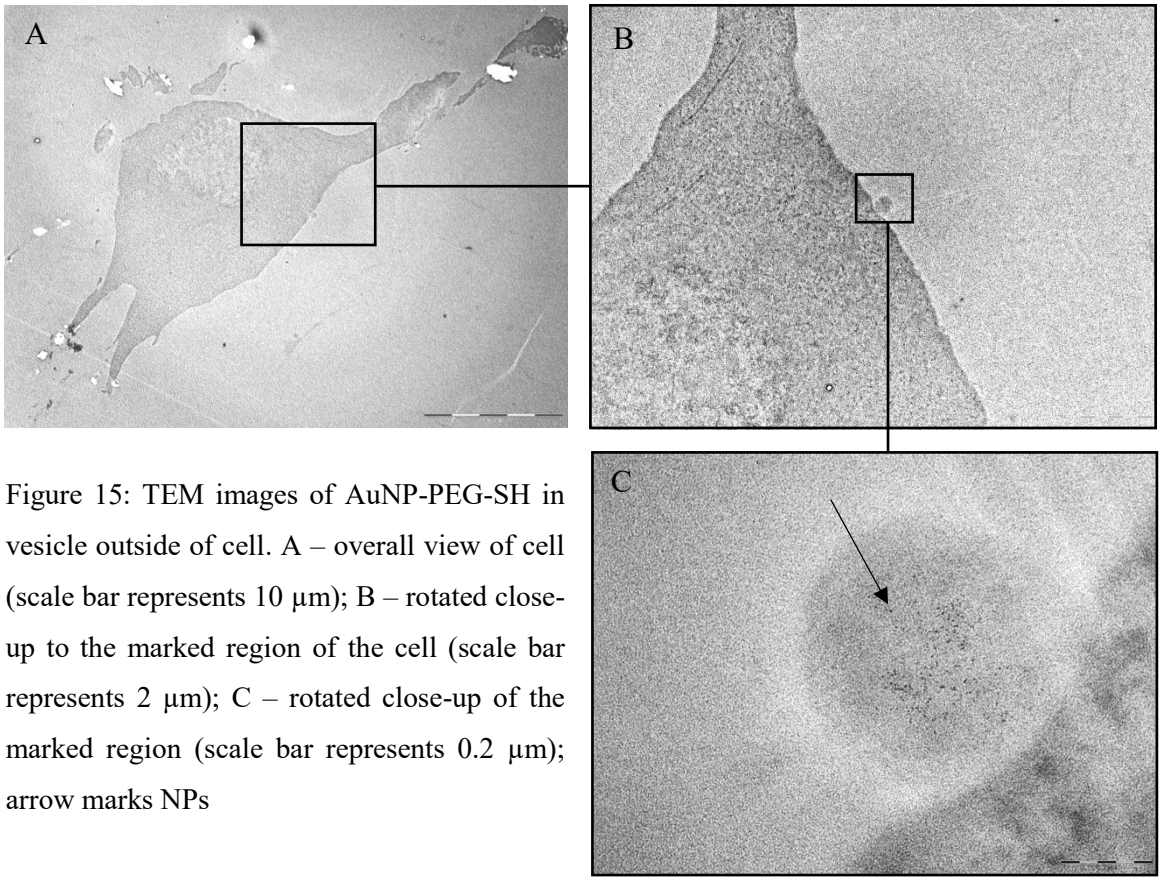

Figure 15: TEM images of AuNP-PEG-SH in vesicle outside of cell. A – overall view of cell (scale bar represents 10 µm); B – rotated close-up to the marked region of the cell (scale bar represents 2 µm); C – rotated close-up of the marked region (scale bar represents 0.2 µm); arrow marks NPs

Raman Spectroscopic Imaging of AuNP-PEG-SH in SAOS-2 Cells

Even though the loss of a distinct extinction peak related to the surface plasmon resonance related absorbance peak of AuNPs after functionalization PEG was reported in Publication D, the possibility to employ Raman spectroscopy and surface enhanced Raman scattering (SERS) for thiol-terminated PEG functionalized AuNPs was tested. The cells were incubated with 14 mg/l of NPs for 24 hours in FBS supplemented medium and subsequently Raman maps cell cytoplasm (lateral *xy*-scan in the equatorial plane of the cell) cross section were recorded. No significant spectral difference was observed between the control sample and AuNP-treated cells. Thus the negative consequences of the disappearance of SERS predicted in Publication D were confirmed. Even though no signs of SERS mechanism either Raman confirmation of the presence of AuNP-PEG-SH in the cells were obtained, the acquired Raman maps were analyzed and presented herein in order to demonstrate analytical possibilities of Raman microscopy for bio-imaging of cells. The True Component Analysis applied for acquired maps analysis is a multivariate method considering spectral differences throughout the spectral region used for the analysis. If the chemical composition of the object is a homogeneous mixture of several components in the relative ratio one to another, only a single spectral component is found, regardless of the fluctuations of the total amount of the homogeneous mixture. However, if the ratio between various components (chemical species) is not constant, the algorithm reveals regions with different compositions and provides characteristic Raman spectra from which one can deduce corresponding spectral differences. Thus, the analysis applied to Raman maps revealed only two distinct components differing in their Raman spectra. The components were called “Biomass A” (red spectra) and “Biomass B” (blue spectra) (Fig. 15A). The corresponding Raman maps (Fig. 15 D, E) show the spatial distribution of the respective components, *i.e.*, regions differing in their composition are highlighted. Furthermore, both components provided rather similar Raman spectra without spectral features which could be assigned to SERS or to Raman signal of functionalized AuNPs. The distinctive Raman signal observed in Fig. 15 E (Biomass B, the bottom part of the image) is most probably caused by some impurity (organic microparticle outside the cell) caught by an optical tweezer formed from the focused laser beam, and thus it has no biological relevancy.

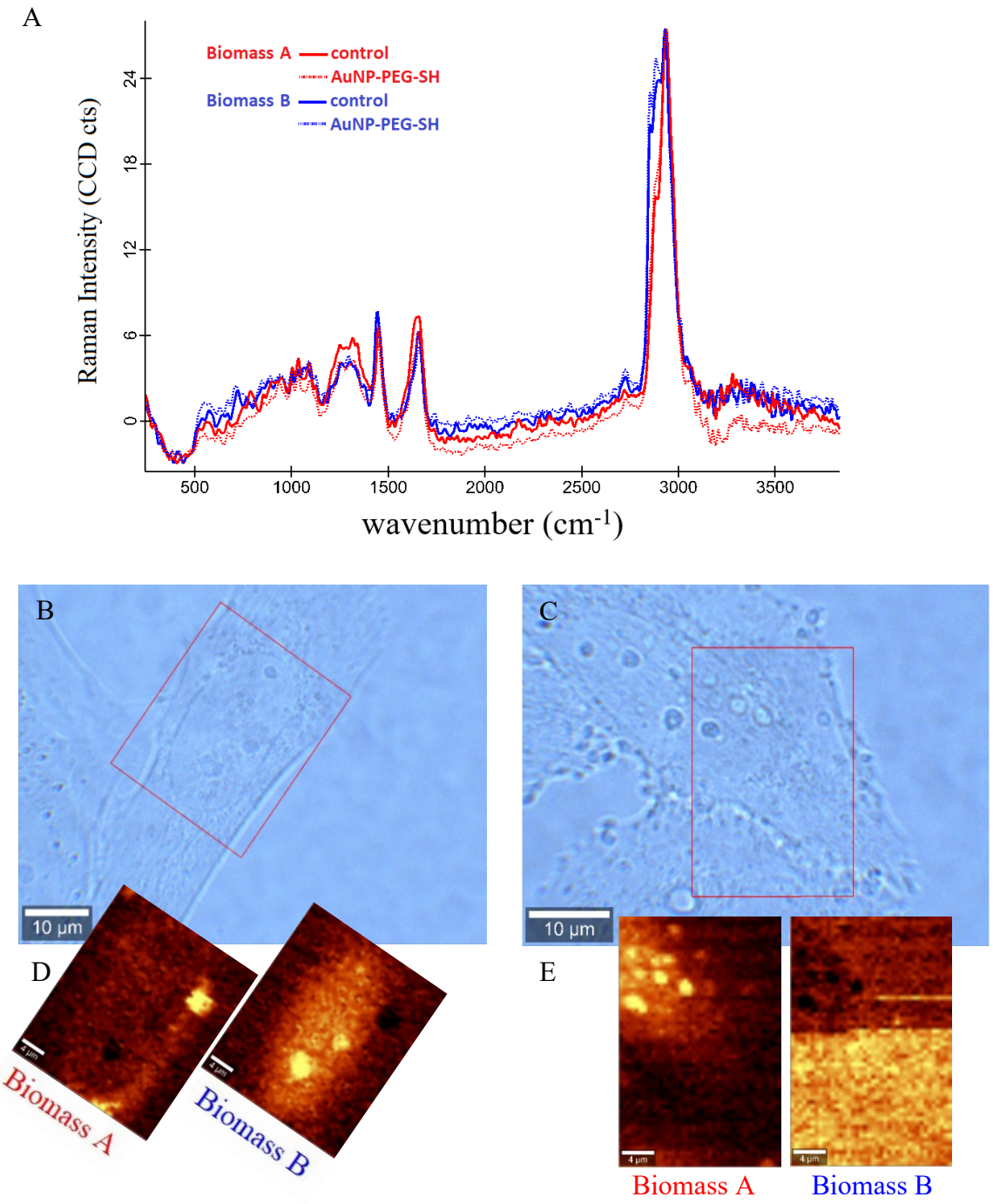

Figure 16: Raman imaging of SAOS-2 cells treated with AuNP-PEG-SH. A – Raman spectral components detected in the studied cells; control cells (solid line) and AuNP-PEG-SH treated cells (dashed line). B – microscopic image of control cells; C – microscopic image of AuNP-PEG-SH treated cells; red rectangles mark measured areas shown in panels D and E. Scale bar represents 10 µm; D, E – reconstructed Raman maps from each spectra of control (D) and AuNP-PEG-SH treated (E) cells. Scale bare represents 4 µm.

6.4. Nanodiamond Nanoparticles Interaction with Proteins and Human Cells

6.4.1. Published Data (Publication E)

Publication E: Machova, Iva, Martin Hubalek, **Tereza Belinova**, Anna Fucikova, Stepan Stehlik, Bohuslav Rezek, and Marie Hubalek Kalbacova. "**The Bio-Chemically Selective Interaction of Hydrogenated and Oxidized Ultra-Small Nanodiamonds with Proteins and Cells**."

In this research a comprehensive study of interactions of ultra-small DNDs with proteins from cultivating medium were broadly characterized and the relation with cells was also discussed. The NPs used herein were DNDs with 2 nm diameter and two different surface terminations; oxidized (O-) and hydrogenated (H-). The NPs themselves were already characterized within the prior studies (Stehlik et al. 2016; Stehlik et al. 2017). Thus, this work focused on composition of PC formed on DNDs and interactions of cells with these DNDs. The DNDs possess differing charges (negative for O-DNDs and positive for H-DNDs) and thus the differences in bound proteins were studied. The NPs were pre-cultured in the cultivation medium (i.e. DMEM) with or without supplementation with 5 % FBS and subsequently zeta potential (electrical charge determining colloidal stability of NPs) was assessed (Table 1 in Publication E). Interestingly, O-DNDs did not show significant shift of zeta potential and thus loss of colloidal stability after transition into DMEM media with or even without FBS. Contrary to this, positively charged H-DNDs shifted their zeta potential closer to 0 mV (approx. 4.9 mV) after transition into simple DMEM making them highly instable in colloids. With addition of FBS, the zeta potential of H-DNDs shifted even to negative charge (- 18.7 mV). Thus these results suggested formation of PC and also H-DND-protein aggregates. The PC formed on such small structures is hardly PC *sensu stricto*, however the composition of protein network formed around both DNDs was analyzed in respect to qualitative and quantitative extent of proteins (Figure 2 and 3 and Table 2 in Publication E). Surprisingly, large amount of proteins was found to be associated with both DNDs (approx. 164 and 173 for H-DNDs and O-DNDs, respectively). Their quantitative analysis furtherly showed that 26 proteins were specific with high fold change for O-DNDs and 12 proteins for H-DNDs. Vast majority of the enriched protein on both DNDs types was smaller than 100 kDa. Charge-vise predominantly negatively charged proteins

were bound to originally positive H-DNDs and conversely, majority of proteins bound to negatively charged O-DNDs were positive.

The PC impact was also assessed in respect to metabolic activity of SAOS-2 cells. The cells were cultured with the increasing concentration (5, 10, 25, 50 and 100 μg/ml) of each DNDs in FBS supplemented and serum-free medium for 6 and 24 hours (Figure 4 in Publication E). O-DNDs exhibited cytotoxic effect on cells only after 24 hours in the serum-free medium. H-DNDs, on the other hand, showed significant dose-dependent cytotoxicity under both conditions and even after shorter time (6 hours). These results showing influence of DNDs on metabolic activity were also accompanied by SEM images, showing cellular morphology and surrounding NPs (Figure 5 in Publication E). Formation of dense aggregates of NPs with proteins was observed with both DNDs. Obvious difference was clearly visible in the size and position of DNDs clusters. O-DNDs formed smaller and more evenly distributed clusters, whereas H-DNDs resulted in larger clusters predominantly covering entire cellular surface.

7. Discussion

7.1. Interactions of Silicon Quantum Dots with Human Cells

The obtained results from SiQDs experiments showed the importance of serum supplementation as a mediator of possible PC formation. This decisive feature was not only of significant importance in respect to cellular metabolic activity and subsequent cytotoxicity of NPs in different types of human cells, but especially important for intracellular localization of the SiQDs and also the detected signal intensity.

It has been long known that the presence of PC can significantly affect uptake of NPs (Lesniak et al. 2012; Lesniak et al. 2013; Saikia et al. 2016). In the Publication A, it was shown that SiQDs 1050 tend to form huge aggregates and lose fluorescence in the cultivation medium, both with and without FBS and thus these NPs were not studied furtherly. On the other hand, SiQDs 1100 showed a nice signal localized in the cells in vesicle-like structures (in medium with 5 % FBS) or a diffused signal most probably originating from cytoplasm (in serum-free medium). It might be speculated that with the presence of PC, SiQDs form aggregates that are recognized by specific receptors associated with endocytic mechanisms and subsequently locates the NPs into (possibly) endosomal vesicles. This presumption had been tested and partially confirmed by Lucie Vrabcova in her PhD thesis, where co-localization studies of SiQD 1100 with endosomal structures with subsequent advanced image analysis were conducted (Section 6.3.1. in (Vrabcova 2019)). The results of co-localization studies showed that the NPs signal co-localizes with late endosomes after 1 hour of incubation in FBS containing medium and with lysosomes after 24 hours. In contrast to FBS containing medium, the absence of the serum proteins (and thus no PC) resulted in diffuse signal of SiQDs 1100, not centralized into vesicles, thus suggesting that the NPs crossed the membrane without endocytosis employment. Such transition through membrane without inducing extreme toxicity was already speculated before (Nakamura et al. 2019).

Furthermore, interesting influence of FBS supplementation on SiQDs fluorescence intensity was observed in the Publication A. In the presence of serum, and thus PC, the signal from NPs was less bright than under the serum-free conditions. A similar signal decrease was detected even by sensitive detectors of fluorescent cytometer (Fig.5 and 6). In case of the cells treated with SiQDs 1100 in the presence of FBS for 2 hours, only approx. 17 % of cells showed fluorescence related to NPs presence. After the same

incubation time, cells treated with SiQDs in the medium without serum (and thus PC) approx. 98 % of the cells showed NPs-related fluorescence. The lack of signal in the presence of FBS might be explained in two ways. Firstly, it is possible that in the short time employed (i.e. 2 hours), not enough particles were internalized by the cells to allow for their detection. Endocytic mechanisms are known to act in the order of minutes whereas direct diffusion or penetration of NPs may happen almost immediately (Watanabe and Boucrot 2017; Taylor, Perrais, and Merrifield 2011). It can be suggested that after longer times, SiQDs accumulate in cells and thus are more detectable as proposed with different types of NPs (Lammel et al. 2019). The accumulation would also imply that the NPs do not leave the cell and remain inside. Secondly, the lower fluorescence intensity might be explained by the formation of PC. It is known that fluorescence signal can be quenched by so called static quenching. This effect is observed when, prior to excitation, the fluorescent probe comes in close contact with substance that has absorption spectrum closely resembling the excitation wavelength of the probe. In that case, the excitation wavelength is absorbed by the substance (i.e. PC) and the probe (i.e. SiQDs) lose their quantum yield. In order to test this second hypothesis, our colleagues from Japan tested differences in quantum yield of SiQD 1100 in the different media (McCoy's 5 A and DMEM) with and without FBS. The results surprisingly showed, that the quenching is not caused by FBS, but by the culture media itself (Fig. 17). Thus, it can be concluded that the medium is responsible for the signal quenching and FBS presence only increases this effect.

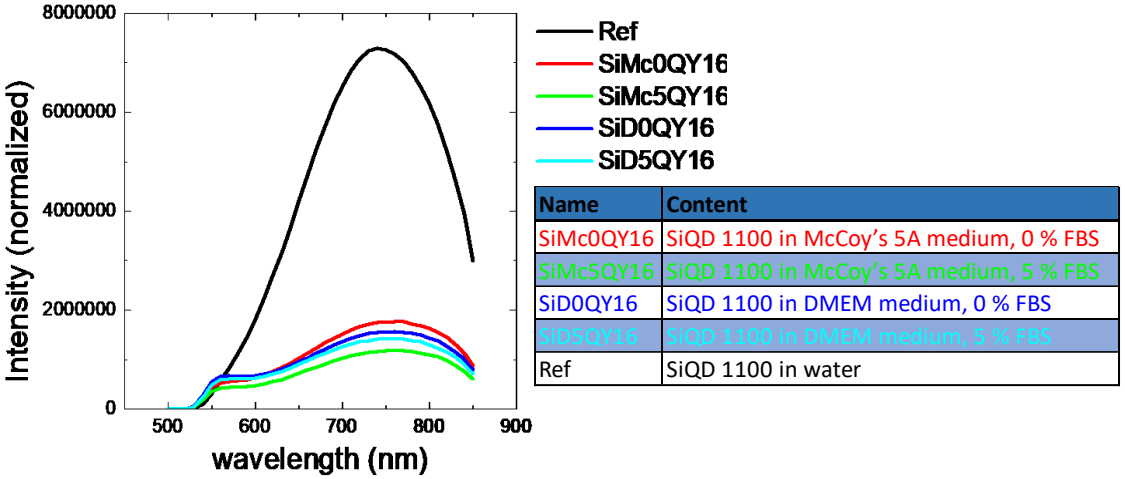

Name	Content
SiMc0QY16	SiQD 1100 in McCoy's 5A medium, 0 % FBS
SiMc5QY16	SiQD 1100 in McCoy's 5A medium, 5 % FBS
SiD0QY16	SiQD 1100 in DMEM medium, 0 % FBS
SiD5QY16	SiQD 1100 in DMEM medium, 5 % FBS
Ref	SiQD 1100 in water

Figure 17: Fluorescence intensity spectra of SiQD 1100 in different media. Data provided by Asuka Inoue, Hiroshi Sugimoto and Minoru Fuuji (Department of Electrical and Electronic Engineering, University of Kobe, Japan).

It must be pointed out that the used method (i.e. flow cytometry) has a huge limitation. The signal origin does not necessarily need to be from inside of the cell, it can also originate from SiQDs attached to cell membrane and thus the results must be interpreted with caution. In biology Trypan mlue stain is commonly used not only to discriminate between healthy and damaged cells (Trypan mlue does not enter cells with intact membrane) but also to eliminate surface-originating green fluorescence in flow cytometry by absorbing the energy of green light emmited by the fluorophore. Simmilar mechanism could be employed in case of SiQD 1100 and another, in biology widely used, stain – Methylen mlue. However, this hypothesis must be tested.

Results obtained from metabolic activity measurements of all tested cell types – osteoblastic SAOS-2 cells, primary human mesenchymal stem cells (hMSC) and two types of immune cells (monocytic and macrophage-like THP-1 cells), again stressed out the importance of PC. The obtained data showed that without FBS (and thus PC) all of the cells respond to the SiQD 1100 by decrease in their metabolic activity to the cytotoxic level (approx. 75 % of control). Such protective effect of PC formation on NPs toxicity have been already described (Wang et al. 2013).

In the Publication B, time-dependent decrease of metabolic activity of SAOS-2 cells was observed after treatment with 100 μg/ml of SiQD 1100, no matter the incubation conditions (i.e. with or without PC). The influence of the treatment on cellular morphology was observed by holographic live cell imaging. The live cell imaging showed that the cells undergo textbook example of apoptosis as soon as after approx. 3 hours when cultured with 100 μg/ml of SiQDs in FBS supplemented medium and thus it can be speculated that the same mechanism is employed even in serum-free medium. It has been reported that USNPs are capable of apoptosis induction in nutrition deprived cells (Kim et al. 2016). In the Publication B, decrease of metabolic activity was correlated to the levels of LDH detected in cell supernatant (and thus necrosis). LDH was detected only after longer cultivation time (i.e. 48 hours) and can be explained not by the NPs directly causing necrosis but by the phenomenon called secondary necrosis which occurs when apoptotic bodies are not eliminated by phagocytes and lose their integrity (Silva 2010; Fink and Cookson 2005).

7.2. Interactions of Silicon Carbide Nanoparticles with Human Cells

SiC-based NPs with different surface terminations showing decent colloidal stability in the biological media, even in the presence of proteins, showed to be especially interesting in respect to modulating immune cells behavior. Once again, the protective influence of PC was described with these NPs, as all toxic or stimulating effects were more obvious under the serum-free conditions. The metabolic activity data acquired for the Publication C suggested that monocytic THP-1 cells must be highly sensitive to surface termination of SiC-based NPs, as a reference cell line of osteoblastic SAOS-2 cells did not respond to any of the SiC-based NPs. In order to test specificity of SiC-x NPs towards immune cells, three other cell types – healthy and cancerous keratinocytes cell lines (HaCaT and A431, respectively) and primary human mesenchymal stem cells (hMSC) were also tested. The results showed that the SiC-x NPs cause significant harm only to monocytic THP-1 cells after 24 hours incubation (as seen in the Publication C). These cells are derived from acute monocytic leukemia and thus the observed selectivity of SiC-x NPs towards them might be of interest in respect of leukemia treatment. It has been shown that iron oxide nanoparticles, approved by the FDA for treatment of iron deficiency, can selectively kill acute myeloid leukemia cells (Trujillo-Alonso et al. 2019). However, more detailed research regarding precise mechanism of the observed effect is highly needed before any application can be proposed.

The various effects of the differently terminated SiC-based NPs on monocytic THP-1 cells led to deeper interest in what exactly is happening with the cells. The method used for detection of changes in the metabolic activity is dependent on the activity of cellular dehydrogenases and commonly misinterpreted to reflect mitochondrial activity. The assumption was, that higher metabolic activity means also higher mitochondrial potential, as presumably mitochondrial dehydrogenases are more active. This presumption led to deeper interest in actual mitochondrial state of cells after the treatment with the SiC-based NPs. The results, however revealed that completely opposite effect (i.e. lower mitochondrial potential) than presumed was observed in SiC-NH_2 treated cells. It has been shown that changes in mitochondrial potential do not necessarily reflect changes in mitochondrial ATP production and dehydrogenases activity (Wu et al. 2005). However, it has been reported that the reduction of tertrazolium salt to formazan responsible for absorbance changes in the metabolic activity test used herein can occur outside of

mitochondria thus suggesting employment of other cellular dehydrogenases beside NADP(H) dehydrogenase in OXPHOS (and thus mitochondria) (Bernas and Dobrucki 2002; Berridge and Tan 1993).

Besides OXPHOS, glycolysis is the main producer of ATP and thus, glyceraldehyde 3-phospate dehydrogenase instead of NADP(H) dehydrogenase could be responsible for the changes in metabolic activity observed in the Publication C. In order to confirm this hypothesis, Seahorse ATP production rate measurement was conducted. The results showed that, compared to control, cells stimulated with 100 μg/ml SiC-NH_2 and SiC-OH NPs for 24 hour showed higher dependence on glycolysis to produce ATP. This might be explained by induction of differentiation of monocytic cells into macrophages. Reactive oxygen species produced in OXPHOS are used in macrophages to eliminate bacteria in human body and thus the switch from OXPHOS to glycolysis can be observed (Freemerman et al. 2014). This presumption is even more supported when combined with long-term cultivation results from differing cellular morphologies acquired from the cells after 7 days shown in the Publication C. SiC-NH_2 stimulated monocytic THP-1 after that time show strong macrophage-like histological phenotype. Very little is known about differentiation of monocytes induced by NPs, however it has been shown that NPs can slow differentiation of THP-1 cells into macrophages (Xu et al. 2015). However, this is not happening in case of SiC-NH_2 NPs and thus, these NPs might be viewed as a potential platform for immunodeficiency treatment. SiC-x treated cells, as opposed to the rest of the samples and control, showed much higher OXPHOS-dependence. The long-term observation of the cells showed that SiC-x treated THP-1 cells do not survive well. In combination with this observation, the increased OXPHOS-dependence of these cells might be connected to ongoing apoptosis. Apoptosis (programmed cell death) is highly energy-dependent process requiring high amounts of ATP (Zamaraeva et al. 2005). Mitochondria play a key role in apoptosis induction as well as ATP production *via* OXPHOS (Kwong et al. 2007). Thus, the shift to highly OXPHOS-dependent metabolism in SiC-x treated cells might indicate early apoptosis caused by these NPs.

The immunomodulatory potential of SiC-based NPs was also shown by increased production of pro-inflammatory cytokines by the monocytic THP-1 cells as reported and discussed in the Publication C. The pro-inflammatory cytokine production was, however significantly lower than positive control (i.e. LPS stimulated cells) mimicking acute inflammatory response. Thus, SiC-based NPs are an immunogenic material, which should

be furtherly exploited. In the past years, immunomodulation has been given rising attention especially in order to direct immune system and subsequently the rest of cells in human body to treat itself. Currently, rising focus in determining immunomodulatory principles is given to exosomes as mediators of intracellular communication (Bellmunt et al. 2019; Kurywchak, Tavormina, and Kalluri 2018). In a pilot test determining if SiC-x NPs can stimulate THP-1 cells to produce more exosomes, interesting results were obtained. The cells that are in metabolically bad shape and in long term are not able to survive produce significantly higher amount of exosomes than control (untreated) cells. Thus the SiC-x treated cells are sending more signals to the surrounding cells. In order to understand the importance of such exosomes, complex study of exosomal content and exosomes' influence on other cells is highly desirable. However, the huge number of exosomes detected from supernatant of SiC-x treated cells might be compromised, as the cells are potentially undergoing apoptosis and thus to certain extent there might be a contamination of the sample with apoptotic bodies present. Detection of CD81 as classical exosomal marker was employed, however some researches point out that this marker can be also found on apoptotic bodies (Crescitelli et al. 2013). Thus detection of other exosomal markers (e.g. CD9 or CD63) along with the precise determination of the vesicular content is highly necessary. This theory can be supported by the fact that no significant difference in signal intensity of CD81 was detected on western blot among SiC-treated sample and control.

Furthermore, the effect of SiC-based NPs on doubling time (and thus proliferation) of THP-1 cells was also tested. The results showed that SiC-x NPs, that overall proved to be the most harmful, increase cell doubling time to 51 hours (i.e. decreased proliferation). This increase is in correspondence with overall toxic effect (low metabolic activity, low mitochondrial potential, lack of long-term survival) of these NPs on THP-1cells. Cells treated with SiC-OH NPs were inert in respect of their metabolic activity and showed just slight changes in OXPHOS/glycolysis metabolic dependence. Their doubling time also remained at approximately the same level as control (untreated) cells. The cells treated with SiC-NH_2 NPs exhibited interesting decrease of their doubling time, which suggests higher proliferation. This was also slightly supported by the long term observation in the Publication C, where after 7 days of treatment with SiC-NH_2, more cells were observed than in the control. It has been shown that amine (-NH_2) termination of NPs and also other materials has highly positive effect on cellular proliferation as well as their adhesion

(Hopper et al. 2014; Faucheux et al. 2004), thus the positive effect of SiC-NH_2 NPs on doubling time of THP-1 cells is not surprising.

In respect of SiC-based NPs detection inside the cells by the means of microscopy, a major drawback has been encountered. These NPs emit fluorescence, which is, however quenched in biological environment into an extent making the NPs undetectable by conventional methods. While classic electron microscopy techniques does not provide sufficient level of contrast for NPs made of biocompatible and also not electron-dense materials such as SiC-based NPs, special microscopic techniques that are nowadays still being developed have to be employed. The pilot study trying to detect silicon (Si) in the cells on elemental level showed that the content of Si in the cells treated with SiC-x NPs is lower than what is needed for cellular mapping, however still detectable by the cryo-TOF-SIMS FIB SEM Microscopy. Due to the transport reasons (cells were prepared in Prague and experiment was conducted in Brno), adherent osteoblastic SAOS-2 cells were used for the detection. These cells however were inert in respect of the NPs and thus the particles might not even be inside the cells, which may be the reason for low concentration of Si detected in the sample. Other possible explanation might also be that the NPs are dispersed in cellular cytoplasm in too low concentration to be precisely detected. However, there are no scientific data to prove either of this hypothesis. The intracellular localization and detection of these SiC-based USNPs is however crucial and must be furtherly studied.

7.3. Interactions of Gold Nanoparticles with Human Cells

PEGylation is commonly used in NPs-related research as an easy and an efficient method to prolong NPs' circulation *in vivo* (by increasing NPs hydrodynamic diameter as well as minimizing recognition of the NPs by immune cells), providing water solubility to hydrophobic NPs and stability to NPs with high tendency to aggregate (Knop et al. 2010; Jokerst et al. 2011). Different termination of PEG used for PEGylation can furtherly affect the interaction of PEGylated NPs with cells. Thiol-terminated PEG provides the resulting PEGylated NPs with negative charge, whereas amine-terminated PEG with positive charge. The data from the Publication D showed that USNPs of gold directly sputtered into thiol-terminated PEG have superior properties than these NPs sputtered into pure PEG or amine-terminated PEG. It have also been proved that the NPs are usable for further biological evaluations, as they did not resulted in significant damage

of the cells. It can be speculated that this superiority might originate from the fact, that thiol functional groups play a key role in biology. They forms a significant parameter in retaining tertial protein structures by formation of cystin from cysteine residues, but it also poses an important role as an enzymatic cofactor or in redox reactions in cells (Poole 2015).

PEGylation is also known to decrease binding of proteins to NPs (and thus PC formation) (Partikel et al. 2019). Herein, the presence of proteins was detected on AuNP-PEG due to the fact that AuNP-PEG-SH (which showed to be superior to the remaining PEGylated NPs in the Publication D) retained extremely high colloidal stability and no detectable pellet to be used for mass spectrometry analysis was acquired. Such superior colloidal stabilization of AuNPs by PEG-SH has been reported previously and marks AuNP-PEG-SH even more as a potential bio-applicable material (Gao et al. 2012). The results obtained from mass spectroscopy analysis of AuNP-PEG incubated in the medium with FBS confirms that PEGylation of AuNPs leads to lower protein binding, as only 39 proteins were detected to be bound to AuNP-PEG (as opposed to more than 160 proteins in case of O-DNDs with similar size and charge (*Section 6.4.1*)).

Influence of PC formation on cytotoxicity of AuNP-PEG-SH was tested in respect to osteoblastic SAOS-2 cells. FBS supplementation of the cultivation medium had obvious impact on cellular metabolic activity. Without the formed PC, AuNP-PEG-SH in higher (7 and 14 mg/l) concentrations caused significant increase of metabolic activity. This can be explained by the role of thiol group in biology, discussed above. However, when the results were compared to control group treated with PEG-SH without AuNPs, obvious resemblance was observed and thus it can be concluded, that the effect of AuNP-PEG-SH might not be directly connected with the USNPs, but with PEG-SH itself. Even though PEG has been approved by the FDA for clinical use and is commonly viewed as inert and non-immunogenic, it has been shown that its presence in the serum-free medium can be a stimulating factor for cell growth (Shintani, Iwamoto, and Kitano 1988).

Typically, AuNPs can enhance Raman spectra by the means of SERS effect, especially molecules or structures in their vicinity (Govindaraju et al. 2015; Nguyen et al. 2012). However, in the Publication D it has been shown that AuNP-PEG-SH used herein did undergo loss of their surface plasmon resonance (which is a prerequisite for SERS excited by wavelengths falling into the plasmon resonance band) due to their small size

and its narrow distribution (Boisselier and Astruc 2009). Even though pure metals as well as corresponding NPs made from them do not provide any Raman signal, it was hypothesized that some absorption for longer wavelengths can be still visible in the absorption spectra of the functionalized AuNPs, which theoretically could provide some surface enhancement Raman scattering of the functional groups attached to AuNPs (i.e. PEG-SH), and thus visualization of the cellular structures penetrated by AuNPs. However, a distinct thiol-related Raman band was not detected, even though it should exist and thus Raman imaging proved to be ineffective in respect to these NPs (Garrell, Szafranski, and Tanner 1990). However, it was demonstrated that Raman imaging can be employed to identify different chemical composition of the sub-cellular structures (e.g. structures containing greater fraction of lipids or presence of nucleoli in nucleus) as shown in Fig. 16.

The AuNPs are the most promising of all NPs reported in this work in respect of their precise detection and tracking in the cells despite being non-fluorescent. TEM was employed in order to detect the NPs and opened new possibilities of studying of AuNP-PEG-SH – cell interaction. The NPs were clearly detectable, enriched in vesicles inside cells. The NPs were even detected in the vesicle outside the cell suggesting NPs exocytosis. As no contrasting and processing of the samples were done, it is without a doubt that the dense particles detected are indeed AuNP-PEG-SH and not staining residues. It can only be speculated in what exact vesicle the NPs were already located inside cells. The intracellular trafficking and endosomal localization of gold NPs has been reported (Liu et al. 2017). However, further study, employing specific antibody staining and identifying of the true nature of the vesicles containing NPs must be conducted. The observed vesicle outside of the cell after 24 hours of incubation of NPs with cells points out that AuNP-PEG-SH undergo complete trafficking, exocytosis including. Thus these NPs could potentially be cleared from body or even trafficked to other cells (Choi et al. 2007; Liu et al. 2019).

7.4. Nanodiamond Nanoparticles Interaction with Proteins and Human Cells

DNDs interactions with proteins and human cells were broadly discussed in the Publication E. No additional unpublished data to broaden the discussion were obtained and thus cannot be discussed herein. However, the results regarding PC composition and

DNDs behavior in biological environment will be set in a broader context with other tested NPs in the next chapter (*Section 7.5.*).

7.5. The Importance of Protein Corona in Nanoparticle Research

As showed multiple times throughout this thesis, PC has a significant influence on interactions of NPs with cells. It has been long established that conventional NPs (>10 nm) interact with proteins by formation of layered PC consisting of tightly bound (hard corona) and loosely bound (soft corona) proteins (Milani et al. 2012). In the case of USNPs (< 5 nm, all NPs used throughout this thesis) such PC composition is highly improbable as these NPs are of the approximately same size, or even smaller, than the proteins forming PC. However, clear connection of PC presence and USNPs influence on cells can be still observed throughout the thesis. All of the used USNPs are less harmful for the cells in the medium supplemented with FBS than in serum-free medium and as suggested in the Publication A it can even play significant role in intracellular localization of the used USNPs. Thus, some form of PC or other USNPs-protein interaction must be present.

It has been shown that USNPs may act like a "binding agent" for proteins and thus forming artificial PC, resembling protein network (Glancy et al. 2019). The composition of such protein network may then affect directly the internalization mechanism in similar manner as PC of bigger NPs (Francia et al. 2019). For example, it has been shown that 100 nm SiO_2 NPs can specifically bind to LDL receptor and be furtherly internalized by the cells while having LDL particulates as a component of their PC (Lara et al. 2017). Herein, LDL particulates were found to be associated with AuNP-PEG by mass spectrometry, thus it might be speculated that such mechanism can be employed also in the case of USNPs. Furthermore, the Publication A showed direct connection of FBS presence or absence in the medium with vesicular or cytoplasmic localization of the fluorescent signal of SiQDs, respectively. Even though the SiQDs formed clusters in the presence of FBS, they still retained the ability to enter cells and so PC has obvious determining effect on NPs' uptake (Lesniak et al. 2012). Contrary to this, some DNDs formed huge aggregates which most probably were unable to penetrate the cells and possibly exerted in different cytotoxic mechanism (e.g. mechanical blocking of cell membrane) as showed in the Publication E. The DNDs-related results showed that physico-chemical properties (e.g. charge or zeta potential) are crucial in respect of

determination of protein corona (or in case of DNDs more of USNPs-protein network) composition.

From results presented herein it is obvious that correct and precise physico-chemical characterization can help with understanding on how the USNPs will interact with proteins in the cultivation medium. In case of larger NPs (> 10 nm) appropriate design of NP in order to avoid creation of PC or even manipulate its composition can lead to major breakthrough for NPs' application in biomedicine (Zhang et al. 2019; Grafe et al. 2016). In case of USNPs, the study of PC formation and composition is even more important, as it may influence not even the mode of interaction of the NPs with cells, but also the fact whether such interaction will even occur. The study and manipulation of PC formation on USNPs is still poorly understood, however rising attention is nowadays directed into this topic (Yin et al. 2020). As recently reviewed by Rampado et al. it is highly important to devote significant effort in studying PC and its possible exploitation in biomedicine (Rampado et al. 2020). However, such research is still highly time- and funding-demanding. Furthermore, currently used methods for studying PC do not allow for precise identification of the nature of USNPs-protein interaction. Indirect methods, such as dynamic light scattering, TEM, SEM or atomic force microscopy do not allow for precise identification of proteins bound to USNPs. Subsequently, direct methods for quantitative and qualitative analysis such as mass spectrometry or SDS-PAGE are in case USNPs somehow artificial (Carrillo-Carrion, Carril, and Parak 2017). These methods require separation of the NPs with PC from the cultivation media, which will eventually lead to bulk pellet of multiple NPs with proteins. The analysis itself then provides only information about proteins generally associating with the NPs, but not about the nature of such interaction with single NP resolution. Thus, if the formation of USNPs-protein network is not obvious from indirect methods (as it was in case of DNDs herein) only general idea of proteins that associate with NPs is obtained. Even though the influence of PC in case of USNPs is certain, the actual form of the PC or protein network remains poorly understood. However, the precise determination of NPs-protein interactions must be investigated in order to describe and possibly exploit these interactions for biomedical applications.

8. Conclusions

8.1. Interactions of Silicon Quantum Dots with Human Cells

The results from phosphorus and boron co-doped SiQDs have showed that protein corona formation is a key factor that determines not only the cellular response but also further trafficking and behavior of SiQDs inside the cells. Furthermore, these NPs showed that different cells respond to SiQDs presence in different manners and thus cell type and origin must be taken into account.

8.2. Interactions of Silicon Carbide Nanoparticles with Human Cells

Surface termination of highly biocompatible SiC-based NPs showed proved to be a determining factor effecting the response of the monocytes *in vitro*. Changes in metabolism, differentiation and cytokine production stimulation as well as increased exosomes production show that these NPs are capable of immunomodulation of monocytic THP-1 cells.

8.3. Interactions of Gold Nanoparticles with Human Cells

The testing of PEGylated AuNPs showed that PEG functionalization has determining effect on response of human osteoblasts to exposure to these NPs. Furthermore, vesicle-related trafficking of AuNP-PEG-SH was showed. With low toxicity and good detectability AuNP-PEG-SH are NPs with huge potential for further studies, especially of vesicle-related trafficking of ultra-small nanoparticles.

8.4. Nanodiamond Nanoparticles Interaction with Proteins and Human Cells

Detonation nanodiamonds with hydrogenated or oxidized surface were shown to interact with different proteins based especially on their physico-chemical properties. Formation of huge protein aggregates mediated by the NPs was showed to have determinant effect to cellular metabolic activity.

9. Supplementary data

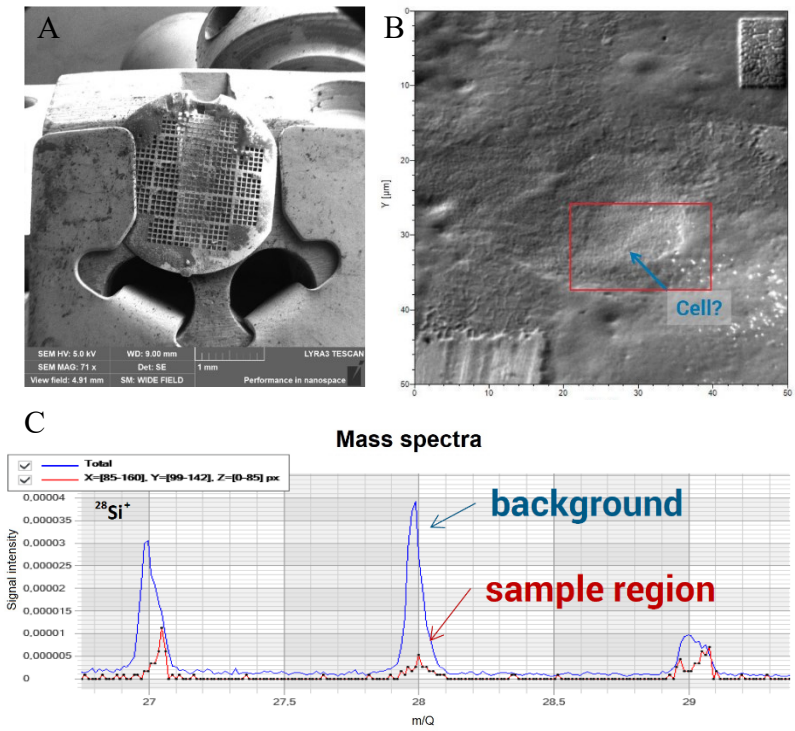

Figure 18: SEM images and spectral analysis of control cells by cryo-TOF-SIMS FIB SEM microscopy. SEM image of damaged grid prior to FIB-SEM (A) possible cell remaining on damaged grid (B). Mass spectra of possible cell area marked by red rectangle – sample region and of background–whole field observed in B (C).

Accession	Name	Function
Proteins with cholesterol transfer, heparin and lipase binding and low-density lipoprotein (LDL) particle receptor binding activity		
E1BNR0	Apolipoprotein B	cholesterol transfer activity, heparin and lipase binding, LDL particle receptor binding
Q03247	Apolipoprotein E	cholesterol transfer activity and heparin binding, LDL particle receptor binding
P15497	Apolipoprotein A-I	cholesterol transfer activity and heparin binding
Proteins associated with hyaluronan metabolic processes		
F1MNW4	Inter-alpha-trypsin inhibitor heavy chain H2	hyaluronan metabolic processes
Q0VCM5	Inter-alpha-trypsin inhibitor heavy chain H1	hyaluronan metabolic processes
Q3T052	Inter-alpha-trypsin inhibitor heavy chain H4	hyaluronan metabolic processes, acute-phase inflammation response
Proteins with cytoskelet and adhesion associated function		
Q28178	Thrombospondin-1	cell-cell or cell-extracellular matrix binding
M0QVY0	Intermediate filament rod domain-containing protein	Keratin filament formation
P06394	Keratin, type I cytoskeletal 10	Intermediate filament formation
Q3ZBS7	Vitronectin	cell-extracellular matrix binding, cell adhesion and migration
A0A140T8C8	Kininogen-1	negative regulation of coagulation and cell adhesion
Q5XQN5	Keratin, type II cytoskeletal 5	epithelial cell differentiation and negative regulation of their proliferation
F1MDH3	Talin 1	actin filament binding and cell adhesion
P63261	Actin, cytoplasmic 2	cell-cell interaction establishment, cytoskeleton formation
F1MC11	Keratin, type I cytoskeletal 14	intermediate filament formation
G3MZ71	Keratin 2	intermediate filament binding and orgaization
Q3SX14	Gelsolin	actin filament binding
P08728	Keratin, type I cytoskeletal 19	organization of myofibers
A1L595	REVERSED Keratin, type I cytoskeletal 17	proliferative activity
G3N0V2	Keratin 1	intermediate filament formation and complement system activation

Table 2A: Mass spectrometry analysis of proteins on AuNP-PEG nanoparticles with protein function included. All proteins originate from *Bos Taurus*.

Accession	Name	Function
		Proteins with hemostatic role in plasma
F1MSZ6	Antithrombin-III	heparin binding, coagulation regulation
P02081	Hemoglobin fetal subunit beta	heme, hemoglobin and oxygen binding, cellular oxidant detoxification
P01966	Hemoglobin subunit alpha	heme, hemoglobin and oxygen binding, cellular oxidant detoxification
Q9N2I2	Plasma serine protease inhibitor	hemostatic role in plasma
P02769	Albumin	osmotic pressure regulation, cell adhesion regulation
		Proteins associated with immune system function
Q2UVX4	Complement C3	activation of the serum complement system (inflammatory process)
P12763	Alpha-2-HS-glycoprotein	endocytosis promotion, opsonization
Q1RMH5	C1QC protein	ormation of first component of the serum complement system
Q5E9E3	Complement C1q subcomponent subunit A	formation of first component of the serum complement system
P28800	Alpha-2-antiplasmin	inhibition of serin-type proteases activity, acute-phase inflamation response
E1BH06	Uncharacterized protein	complement activation, endopeptidase inhibition activity
		Proteins with various proteinase and inhibitory activity
Q7SIH1	Alpha-2-macroglobulin	various proteinasse inhibitor activity
A6QPP2	SERPIND1 protein	inhibition of serin-type endopeptidases activity
P00760	Cationic trypsin	protein digestion, proteolysis
P34955	Alpha-1-antiproteinase	inhibition of serin-type proteases activity
		Proteins associated with cellular metabolism
Q3MHL4	Adenosylhomocysteinase	control of methylations via regulation of the intracellular concentration of adenosylhomocysteine
P10096	Glyceraldehyde-3-phosphate dehydrogenase	glycolysis regulation, microtubule cytoskeleton organization
A5D984	Pyruvate kinase	production of ATP, cellular response to insulin
P19858	L-lactate dehydrogenase A chain	various metabolic processes

Table 2B: Mass spectrometry analysis of proteins on AuNP-PEG nanoparticles with protein function included. All proteins originate from *Bos Taurus*.

10. References

Acar, H., R. Samaeekia, M. R. Schnorenberg, D. K. Sasmal, J. Huang, M. V. Tirrell, and J. L. LaBelle. 2017. 'Cathepsin-Mediated Cleavage of Peptides from Peptide Amphiphiles Leads to Enhanced Intracellular Peptide Accumulation', *Bioconjug Chem*, 28: 2316-26.

Aderem, A., and D. M. Underhill. 1999. 'Mechanisms of phagocytosis in macrophages', *Annu Rev Immunol*, 17: 593-623.

Ali, Moustafa R. K., Yue Wu, and Mostafa A. El-Sayed. 2019. 'Gold-Nanoparticle-Assisted Plasmonic Photothermal Therapy Advances Toward Clinical Application', *The Journal of Physical Chemistry C*, 123: 15375-93.

Arayne, M. S., and N. Sultana. 2006. 'Porous nanoparticles in drug delivery systems', *Pak J Pharm Sci*, 19: 158-69.

Artioli, G., I. Angelini, and A. Polla. 2008. 'Crystals and phase transitions in protohistoric glass materials', *Phase Transitions*, 81: 233-52.

Beke, David, Zsolt Szekrényes, István Balogh, Zsolt Czigány, Katalin Kamarás, and Adam Gali. 2012. 'Preparation of small silicon carbide quantum dots by wet chemical etching', *Journal of Materials Research*, 28: 44-49.

Bellmunt, A. M., L. Lopez-Puerto, J. Lorente, and D. Closa. 2019. 'Involvement of extracellular vesicles in the macrophage-tumor cell communication in head and neck squamous cell carcinoma', *PLoS One*, 14: e0224710.

Benyettou, F., R. Rezgui, F. Ravaux, T. Jaber, K. Blumer, M. Jouiad, L. Motte, J. C. Olsen, C. Platas-Iglesias, M. Magzoub, and A. Trabolsi. 2015. 'Synthesis of silver nanoparticles for the dual delivery of doxorubicin and alendronate to cancer cells', *J Mater Chem B*, 3: 7237-45.

Bernas, T., and J. Dobrucki. 2002. 'Mitochondrial and nonmitochondrial reduction of MTT: interaction of MTT with TMRE, JC-1, and NAO mitochondrial fluorescent probes', *Cytometry*, 47: 236-42.

Bernhard, C., S. J. Roeters, J. Franz, T. Weidner, M. Bonn, and G. Gonella. 2017. 'Repelling and ordering: the influence of poly(ethylene glycol) on protein adsorption', *Phys Chem Chem Phys*, 19: 28182-88.

Berridge, M. V., and A. S. Tan. 1993. 'Characterization of the cellular reduction of 3-(4,5-dimethylthiazol-2-yl)-2,5-diphenyltetrazolium bromide (MTT): subcellular localization, substrate dependence, and involvement of mitochondrial electron transport in MTT reduction', *Arch Biochem Biophys*, 303: 474-82.

Boisselier, E., and D. Astruc. 2009. 'Gold nanoparticles in nanomedicine: preparations, imaging, diagnostics, therapies and toxicity', *Chemical Society Reviews*, 38: 1759-82.

Bradac, Carlo, Ishan Das Rastogi, Nicole M. Cordina, Alfonso Garcia-Bennett, and Louise J. Brown. 2018. 'Influence of surface composition on the colloidal stability of ultra-small detonation nanodiamonds in biological media', *Diamond and Related Materials*, 83: 38-45.

Buzea, C., Pacheco, II, and K. Robbie. 2007. 'Nanomaterials and nanoparticles: sources and toxicity', *Biointerphases*, 2: MR17-71.

Caracciolo, G., S. Palchetti, V. Colapicchioni, L. Digiacomo, D. Pozzi, A. L. Capriotti, G. La Barbera, and A. Lagana. 2015. 'Stealth effect of biomolecular corona on nanoparticle uptake by immune cells', *Langmuir*, 31: 10764-73.

Carrillo-Carrion, C., M. Carril, and W. J. Parak. 2017. 'Techniques for the experimental investigation of the protein corona', *Curr Opin Biotechnol*, 46: 106-13.

Contini, Claudia, Matthew Schneemilch, Simon Gaisford, and Nick Quirke. 2017. 'Nanoparticle–membrane interactions', *Journal of Experimental Nanoscience*, 13: 62-81.

Crescitelli, R., C. Lasser, T. G. Szabo, A. Kittel, M. Eldh, I. Dianzani, E. I. Buzas, and J. Lotvall. 2013. 'Distinct RNA profiles in subpopulations of extracellular vesicles: apoptotic bodies, microvesicles and exosomes', *J Extracell Vesicles*, 2.

Dalal, C., and N. R. Jana. 2017. 'Multivalency Effect of TAT-Peptide-Functionalized Nanoparticle in Cellular Endocytosis and Subcellular Trafficking', *J Phys Chem B*, 121: 2942-51.

Damm, E. M., L. Pelkmans, J. Kartenbeck, A. Mezzacasa, T. Kurzchalia, and A. Helenius. 2005. 'Clathrin- and caveolin-1-independent endocytosis: entry of simian virus 40 into cells devoid of caveolae', *J Cell Biol*, 168: 477-88.

De S. Reboucas, J., J. M. Irache, A. I. Camacho, G. Gastaminza, M. L. Sanz, M. Ferrer, and C. Gamazo. 2014. 'Immunogenicity of peanut proteins containing poly(anhydride) nanoparticles', *Clin Vaccine Immunol*, 21: 1106-12.

Ding, T., and J. Sun. 2019. 'Formation of Protein Corona on Nanoparticle Affects Different Complement Activation Pathways Mediated by C1q', *Pharm Res*, 37: 10.

Dravecz, G., T. Z. Janosi, D. Beke, D. A. Major, G. Karolyhazy, J. Erostyak, K. Kamaras, and A. Gali. 2018. 'Identification of the binding site between bovine serum albumin and ultrasmall SiC fluorescent biomarkers', *Phys Chem Chem Phys*, 20: 13419-29.

Dulkeith, E., M. Ringler, T. A. Klar, J. Feldmann, A. Munoz Javier, and W. J. Parak. 2005. 'Gold nanoparticles quench fluorescence by phase induced radiative rate suppression', *Nano Lett*, 5: 585-9.

Ehlerding, E. B., F. Chen, and W. Cai. 2016. 'Biodegradable and Renal Clearable Inorganic Nanoparticles', *Adv Sci (Weinh)*, 3.

El-Say, K. M., and H. S. El-Sawy. 2017. 'Polymeric nanoparticles: Promising platform for drug delivery', *Int J Pharm*, 528: 675-91.

Erogbogbo, F., K. T. Yong, I. Roy, R. Hu, W. C. Law, W. Zhao, H. Ding, F. Wu, R. Kumar, M. T. Swihart, and P. N. Prasad. 2011. 'In vivo targeted cancer imaging, sentinel lymph node mapping and multi-channel imaging with biocompatible silicon nanocrystals', *ACS Nano*, 5: 413-23.

Evans, B. C., R. B. Fletcher, K. V. Kilchrist, E. A. Dailing, A. J. Mukalel, J. M. Colazo, M. Oliver, J. Cheung-Flynn, C. M. Brophy, J. W. Tierney, J. S. Isenberg, K. D. Hankenson, K. Ghimire, C. Lander, C. A. Gersbach, and C. L. Duvall. 2019. 'An anionic, endosome-escaping polymer to potentiate intracellular delivery of cationic peptides, biomacromolecules, and nanoparticles', *Nat Commun*, 10: 5012.

Faraday, M. 1856. "Faraday's notebooks: Gold colloids " In.

———. 1857. 'X. The Bakerian Lecture. —Experimental relations of gold (and other metals) to light', *Philosophical Transactions of the Royal Society of London*, 147: 145-81.

Faucheux, N., R. Schweiss, K. Lutzow, C. Werner, and T. Groth. 2004. 'Self-assembled monolayers with different terminating groups as model substrates for cell adhesion studies', *Biomaterials*, 25: 2721-30.

Fink, S. L., and B. T. Cookson. 2005. 'Apoptosis, pyroptosis, and necrosis: mechanistic description of dead and dying eukaryotic cells', *Infect Immun*, 73: 1907-16.

Flahaut, E., M. C. Durrieu, M. Remy-Zolghadri, R. Bareille, and Ch Baquey. 2006. 'Investigation of the cytotoxicity of CCVD carbon nanotubes towards human umbilical vein endothelial cells', *Carbon*, 44: 1093-99.

Flessau, S., C. Wolter, E. Poselt, E. Kroger, A. Mews, and T. Kipp. 2014. 'Fluorescence spectroscopy of individual semiconductor nanoparticles in different ethylene glycols', *Phys Chem Chem Phys*, 16: 10444-55.

Francia, V., K. Yang, S. Deville, C. Reker-Smit, I. Nelissen, and A. Salvati. 2019. 'Corona Composition Can Affect the Mechanisms Cells Use to Internalize Nanoparticles', *ACS Nano*, 13: 11107-21.

Freemerman, A. J., A. R. Johnson, G. N. Sacks, J. J. Milner, E. L. Kirk, M. A. Troester, A. N. Macintyre, P. Goraksha-Hicks, J. C. Rathmell, and L. Makowski. 2014. 'Metabolic reprogramming of macrophages: glucose transporter 1 (GLUT1)-mediated glucose metabolism drives a proinflammatory phenotype', *J Biol Chem*, 289: 7884-96.

Fujii, M., H. Sugimoto, and K. Imakita. 2016. 'All-inorganic colloidal silicon nanocrystals-surface modification by boron and phosphorus co-doping', *Nanotechnology*, 27: 262001.

Gagner, J. E., X. Qian, M. M. Lopez, J. S. Dordick, and R. W. Siegel. 2012. 'Effect of gold nanoparticle structure on the conformation and function of adsorbed proteins', *Biomaterials*, 33: 8503-16.

Gallud, A., K. Kloditz, J. Ytterberg, N. Ostberg, S. Katayama, T. Skoog, V. Gogvadze, Y. Z. Chen, D. Xue, S. Moya, J. Ruiz, D. Astruc, R. Zubarev, J. Kere, and B. Fadeel. 2019. 'Cationic gold nanoparticles elicit mitochondrial dysfunction: a multi-omics study', *Sci Rep*, 9: 4366.

Gao, H., Z. Yang, S. Zhang, S. Cao, S. Shen, Z. Pang, and X. Jiang. 2013. 'Ligand modified nanoparticles increases cell uptake, alters endocytosis and elevates glioma distribution and internalization', *Sci Rep*, 3: 2534.

Gao, J., X. Huang, H. Liu, F. Zan, and J. Ren. 2012. 'Colloidal stability of gold nanoparticles modified with thiol compounds: bioconjugation and application in cancer cell imaging', *Langmuir*, 28: 4464-71.

Garrell, Robin L., Cory Szafranski, and Weslene Tanner. 1990. "Surface-enhanced Raman spectroscopy of thiols and disulfides." In *34th Annual International Technical Symposium on Optical and Optoelectronic Applied Science and Engineering*. San Diego, CA.

Glancy, D., Y. Zhang, J. L. Y. Wu, B. Ouyang, S. Ohta, and W. C. W. Chan. 2019. 'Characterizing the protein corona of sub-10nm nanoparticles', *J Control Release*, 304: 102-10.

Gliga, Anda R., Jessica De Loma, Sebastiano Di Bucchianico, Sara Skoglund, Sandeep Keshavan, Inger Odnevall Wallinder, Hanna L. Karlsson, and Bengt Fadeel. 2020. 'Silver nanoparticles modulate lipopolysaccharide-triggered Toll-like receptor signaling in immune-competent human cell lines', *Nanoscale Advances*, 2: 648-58.

Gomez, D. M., S. Urcuqui-Inchima, and J. C. Hernandez. 2017. 'Silica nanoparticles induce NLRP3 inflammasome activation in human primary immune cells', *Innate Immun*, 23: 697-708.
Govindaraju, S., M. Ramasamy, R. Baskaran, S. J. Ahn, and K. Yun. 2015. 'Ultraviolet light and laser irradiation enhances the antibacterial activity of glucosamine-functionalized gold nanoparticles', *Int J Nanomedicine*, 10 Spec Iss: 67-78.
Grafe, C., A. Weidner, M. V. Luhe, C. Bergemann, F. H. Schacher, J. H. Clement, and S. Dutz. 2016. 'Intentional formation of a protein corona on nanoparticles: Serum concentration affects protein corona mass, surface charge, and nanoparticle-cell interaction', *Int J Biochem Cell Biol*, 75: 196-202.
Guerrero-Florez, V., S. C. Mendez-Sanchez, O. A. Patron-Soberano, V. Rodriguez-Gonzalez, D. Blach, and O. F. Martinez. 2020. 'Gold nanoparticle-mediated generation of reactive oxygen species during plasmonic photothermal therapy: a comparative study for different particle sizes, shapes, and surface conjugations', *J Mater Chem B*, 8: 2862-75.
Harvey, Sean, Marco Raabe, Anna Ermakova, Yingke Wu, Todd Zapata, Chaojian Chen, Hao Lu, Fedor Jelezko, David Y. W. Ng, and Tanja Weil. 2019. 'Transferrin-Coated Nanodiamond–Drug Conjugates for Milliwatt Photothermal Applications', *Advanced Therapeutics*, 2.
Hirai, T., Y. Yoshioka, N. Izumi, K. Ichihashi, T. Handa, N. Nishijima, E. Uemura, K. Sagami, H. Takahashi, M. Yamaguchi, K. Nagano, Y. Mukai, H. Kamada, S. Tsunoda, K. J. Ishii, K. Higashisaka, and Y. Tsutsumi. 2016. 'Metal nanoparticles in the presence of lipopolysaccharides trigger the onset of metal allergy in mice', *Nat Nanotechnol*, 11: 808-16.
Hopper, A. P., J. M. Dugan, A. A. Gill, O. J. Fox, P. W. May, J. W. Haycock, and F. Claeyssens. 2014. 'Amine functionalized nanodiamond promotes cellular adhesion, proliferation and neurite outgrowth', *Biomed Mater*, 9: 045009.
Horisberger, M., and J. Rosset. 1977. 'Colloidal gold, a useful marker for transmission and scanning electron microscopy', *J Histochem Cytochem*, 25: 295-305.
Hosea, Michael, Benjamin Greene, Robert McPherson, Michael Henzl, M. Dale Alexander, and Dennis W. Darnall. 1986. 'Accumulation of elemental gold on the alga Chlorella vulgaris', *Inorganica Chimica Acta*, 123: 161-65.
Huo, S., S. Jin, X. Ma, X. Xue, K. Yang, A. Kumar, P. C. Wang, J. Zhang, Z. Hu, and X. J. Liang. 2014. 'Ultrasmall gold nanoparticles as carriers for nucleus-based gene therapy due to size-dependent nuclear entry', *ACS Nano*, 8: 5852-62.
Chang, Be-Ming, Hsin-Hung Lin, Long-Jyun Su, Wen-Der Lin, Ruey-Jen Lin, Yan-Kai Tzeng, Reiko T. Lee, Yuan C. Lee, Alice L. Yu, and Huan-Cheng Chang. 2013. 'Highly Fluorescent Nanodiamonds Protein-Functionalized for Cell Labeling and Targeting', *Advanced Functional Materials*, 23: 5737-45.
Chatterjee, S., and T. K. Mukherjee. 2014. 'Spectroscopic investigation of interaction between bovine serum albumin and amine-functionalized silicon quantum dots', *Phys Chem Chem Phys*, 16: 8400-8.
Choi, H. S., W. Liu, P. Misra, E. Tanaka, J. P. Zimmer, B. Itty Ipe, M. G. Bawendi, and J. V. Frangioni. 2007. 'Renal clearance of quantum dots', *Nat Biotechnol*, 25: 1165-70.
Iversen, T. G., N. Frerker, and K. Sandvig. 2012. 'Uptake of ricinB-quantum dot nanoparticles by a macropinocytosis-like mechanism', *J Nanobiotechnology*, 10: 33.
Jatana, S., B. C. Palmer, S. J. Phelan, and L. A. DeLouise. 2017. 'Immunomodulatory Effects of Nanoparticles on Skin Allergy', *Sci Rep*, 7: 3979.
Jiang, P., Y. Wang, L. Zhao, C. Ji, D. Chen, and L. Nie. 2018. 'Applications of Gold Nanoparticles in Non-Optical Biosensors', *Nanomaterials (Basel)*, 8.
Jiang, X., C. Rocker, M. Hafner, S. Brandholt, R. M. Dorlich, and G. U. Nienhaus. 2010. 'Endo- and exocytosis of zwitterionic quantum dot nanoparticles by live HeLa cells', *ACS Nano*, 4: 6787-97.
Jiang, Y., S. Huo, T. Mizuhara, R. Das, Y. W. Lee, S. Hou, D. F. Moyano, B. Duncan, X. J. Liang, and V. M. Rotello. 2015. 'The Interplay of Size and Surface Functionality on the Cellular Uptake of Sub-10 nm Gold Nanoparticles', *ACS Nano*, 9: 9986-93.
Johansen, P. L., F. Fenaroli, L. Evensen, G. Griffiths, and G. Koster. 2016. 'Optical micromanipulation of nanoparticles and cells inside living zebrafish', *Nat Commun*, 7: 10974.
Johnson-McDaniel, D., C. A. Barrett, A. Sharafi, and T. T. Salguero. 2013. 'Nanoscience of an ancient pigment', *J Am Chem Soc*, 135: 1677-9.
Jokerst, J. V., T. Lobovkina, R. N. Zare, and S. S. Gambhir. 2011. 'Nanoparticle PEGylation for imaging and therapy', *Nanomedicine (Lond)*, 6: 715-28.
Kabe, Y., S. Sakamoto, M. Hatakeyama, Y. Yamaguchi, M. Suematsu, M. Itonaga, and H. Handa. 2019. 'Application of high-performance magnetic nanobeads to biological sensing devices', *Anal Bioanal Chem*, 411: 1825-37.

Kagawa, Jun. 2002. 'Health effects of diesel exhaust emissions—a mixture of air pollutants of worldwide concern', *Toxicology*, 181-182: 349-53.
Kailasa, S. K., K. H. Cheng, and H. F. Wu. 2013. 'Semiconductor Nanomaterials-Based Fluorescence Spectroscopic and Matrix-Assisted Laser Desorption/Ionization (MALDI) Mass Spectrometric Approaches to Proteome Analysis', *Materials (Basel)*, 6: 5763-95.
Kaksonen, M., and A. Roux. 2018. 'Mechanisms of clathrin-mediated endocytosis', *Nat Rev Mol Cell Biol*, 19: 313-26.
Kasper, J., M. I. Hermanns, C. Bantz, S. Utech, O. Koshkina, M. Maskos, C. Brochhausen, C. Pohl, S. Fuchs, R. E. Unger, and C. J. Kirkpatrick. 2013. 'Flotillin-involved uptake of silica nanoparticles and responses of an alveolar-capillary barrier in vitro', *Eur J Pharm Biopharm*, 84: 275-87.
Kaur, R., and I. Badea. 2013. 'Nanodiamonds as novel nanomaterials for biomedical applications: drug delivery and imaging systems', *Int J Nanomedicine*, 8: 203-20.
Kerr, M. C., and R. D. Teasdale. 2009. 'Defining macropinocytosis', *Traffic*, 10: 364-71.
Kettiger, H., A. Schipanski, P. Wick, and J. Huwyler. 2013. 'Engineered nanomaterial uptake and tissue distribution: from cell to organism', *Int J Nanomedicine*, 8: 3255-69.
Kim, C., G. Y. Tonga, B. Yan, C. S. Kim, S. T. Kim, M. H. Park, Z. Zhu, B. Duncan, B. Creran, and V. M. Rotello. 2015. 'Regulating exocytosis of nanoparticles via host-guest chemistry', *Org Biomol Chem*, 13: 2474-79.
Kim, J., H. R. Cho, H. Jeon, D. Kim, C. Song, N. Lee, S. H. Choi, and T. Hyeon. 2017. 'Continuous O2-Evolving MnFe2O4 Nanoparticle-Anchored Mesoporous Silica Nanoparticles for Efficient Photodynamic Therapy in Hypoxic Cancer', *J Am Chem Soc*, 139: 10992-95.
Kim, S. E., L. Zhang, K. Ma, M. Riegman, F. Chen, I. Ingold, M. Conrad, M. Z. Turker, M. Gao, X. Jiang, S. Monette, M. Pauliah, M. Gonen, P. Zanzonico, T. Quinn, U. Wiesner, M. S. Bradbury, and M. Overholtzer. 2016. 'Ultrasmall nanoparticles induce ferroptosis in nutrient-deprived cancer cells and suppress tumour growth', *Nat Nanotechnol*, 11: 977-85.
Knop, K., R. Hoogenboom, D. Fischer, and U. S. Schubert. 2010. 'Poly(ethylene glycol) in drug delivery: pros and cons as well as potential alternatives', *Angew Chem Int Ed Engl*, 49: 6288-308.
Koh, B., and W. Cheng. 2014. 'Mechanisms of carbon nanotube aggregation and the reversion of carbon nanotube aggregates in aqueous medium', *Langmuir*, 30: 10899-909.
Kong, F. Y., J. W. Zhang, R. F. Li, Z. X. Wang, W. J. Wang, and W. Wang. 2017. 'Unique Roles of Gold Nanoparticles in Drug Delivery, Targeting and Imaging Applications', *Molecules*, 22.
Korangath, P., J. D. Barnett, A. Sharma, E. T. Henderson, J. Stewart, S. H. Yu, S. K. Kandala, C. T. Yang, J. S. Caserto, M. Hedayati, T. D. Armstrong, E. Jaffee, C. Gruettner, X. C. Zhou, W. Fu, C. Hu, S. Sukumar, B. W. Simons, and R. Ivkov. 2020. 'Nanoparticle interactions with immune cells dominate tumor retention and induce T cell-mediated tumor suppression in models of breast cancer', *Sci Adv*, 6: eaay1601.
Kuhn, D. A., D. Vanhecke, B. Michen, F. Blank, P. Gehr, A. Petri-Fink, and B. Rothen-Rutishauser. 2014. 'Different endocytotic uptake mechanisms for nanoparticles in epithelial cells and macrophages', *Beilstein J Nanotechnol*, 5: 1625-36.
Kumar, S., I. Yadav, V. K. Aswal, and J. Kohlbrecher. 2018. 'Structure and Interaction of Nanoparticle-Protein Complexes', *Langmuir*, 34: 5679-95.
Kumari, S., S. Mg, and S. Mayor. 2010. 'Endocytosis unplugged: multiple ways to enter the cell', *Cell Res*, 20: 256-75.
Kurywchak, P., J. Tavormina, and R. Kalluri. 2018. 'The emerging roles of exosomes in the modulation of immune responses in cancer', *Genome Med*, 10: 23.
Kwong, J. Q., M. S. Henning, A. A. Starkov, and G. Manfredi. 2007. 'The mitochondrial respiratory chain is a modulator of apoptosis', *J Cell Biol*, 179: 1163-77.
Lalwani, Gaurav, and Balaji Sitharaman. 2013. 'Multifunctional Fullerene- and Metallofullerene-Based Nanobiomaterials', *Nano LIFE*, 03.
Lammel, T., A. Mackevica, B. R. Johansson, and J. Sturve. 2019. 'Endocytosis, intracellular fate, accumulation, and agglomeration of titanium dioxide (TiO2) nanoparticles in the rainbow trout liver cell line RTL-W1', *Environ Sci Pollut Res Int*, 26: 15354-72.
Lara, S., F. Alnasser, E. Polo, D. Garry, M. C. Lo Giudice, D. R. Hristov, L. Rocks, A. Salvati, Y. Yan, and K. A. Dawson. 2017. 'Identification of Receptor Binding to the Biomolecular Corona of Nanoparticles', *ACS Nano*, 11: 1884-93.
Lazarovits, J., Y. Y. Chen, E. A. Sykes, and W. C. Chan. 2015. 'Nanoparticle-blood interactions: the implications on solid tumour targeting', *Chem Commun (Camb)*, 51: 2756-67.
Le, P. U., and I. R. Nabi. 2003. 'Distinct caveolae-mediated endocytic pathways target the Golgi apparatus and the endoplasmic reticulum', *J Cell Sci*, 116: 1059-71.

Lee, C., L. Jose, K. Shim, S. S. A. An, S. Jang, J. K. Song, J. O. Jin, and H. J. Paik. 2019. 'Influenza mimetic protein-polymer nanoparticles as antigen delivery vehicles to dendritic cells for cancer immunotherapy', *Nanoscale*, 11: 13878-84.

Lesniak, A., F. Fenaroli, M. P. Monopoli, C. Aberg, K. A. Dawson, and A. Salvati. 2012. 'Effects of the presence or absence of a protein corona on silica nanoparticle uptake and impact on cells', *ACS Nano*, 6: 5845-57.

Lesniak, A., A. Salvati, M. J. Santos-Martinez, M. W. Radomski, K. A. Dawson, and C. Aberg. 2013. 'Nanoparticle adhesion to the cell membrane and its effect on nanoparticle uptake efficiency', *J Am Chem Soc*, 135: 1438-44.

Liu, M., Q. Li, L. Liang, J. Li, K. Wang, J. Li, M. Lv, N. Chen, H. Song, J. Lee, J. Shi, L. Wang, R. Lal, and C. Fan. 2017. 'Real-time visualization of clustering and intracellular transport of gold nanoparticles by correlative imaging', *Nat Commun*, 8: 15646.

Liu, X., and D. Ghosh. 2019. 'Intracellular nanoparticle delivery by oncogenic KRAS-mediated macropinocytosis', *Int J Nanomedicine*, 14: 6589-600.

Liu, Y., Y. Huo, L. Yao, Y. Xu, F. Meng, H. Li, K. Sun, G. Zhou, D. S. Kohane, and K. Tao. 2019. 'Transcytosis of Nanomedicine for Tumor Penetration', *Nano Lett*, 19: 8010-20.

Lolicato, F., L. Joly, H. Martinez-Seara, G. Fragneto, E. Scoppola, F. Baldelli Bombelli, I. Vattulainen, J. Akola, and M. Maccarini. 2019. 'The Role of Temperature and Lipid Charge on Intake/Uptake of Cationic Gold Nanoparticles into Lipid Bilayers', *Small*, 15: e1805046.

Luo, N., J. K. Weber, S. Wang, B. Luan, H. Yue, X. Xi, J. Du, Z. Yang, W. Wei, R. Zhou, and G. Ma. 2017. 'PEGylated graphene oxide elicits strong immunological responses despite surface passivation', *Nat Commun*, 8: 14537.

Lv, Y., L. Hao, W. Hu, Y. Ran, Y. Bai, and L. Zhang. 2016. 'Novel multifunctional pH-sensitive nanoparticles loaded into microbubbles as drug delivery vehicles for enhanced tumor targeting', *Sci Rep*, 6: 29321.

Ma, D. D., and W. X. Yang. 2016. 'Engineered nanoparticles induce cell apoptosis: potential for cancer therapy', *Oncotarget*, 7: 40882-903.

Melamed, J. R., S. A. Ioele, A. J. Hannum, V. M. Ullman, and E. S. Day. 2018. 'Polyethylenimine-Spherical Nucleic Acid Nanoparticles against Gli1 Reduce the Chemoresistance and Stemness of Glioblastoma Cells', *Mol Pharm*, 15: 5135-45.

Meyers, J. D., Y. Cheng, A. M. Broome, R. S. Agnes, M. D. Schluchter, S. Margevicius, X. Wang, M. E. Kenney, C. Burda, and J. P. Basilion. 2015. 'Peptide-Targeted Gold Nanoparticles for Photodynamic Therapy of Brain Cancer', *Part Part Syst Charact*, 32: 448-57.

Milani, S., F. B. Bombelli, A. S. Pitek, K. A. Dawson, and J. Radler. 2012. 'Reversible versus irreversible binding of transferrin to polystyrene nanoparticles: soft and hard corona', *ACS Nano*, 6: 2532-41.

Milla, P., F. Dosio, and L. Cattel. 2012. 'PEGylation of proteins and liposomes: a powerful and flexible strategy to improve the drug delivery', *Curr Drug Metab*, 13: 105-19.

Miller, H. A., A. W. Magsam, A. W. Tarudji, S. Romanova, L. Weber, C. C. Gee, G. L. Madsen, T. K. Bronich, and F. M. Kievit. 2019. 'Evaluating differential nanoparticle accumulation and retention kinetics in a mouse model of traumatic brain injury via K(trans) mapping with MRI', *Sci Rep*, 9: 16099.

Mirshafiee, V., M. Mahmoudi, K. Lou, J. Cheng, and M. L. Kraft. 2013. 'Protein corona significantly reduces active targeting yield', *Chem Commun (Camb)*, 49: 2557-9.

Monopoli, M. P., C. Aberg, A. Salvati, and K. A. Dawson. 2012. 'Biomolecular coronas provide the biological identity of nanosized materials', *Nat Nanotechnol*, 7: 779-86.

Nakamura, H., K. Sezawa, M. Hata, S. Ohsaki, and S. Watano. 2019. 'Direct translocation of nanoparticles across a model cell membrane by nanoparticle-induced local enhancement of membrane potential', *Phys Chem Chem Phys*, 21: 18830-38.

"Nanotechnologies — Vocabulary — Part 2: Nano-objects." In. 2015. edited by International Organization for Standardization, 10

Nguyen, The Binh, Thi Khanh Thu Vu, Quang Dong Nguyen, Thanh Dinh Nguyen, The An Nguyen, and Thi Hue Trinh. 2012. 'Preparation of metal nanoparticles for surface enhanced Raman scattering by laser ablation method', *Advances in Natural Sciences: Nanoscience and Nanotechnology*, 3.

Ning, Z., C. S. Cheung, J. Fu, M. A. Liu, and M. A. Schnell. 2006. 'Experimental study of environmental tobacco smoke particles under actual indoor environment', *Sci Total Environ*, 367: 822-30.

Oh, J. Y., H. S. Kim, L. Palanikumar, E. M. Go, B. Jana, S. A. Park, H. Y. Kim, K. Kim, J. K. Seo, S. K. Kwak, C. Kim, S. Kang, and J. H. Ryu. 2018. 'Cloaking nanoparticles with protein corona shield for targeted drug delivery', *Nat Commun*, 9: 4548.

Oh, N., and J. H. Park. 2014. 'Surface chemistry of gold nanoparticles mediates their exocytosis in macrophages', *ACS Nano*, 8: 6232-41.

Oh, P., J. E. Testa, P. Borgstrom, H. Witkiewicz, Y. Li, and J. E. Schnitzer. 2014. 'In vivo proteomic imaging analysis of caveolae reveals pumping system to penetrate solid tumors', *Nat Med*, 20: 1062-8.

Paatero, I., E. Casals, R. Niemi, E. Ozliseli, J. M. Rosenholm, and C. Sahlgren. 2017. 'Analyses in zebrafish embryos reveal that nanotoxicity profiles are dependent on surface-functionalization controlled penetrance of biological membranes', *Sci Rep*, 7: 8423.

Park, J. H., L. Gu, G. von Maltzahn, E. Ruoslahti, S. N. Bhatia, and M. J. Sailor. 2009. 'Biodegradable luminescent porous silicon nanoparticles for in vivo applications', *Nat Mater*, 8: 331-6.

Park, S., W. J. Lee, S. Park, D. Choi, S. Kim, and N. Park. 2019. 'Reversibly pH-responsive gold nanoparticles and their applications for photothermal cancer therapy', *Sci Rep*, 9: 20180.

Partikel, K., R. Korte, N. C. Stein, D. Mulac, F. C. Herrmann, H. U. Humpf, and K. Langer. 2019. 'Effect of nanoparticle size and PEGylation on the protein corona of PLGA nanoparticles', *Eur J Pharm Biopharm*, 141: 70-80.

Parton, R. G., and K. Simons. 2007. 'The multiple faces of caveolae', *Nat Rev Mol Cell Biol*, 8: 185-94.

Pelaz, B., P. del Pino, P. Maffre, R. Hartmann, M. Gallego, S. Rivera-Fernandez, J. M. de la Fuente, G. U. Nienhaus, and W. J. Parak. 2015. 'Surface Functionalization of Nanoparticles with Polyethylene Glycol: Effects on Protein Adsorption and Cellular Uptake', *ACS Nano*, 9: 6996-7008.

Perica, K., J. C. Varela, M. Oelke, and J. Schneck. 2015. 'Adoptive T cell immunotherapy for cancer', *Rambam Maimonides Med J*, 6: e0004.

Petryayeva, E., and U. J. Krull. 2011. 'Localized surface plasmon resonance: nanostructures, bioassays and biosensing--a review', *Anal Chim Acta*, 706: 8-24.

Phonesouk, E., S. Lechevallier, A. Ferrand, M. P. Rols, C. Bezombes, M. Verelst, and M. Golzio. 2019. 'Increasing Uptake of Silica Nanoparticles with Electroporation: From Cellular Characterization to Potential Applications', *Materials (Basel)*, 12.

Piella, J., N. G. Bastus, and V. Puntes. 2017. 'Size-Dependent Protein-Nanoparticle Interactions in Citrate-Stabilized Gold Nanoparticles: The Emergence of the Protein Corona', *Bioconjug Chem*, 28: 88-97.

Plane, J. M. 2012. 'Cosmic dust in the earth's atmosphere', *Chemical Society Reviews*, 41: 6507-18.

Poole, L. B. 2015. 'The basics of thiols and cysteines in redox biology and chemistry', *Free Radic Biol Med*, 80: 148-57.

Pramanik, Sunipa, Samantha K. E. Hill, Bo Zhi, Natalie V. Hudson-Smith, Jeslin J. Wu, Jacob N. White, Eileen A. McIntire, V. S. Santosh K. Kondeti, Amani L. Lee, Peter J. Bruggeman, Uwe R. Kortshagen, and Christy L. Haynes. 2018. 'Comparative toxicity assessment of novel Si quantum dots and their traditional Cd-based counterparts using bacteria models Shewanella oneidensis and Bacillus subtilis', *Environmental Science: Nano*, 5: 1890-901.

Qie, Y., H. Yuan, C. A. von Roemeling, Y. Chen, X. Liu, K. D. Shih, J. A. Knight, H. W. Tun, R. E. Wharen, W. Jiang, and B. Y. Kim. 2016. 'Surface modification of nanoparticles enables selective evasion of phagocytic clearance by distinct macrophage phenotypes', *Sci Rep*, 6: 26269.

Qing, Y., L. Cheng, R. Li, G. Liu, Y. Zhang, X. Tang, J. Wang, H. Liu, and Y. Qin. 2018. 'Potential antibacterial mechanism of silver nanoparticles and the optimization of orthopedic implants by advanced modification technologies', *Int J Nanomedicine*, 13: 3311-27.

Raj, S., S. Jose, U. S. Sumod, and M. Sabitha. 2012. 'Nanotechnology in cosmetics: Opportunities and challenges', *J Pharm Bioallied Sci*, 4: 186-93.

Rampado, R., S. Crotti, P. Caliceti, S. Pucciarelli, and M. Agostini. 2020. 'Recent Advances in Understanding the Protein Corona of Nanoparticles and in the Formulation of "Stealthy" Nanomaterials', *Front Bioeng Biotechnol*, 8: 166.

Reznickova, A., N. Slavikova, Z. Kolska, K. Kolarova, T. Belinova, M. Hubalek Kalbacova, M. Cieslar, and V. Svorcik. 2019. 'PEGylated gold nanoparticles: Stability, cytotoxicity and antibacterial activity', *Colloids and Surfaces A: Physicochemical and Engineering Aspects*, 560: 26-34.

Reznickova, A., P. Slepicka, N. Slavikova, M. Staszek, and V. Svorcik. 2017. 'Preparation, aging and temperature stability of PEGylated gold nanoparticles', *Colloids and Surfaces A: Physicochemical and Engineering Aspects*, 523: 91-97.

Saikia, J., M. Yazdimamaghani, S. P. Hadipour Moghaddam, and H. Ghandehari. 2016. 'Differential Protein Adsorption and Cellular Uptake of Silica Nanoparticles Based on Size and Porosity', *ACS Appl Mater Interfaces*, 8: 34820-32.

Salvati, A., A. S. Pitek, M. P. Monopoli, K. Prapainop, F. B. Bombelli, D. R. Hristov, P. M. Kelly, C. Aberg, E. Mahon, and K. A. Dawson. 2013. 'Transferrin-functionalized nanoparticles lose their targeting capabilities when a biomolecule corona adsorbs on the surface', *Nat Nanotechnol*, 8: 137-43.

Sancho-Albero, M., M. D. M. Encabo-Berzosa, M. Beltran-Visiedo, L. Fernandez-Messina, V. Sebastian, F. Sanchez-Madrid, M. Arruebo, J. Santamaria, and P. Martin-Duque. 2019. 'Efficient encapsulation of theranostic nanoparticles in cell-derived exosomes: leveraging the exosomal biogenesis pathway to obtain hollow gold nanoparticle-hybrids', *Nanoscale*, 11: 18825-36.

Santos, Cátia S. C., Barbara Gabriel, Marilys Blanchy, Olivia Menes, Denise García, Miren Blanco, Noemí Arconada, and Victor Neto. 2015. 'Industrial Applications of Nanoparticles – A Prospective Overview', *Materials Today: Proceedings*, 2: 456-65.

Satterlee, A. B., J. D. Rojas, P. A. Dayton, and L. Huang. 2017. 'Enhancing Nanoparticle Accumulation and Retention in Desmoplastic Tumors via Vascular Disruption for Internal Radiation Therapy', *Theranostics*, 7: 253-69.

Sciau, Philippe, Claude Mirguet, Christian Roucau, Delhia Chabanne, and Max Schvoerer. 2009. 'Double Nanoparticle Layer in a 12th Century Lustreware Decoration: Accident or Technological Mastery?', *Journal of Nano Research*, 8: 133-39.

Secret, E., M. Maynadier, A. Gallud, M. Gary-Bobo, A. Chaix, E. Belamie, P. Maillard, M. J. Sailor, M. Garcia, J. O. Durand, and F. Cunin. 2013. 'Anionic porphyrin-grafted porous silicon nanoparticles for photodynamic therapy', *Chem Commun (Camb)*, 49: 4202-4.

Senapati, V. A., A. Kumar, G. S. Gupta, A. K. Pandey, and A. Dhawan. 2015. 'ZnO nanoparticles induced inflammatory response and genotoxicity in human blood cells: A mechanistic approach', *Food Chem Toxicol*, 85: 61-70.

Sharifi, Ibrahim, H. Shokrollahi, and S. Amiri. 2012. 'Ferrite-based magnetic nanofluids used in hyperthermia applications', *Journal of Magnetism and Magnetic Materials*, 324: 903-15.

Shintani, Yasushi, Keiji Iwamoto, and Kazuaki Kitano. 1988. 'Polyethylene glycols for promoting the growth of mammalian cells', *Applied Microbiology and Biotechnology*, 27: 533-37.

Scholz, M., S. Yep, M. Chancey, C. Kelly, K. Chau, J. Turner, R. Lam, and C. G. Drake. 2017. 'Phase I clinical trial of sipuleucel-T combined with escalating doses of ipilimumab in progressive metastatic castrate-resistant prostate cancer', *Immunotargets Ther*, 6: 11-16.

Silva, M. T. 2010. 'Secondary necrosis: the natural outcome of the complete apoptotic program', *FEBS Lett*, 584: 4491-9.

Simakov, S. K. 2018. 'Nano- and micron-sized diamond genesis in nature: An overview', *Geoscience Frontiers*, 9: 1849-58.

Stayton, I., J. Winiarz, K. Shannon, and Y. Ma. 2009. 'Study of uptake and loss of silica nanoparticles in living human lung epithelial cells at single cell level', *Anal Bioanal Chem*, 394: 1595-608.

Stefani, D., D. Wardman, and T. Lambert. 2005. 'The implosion of the Calgary General Hospital: ambient air quality issues', *J Air Waste Manag Assoc*, 55: 52-9.

Stehlik, S., M. Varga, M. Ledinsky, D. Miliaieva, H. Kozak, V. Skakalova, C. Mangler, T. J. Pennycook, J. C. Meyer, A. Kromka, and B. Rezek. 2016. 'High-yield fabrication and properties of 1.4 nm nanodiamonds with narrow size distribution', *Sci Rep*, 6: 38419.

Stehlik, S., M. Varga, P. Stenclova, L. Ondic, M. Ledinsky, J. Pangrac, O. Vanek, J. Lipov, A. Kromka, and B. Rezek. 2017. 'Ultrathin Nanocrystalline Diamond Films with Silicon Vacancy Color Centers via Seeding by 2 nm Detonation Nanodiamonds', *ACS Appl Mater Interfaces*, 9: 38842-53.

Stojanovic, V., F. Cunin, J. O. Durand, M. Garcia, and M. Gary-Bobo. 2016. 'Potential of porous silicon nanoparticles as an emerging platform for cancer theranostics', *J Mater Chem B*, 4: 7050-59.

Su, L. J., M. S. Wu, Y. Y. Hui, B. M. Chang, L. Pan, P. C. Hsu, Y. T. Chen, H. N. Ho, Y. H. Huang, T. Y. Ling, H. H. Hsu, and H. C. Chang. 2017. 'Fluorescent nanodiamonds enable quantitative tracking of human mesenchymal stem cells in miniature pigs', *Sci Rep*, 7: 45607.

Szekrényes, Zsolt, Bálint Somogyi, Dávid Beke, Gyula Károlyházy, István Balogh, Katalin Kamarás, and Adam Gali. 2014. 'Chemical Transformation of Carboxyl Groups on the Surface of Silicon Carbide Quantum Dots', *The Journal of Physical Chemistry C*, 118: 19995-20001.

Tamba, B. I., A. Dondas, M. Leon, A. N. Neagu, G. Dodi, C. Stefanescu, and A. Tijani. 2015. 'Silica nanoparticles: preparation, characterization and in vitro/in vivo biodistribution studies', *Eur J Pharm Sci*, 71: 46-55.

Tavano, R., L. Gabrielli, E. Lubian, C. Fedeli, S. Visentin, P. Polverino De Laureto, G. Arrigoni, A. Geffner-Smith, F. Chen, D. Simberg, G. Morgese, E. M. Benetti, L. Wu, S. M. Moghimi, F. Mancin, and E. Papini. 2018. 'C1q-Mediated Complement Activation and C3 Opsonization Trigger Recognition of Stealth Poly(2-methyl-2-oxazoline)-Coated Silica Nanoparticles by Human Phagocytes', *ACS Nano*, 12: 5834-47.

Taylor, M. J., D. Perrais, and C. J. Merrifield. 2011. 'A high precision survey of the molecular dynamics of mammalian clathrin-mediated endocytosis', *PLoS Biol*, 9: e1000604.

Temchura, V. V., D. Kozlova, V. Sokolova, K. Uberla, and M. Epple. 2014. 'Targeting and activation of antigen-specific B-cells by calcium phosphate nanoparticles loaded with protein antigen', *Biomaterials*, 35: 6098-105.

Thakur, S., R. V. Saini, P. Singh, P. Raizada, V. K. Thakur, and A. K. Saini. 2020. 'Nanoparticles as an emerging tool to alter the gene expression: Preparation and conjugation methods', *Materials Today Chemistry*, 17.

Tiefenboeck, P., J. A. Kim, F. Trunk, T. Eicher, E. Russo, A. Teijeira, C. Halin, and J. C. Leroux. 2017. 'Microinjection for the ex Vivo Modification of Cells with Artificial Organelles', *ACS Nano*, 11: 7758-69.

Torrano, A. A., R. Herrmann, C. Strobel, M. Rennhak, H. Engelke, A. Reller, I. Hilger, A. Wixforth, and C. Brauchle. 2016. 'Cell membrane penetration and mitochondrial targeting by platinum-decorated ceria nanoparticles', *Nanoscale*, 8: 13352-67.

Trujillo-Alonso, V., E. C. Pratt, H. Zong, A. Lara-Martinez, C. Kaittanis, M. O. Rabie, V. Longo, M. W. Becker, G. J. Roboz, J. Grimm, and M. L. Guzman. 2019. 'FDA-approved ferumoxytol displays anti-leukaemia efficacy against cells with low ferroportin levels', *Nat Nanotechnol*, 14: 616-22.

Tucci, P., G. Porta, M. Agostini, D. Dinsdale, I. Iavicoli, K. Cain, A. Finazzi-Agro, G. Melino, and A. Willis. 2013. 'Metabolic effects of TiO2 nanoparticles, a common component of sunscreens and cosmetics, on human keratinocytes', *Cell Death Dis*, 4: e549.

Ventola, C. L. 2017. 'Progress in Nanomedicine: Approved and Investigational Nanodrugs', *P T*, 42: 742-55.

Vert, Michel, Yoshiharu Doi, Karl-Heinz Hellwich, Michael Hess, Philip Hodge, Przemyslaw Kubisa, Marguerite Rinaudo, and François Schué. 2012. 'Terminology for biorelated polymers and applications (IUPAC Recommendations 2012)', *Pure and Applied Chemistry*, 84: 377-410.

Vivier, E., and B. Malissen. 2005. 'Innate and adaptive immunity: specificities and signaling hierarchies revisited', *Nat Immunol*, 6: 17-21.

Vrabcova, Lucie. 2019. 'The cell-nanomaterial interactions and their application in biomedicine', disertation, Charles University.

Walter, P., E. Welcomme, P. Hallegot, N. J. Zaluzec, C. Deeb, J. Castaing, P. Veyssiere, R. Breniaux, J. L. Leveque, and G. Tsoucaris. 2006. 'Early use of PbS nanotechnology for an ancient hair dyeing formula', *Nano Lett*, 6: 2215-9.

Wang, F., L. Yu, M. P. Monopoli, P. Sandin, E. Mahon, A. Salvati, and K. A. Dawson. 2013. 'The biomolecular corona is retained during nanoparticle uptake and protects the cells from the damage induced by cationic nanoparticles until degraded in the lysosomes', *Nanomedicine*, 9: 1159-68.

Wang, M., O. J. R. Gustafsson, E. H. Pilkington, A. Kakinen, I. Javed, A. Faridi, T. P. Davis, and P. C. Ke. 2018. 'Nanoparticle-proteome in vitro and in vivo', *J Mater Chem B*, 6: 6026-41.

Wang, S., H. Guo, Y. Li, and X. Li. 2019. 'Penetration of nanoparticles across a lipid bilayer: effects of particle stiffness and surface hydrophobicity', *Nanoscale*, 11: 4025-34.

Wang, T., J. Bai, X. Jiang, and G. U. Nienhaus. 2012. 'Cellular uptake of nanoparticles by membrane penetration: a study combining confocal microscopy with FTIR spectroelectrochemistry', *ACS Nano*, 6: 1251-9.

Wang, Wenqian, Katharina Gaus, Richard D. Tilley, and J. Justin Gooding. 2019. 'The impact of nanoparticle shape on cellular internalisation and transport: what do the different analysis methods tell us?', *Materials Horizons*, 6: 1538-47.

Wang, Z., C. Tiruppathi, J. Cho, R. D. Minshall, and A. B. Malik. 2011. 'Delivery of nanoparticle: complexed drugs across the vascular endothelial barrier via caveolae', *IUBMB Life*, 63: 659-67.

Watanabe, S., and E. Boucrot. 2017. 'Fast and ultrafast endocytosis', *Curr Opin Cell Biol*, 47: 64-71.

Weber, C., J. Simon, V. Mailander, S. Morsbach, and K. Landfester. 2018. 'Preservation of the soft protein corona in distinct flow allows identification of weakly bound proteins', *Acta Biomater*, 76: 217-24.

Winchester, B., A. Vellodi, and E. Young. 2000. 'The molecular basis of lysosomal storage diseases and their treatment', *Biochem Soc Trans*, 28: 150-4.

Winzen, S., S. Schoettler, G. Baier, C. Rosenauer, V. Mailaender, K. Landfester, and K. Mohr. 2015. 'Complementary analysis of the hard and soft protein corona: sample preparation critically effects corona composition', *Nanoscale*, 7: 2992-3001.

Wu, G. J., Y. T. Tai, T. L. Chen, L. L. Lin, Y. F. Ueng, and R. M. Chen. 2005. 'Propofol specifically inhibits mitochondrial membrane potential but not complex I NADH dehydrogenase activity, thus reducing cellular ATP biosynthesis and migration of macrophages', *Ann N Y Acad Sci*, 1042: 168-76.

Wu, X., M. Bruschi, T. Waag, S. Schweeberg, Y. Tian, T. Meinhardt, R. Stigler, K. Larsson, M. Funk, D. Steinmuller-Nethl, M. Rasse, and A. Krueger. 2017. 'Functionalization of bone implants with

nanodiamond particles and angiopoietin-1 to improve vascularization and bone regeneration', *J Mater Chem B*, 5: 6629-36.
Wu, Yue, Moustafa R. K. Ali, Kuangcai Chen, Ning Fang, and Mostafa A. El-Sayed. 2019. 'Gold nanoparticles in biological optical imaging', *Nano Today*, 24: 120-40.
Xie, H., M. M. Mason, and J. P. Wise, Sr. 2011. 'Genotoxicity of metal nanoparticles', *Rev Environ Health*, 26: 251-68.
Xie, X., J. Liao, X. Shao, Q. Li, and Y. Lin. 2017. 'The Effect of shape on Cellular Uptake of Gold Nanoparticles in the forms of Stars, Rods, and Triangles', *Sci Rep*, 7: 3827.
Xin, X., X. Pei, X. Yang, Y. Lv, L. Zhang, W. He, and L. Yin. 2017. 'Rod-Shaped Active Drug Particles Enable Efficient and Safe Gene Delivery', *Adv Sci (Weinh)*, 4: 1700324.
Xu, Y., L. Wang, R. Bai, T. Zhang, and C. Chen. 2015. 'Silver nanoparticles impede phorbol myristate acetate-induced monocyte-macrophage differentiation and autophagy', *Nanoscale*, 7: 16100-9.
Yang, Y., N. Gao, Y. Hu, C. Jia, T. Chou, H. Du, and H. Wang. 2015. 'Gold nanoparticle-enhanced photodynamic therapy: effects of surface charge and mitochondrial targeting', *Ther Deliv*, 6: 307-21.
Yassin, M. A., K. Mustafa, Z. Xing, Y. Sun, K. E. Fasmer, T. Waag, A. Krueger, D. Steinmuller-Nethl, A. Finne-Wistrand, and K. N. Leknes. 2017. 'A Copolymer Scaffold Functionalized with Nanodiamond Particles Enhances Osteogenic Metabolic Activity and Bone Regeneration', *Macromol Biosci*, 17.
Yin, M. M., W. Q. Chen, Y. Q. Lu, J. Y. Han, Y. Liu, and F. L. Jiang. 2020. 'A model beyond protein corona: thermodynamics and binding stoichiometries of the interactions between ultrasmall gold nanoclusters and proteins', *Nanoscale*, 12: 4573-85.
Yu, M. F., O. Lourie, M. J. Dyer, K. Moloni, T. F. Kelly, and R. S. Ruoff. 2000. 'Strength and breaking mechanism of multiwalled carbon nanotubes under tensile load', *Science*, 287: 637-40.
Yu, Xiaoya, Xiao Liu, Wanchuan Ding, Jun Wang, and Gang Ruan. 2019. 'Spontaneous and instant formation of highly stable protein–nanoparticle supraparticle co-assemblies driven by hydrophobic interaction', *Nanoscale Advances*, 1: 4137-47.
Yu, Yue, Xi Yang, Ming Liu, Masahiro Nishikawa, Takahiro Tei, and Eijiro Miyako. 2019. 'Anticancer drug delivery to cancer cells using alkyl amine-functionalized nanodiamond supraparticles', *Nanoscale Advances*, 1: 3406-12.
Yu, Yun, Jing Wang, Juqiang Lin, Duo Lin, Weiwei Chen, Shangyuan Feng, Zufang Huang, Yongzeng Li, Hao Huang, Hong Shi, and Rong Chen. 2016. 'An optimized electroporation method for delivering nanoparticles into living cells for surface-enhanced Raman scattering imaging', *Applied Physics Letters*, 108.
Zamaraeva, M. V., R. Z. Sabirov, E. Maeno, Y. Ando-Akatsuka, S. V. Bessonova, and Y. Okada. 2005. 'Cells die with increased cytosolic ATP during apoptosis: a bioluminescence study with intracellular luciferase', *Cell Death Differ*, 12: 1390-7.
Zarschler, K., L. Rocks, N. Licciardello, L. Boselli, E. Polo, K. P. Garcia, L. De Cola, H. Stephan, and K. A. Dawson. 2016. 'Ultrasmall inorganic nanoparticles: State-of-the-art and perspectives for biomedical applications', *Nanomedicine*, 12: 1663-701.
Zhang, B., Y. Xing, Z. Li, H. Zhou, Q. Mu, and B. Yan. 2009. 'Functionalized carbon nanotubes specifically bind to alpha-chymotrypsin's catalytic site and regulate its enzymatic function', *Nano Lett*, 9: 2280-4.
Zhang, Z., J. Guan, Z. Jiang, Y. Yang, J. Liu, W. Hua, Y. Mao, C. Li, W. Lu, J. Qian, and C. Zhan. 2019. 'Brain-targeted drug delivery by manipulating protein corona functions', *Nat Commun*, 10: 3561.
Zhao, Jiacheng, and Martina H. Stenzel. 2018. 'Entry of nanoparticles into cells: the importance of nanoparticle properties', *Polymer Chemistry*, 9: 259-72.
Zhu, L., B. Pelaz, I. Chakraborty, and W. J. Parak. 2019. 'Investigating Possible Enzymatic Degradation on Polymer Shells around Inorganic Nanoparticles', *Int J Mol Sci*, 20.

11. Full-texts of Author's Publications

Publication A: Ostrovska, Lucie, Antonin Broz, Anna Fucikova, **Tereza Belinova**, Hiroshi Sugimoto, Takashi Kanno, Minoru Fujii, Jan Valenta, and Marie Hubalek Kalbacova. "**The Impact of Doped Silicon Quantum Dots on Human Osteoblasts**." RSC Advances 6, no. 68 (2016): 63403-13, IF = 3,289

Publication B: Belinova, Tereza, Lucie Vrabcova, Iva Machova, Anna Fucikova, Jan Valenta, Hiroshi Sugimoto, Minoru Fujii, and Marie Hubalek Kalbacova. "**Silicon Quantum Dots and Their Impact on Different Human Cells**." physica status solidi (b) 255, no. 10 (2018). IF = 1.729

Publication C: Bělinová, Tereza, Iva Machová, David Beke, Anna Fučíková, Adam Gali, Zuzana Humlová, Jan Valenta, and Marie Hubálek Kalbáčová. "**Immunomodulatory Potential of Differently-Terminated Ultra-Small Silicon Carbide Nanoparticles.**" Nanomaterials 10, no. 3 (2020), IF = 4.324

Publication D: Reznickova, A., N. Slavikova, Z. Kolska, K. Kolarova, **T. Belinova**, M. Hubalek Kalbacova, M. Cieslar, and V. Svorcik. "**Pegylated Gold Nanoparticles: Stability, Cytotoxicity and Antibacterial Activity**." Colloids and Surfaces A: Physicochemical and Engineering Aspects 560 (2019): 26-34, IF = 2.829

Publication E: Machova, Iva, Martin Hubalek, **Tereza Belinova**, Anna Fucikova, Stepan Stehlik, Bohuslav Rezek, and Marie Hubalek Kalbacova. "**The Bio-Chemically Selective Interaction of Hydrogenated and Oxidized Ultra-Small Nanodiamonds with Proteins and Cells**." Carbon (2020), IF = 8.821